Accepted Manuscript

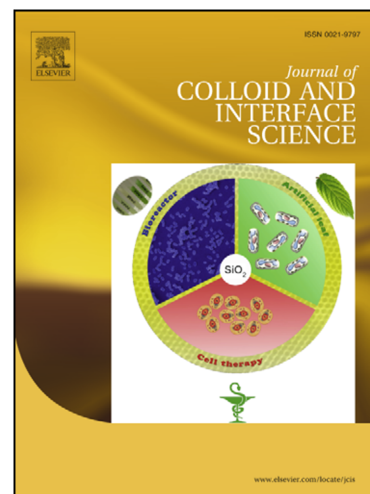

Self-Assembled Templates for the Generation of Arrays of 1-Dimenisonal Nanostructures: From Molecules to Devices

Richard A. Farrell, Nikolay Petkov, Michael A. Morris, Justin D. Holmes

PII: S0021-9797(10)00442-X
DOI: 10.1016/j.jcis.2010.04.041
Reference: YJCIS 15793

To appear in: *Journal of Colloid and Interface Science*

Received Date: 20 December 2009
Accepted Date: 19 April 2010

Please cite this article as: R.A. Farrell, N. Petkov, M.A. Morris, J.D. Holmes, Self-Assembled Templates for the Generation of Arrays of 1-Dimenisonal Nanostructures: From Molecules to Devices, *Journal of Colloid and Interface Science* (2010), doi: 10.1016/j.jcis.2010.04.041

This is a PDF file of an unedited manuscript that has been accepted for publication. As a service to our customers we are providing this early version of the manuscript. The manuscript will undergo copyediting, typesetting, and review of the resulting proof before it is published in its final form. Please note that during the production process errors may be discovered which could affect the content, and all legal disclaimers that apply to the journal pertain.

ACCEPTED MANUSCRIPT

Self-Assembled Templates for the Generation of Arrays of 1-Dimenisonal Nanostructures: From Molecules to Devices

Richard A. Farrell[†,ϕ,§], Nikolay Petkov[‡], Michael A. Morris[†,ϕ] and Justin D. Holmes[†,ϕ,*]

[†]Materials and Supercritical Fluid Group, Department of Chemistry and the Tyndall National Institute, University College Cork, Cork, Ireland. [ϕ]Centre for Research on Adaptive Nanostructures and Nanodevices (CRANN), Trinity College Dublin, Dublin 2, Ireland. [§]Department of Chemistry and Biochemistry, University of California Los Angeles (UCLA), 607 Charles E. Young Drive East, Los Angeles, CA., 90095-1569. [‡]Electron Microscopy and Analysis Facility (EMAF), Tyndall National Institute, Lee Maltings, Prospect Row, Ireland.

RECEIVED DATE (to be automatically inserted after your manuscript is accepted if required according to the journal that you are submitting your paper to)

*To whom correspondence should be addressed Tel: +353 (0)21 4903608; Fax, +353 (0)21 4274097; Email: j.holmes@ucc.ie

ACCEPTED MANUSCRIPT

ACCEPTED MANUSCRIPT

KEYWORDS

Self-assembly, Nanostructures, Templates, Block Copolymers, Mesoporous Materials, Porous Anodic Alumina.

ABSTRACT

Self-assembled nanoscale porous architectures, such as mesoporous silica films (MPS), block copolymer films (BCP) and porous anodic aluminas (PAAs), are ideal hosts for templating one dimension (1 D) nano-entities for a wide range of electronic, photonic, magnetic and environmental applications. All three templates offer dimensional scalability and tunability over a wide range, with critical pore sizes for each system well below the 20 nm threshold [1-3]. Recently, research has progressed towards controlling the pore direction, orientation and long range order of these nanostructures through so called directed self-assembly (DSA). Significantly, the introduction of a wide range of top-down chemically and physically pre-patterning substrates has facilitated the DSA of nanostructures into functional device arrays. The following review begins with an overview of the fundamental aspects of self-assembly and ordering processes during the formation of PAAs, BCPs and MPS films. Special attention is given to the different ways of directing self-assembly, concentrating on properties such as uni-directional alignment, precision placement and registry of the self-assembled structures to hierarchal or top down architectures. Finally, to distinguish this review from other articles we focus on research where nanostructures have been utilised in part to fabricate arrays of functioning devices below the sub 50 nm threshold, by subtractive transfer and additive methods. Where possible, we attempt to compare and contrast the different templating approaches and highlight the strengths and/or limitations that will be important for their potential integration into downstream processes.

ACCEPTED MANUSCRIPT

ACCEPTED MANUSCRIPT

SECTION 1.0: SELF ASSEMBLY AND NANO-ARCHITETCURES

The diversity of self-assembled nanostructures and more importantly, their precise orientation within a thin film (fixed to a substrate) ultimately determines their function and overall application. A large population of research reports to date have focused on identifying these orientations and related periodicities, using x-ray and microscopy tools, as well the development of methods for readily manipulating nanostructures, such as pre-patterning of silicon substrates for the alignment of block copolymers (BCPs) [4] and mesoporous thin films (MTFs) [5] and altering the growth direction of porous anodic alumina (PAA) templates [6]. In this section, a brief synopsis of the mechanisms behind the self-assembly/organisation of each system and highlight nanoscale architectures (and orientations), which are important from a device perspective.

1.1. Templated mesoporous thin films

Ordered mesoporous powders were first discovered by researchers at the Mobil Petrochemical Corporation in 1992 and shortly after, sol-gel derived mesoporous silica films were fabricated [1, 7]. The first series of ordered mesoporous films were reported by Yang *et al*. in 1996 [8], prepared using initial surfactant concentrations above their critical micelle concentration (CMC). However the films prepared films prepared were relatively thick and similar to their powder analogues. In 1997, Lu and co-workers [9] synthesised well-structured and homogenous mesoporous silica films by templating with the surfactant CTAB, designating this technique as evaporation induced self assembly (EISA) [10-12]. In this regime, approach the surfactant monomers organise themselves through non-covalent interactions (hydrogen bonding, Van der Waals forces, electrostatic and hydrophobic forces), around silica oligomers to form highly ordered mesostructured thin film oxides, by the rapid evaporation of a volatile solvent during either spin-coating or dip-coating of the sol. This technique differs from the aforementioned

ACCEPTED MANUSCRIPT

ACCEPTED MANUSCRIPT

methods as the surfactant concentration used was well below the CMC prior to sol deposition; acting as a driving force for self-assembly as the solvent evaporates during deposition.

Figure 1 is a schematic depicting the mechanism of formation during dip-coating (or a thinning fluid) for a mesoporous film. At the outset a mixture of water, inorganic precursor, alcohol and surfactant exist as a thick film. As the film thickness is carefully reduced, solvent evaporation becomes significant (transition of the film from bulk to nanoscale), resulting in the formation of an ordered structure. The drying stage allows for precision control of the final mesostructure by regulating the humidity of the system which can swell/contract the hydrophilic portion of the film. By controlling the solvent evaporation rate, temperature, silicate/polymer ratio and humidity, the 3 D nanostructuring of the film can be tailored into a variety of different pore assemblies, such as cubic and hexagonal [10-14]. Figure 1(b) displays a P6m/2D hexagonally structured film, ~700 nm thick; templated by Pluronic F127 with its porous channels adopting a parallel orientation with respect to the substrate. The EISA method is extremely efficient as it produces films with high uniformity and uni-modal pore size distributions. Elimination of the surfactant templates by calcination creates a silica fossil which is essentially the inverse of the liquid crystal template. Spin and dip coating are the most frequent methods used for depositing self-assembled mesoporous films, although it has become widely accepted that dip-coating provides greater control and ordering of the final nanostructures generated [15-16].

Self-assembled mesoporous silica films have also been prepared *via* aerosol-assisted deposition [17] and pre-organised template/supercritical fluid inclusion techniques [18]. The later one represents an appealing avenue for tailoring mesoporous silica architectures since the organic structure directing agents (tri-block copolymer from the Pluronic family) are deposited in an initial first step before the inorganic component is infiltrated via supercritical inclusion/swelling. The authors argue that the mesophase structure that has already been developed by the self-assembly of the block co-polymer can serve as a static scaffold for further incorporation of the inorganic component. This approach is extremely powerful because the ordering and the orientation of tri-block co-polymers can be controlled

ACCEPTED MANUSCRIPT

ACCEPTED MANUSCRIPT

separately. Thus mesophases and orientations that are difficult to obtain through organic-inorganic co-operative self-assembly, as for example those obtained by EISA method, can be accessed. Unfortunately, the authors of this pioneering work limited themselves to investigating 2 D-hexagonal ordered channels (parallel orientation to the substrate surface) which is the most commonly and easily obtainable mesophase structure obtainable by the EISA method. Mesoporous silica films have also been prepared by spin coating a suspension of sub-100 nm mesoporous particles with a radial pore orientation [19]. These particles have limited application as templates for nanostructures because of the random orientation of the porous system and the granular nature of the films, but can have excellent separation and absorption properties [20].

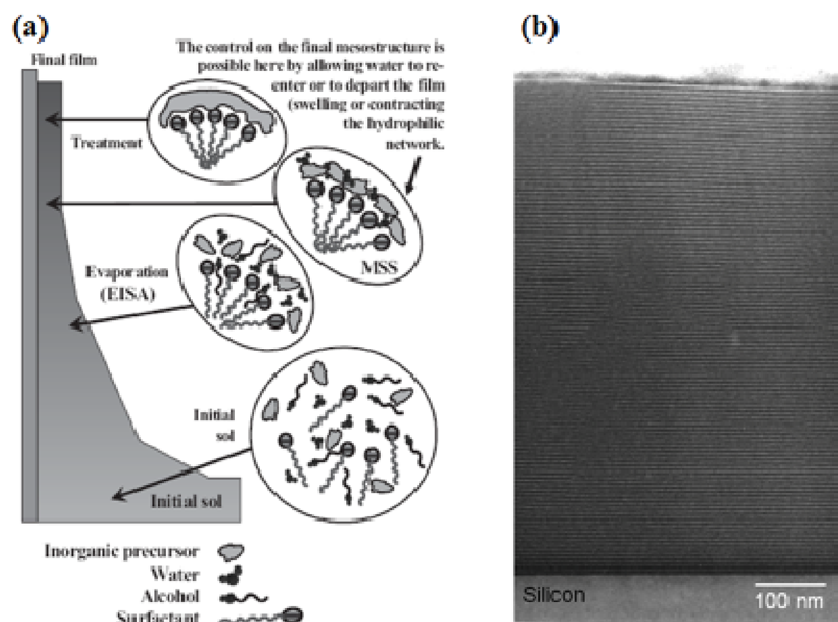

FIGURE 1: (a) Schematic of evaporation induced self-assembly (EISA), cartoon represents 4 stages of film formation – initial sol, evaporation driven self-assembly, equilibrium with environment and condensation of silica network (reproduced with permission from reference [12]). (b) TEM cross section of a film formed by the EISA methods, film of ~700 nm with a p6m 2D hexagonal structure was fabricated through a dip-coating process where Pluronic F127 was the template used (unpublished work). Careful control during deposition (humidity and precursor concentrations) ensures the formation of well-ordered periodic nanostructures.

ACCEPTED MANUSCRIPT

Mesoporous silica films have potential applications in many fields including sensing [21], catalysis [22], optics [23] and microfluidics [16]. For additional reading, Brinker [10-11] and Grosso [12] provide in-depth and comprehensive reviews on films synthesised *via* EISA techniques and their potential applications.

1.2. Block copolymer (BCP) thin films

Block copolymers are an important class of macromolecules with a promising future in the nanoelectronics industry as they can function as the template for periodic porous low-*k* silicon dioxide intermetal/interlevel dielectrics [24] and as self-assembled nano-lithographic resists for patterning/templating front-end nanodevices [25]. Numerous reviews exist on block copolymers ranging from their thermodynamic properties to more applied research [26-36]. In this section, a short introduction to A-B diblock copolymer thin film nanostructures and the mechanisms behind the formation of ordered block copolymer nanopatterns are provided.

Block copolymers comprise of two or more copolymer units covalently bonded together which undergo microphase separation; progressing from a homogenous mixture of the constituent blocks (phase mixed) into discrete heterogonous polymer domains (microphase separated) when thermally annealed above the glass transition temperature (T_g). A wide variety of nanostructures with reported feature sizes close to 7-10 nm have been reported [2, 37-38]. Microphase separation can also be induced by swelling the polymer films in a saturated solvent environment [39]. The final morphology for an A-B block copolymer film is governed by three parameters; the mole fraction of one block (f) with respect to the other block, the degree of polymerisation for the entire polymer (N) and the segmental interaction parameter, known as the Flory-Huggins interaction parameter (χ). Figure 2(a) displays the rich variety of nanostructures which can be formed by tailoring the molar fraction (f) and the degree of polymerisation (N) for a given A-B block copolymer, based on the self-consistent-mean-field (SCMF) theory. According to SCMF theory and experimental analysis of a symmetric block

ACCEPTED MANUSCRIPT

copolymer phase diagram, by decreasing the concentration of the A-block dominant system towards an equal molar fraction for both blocks, phases such closed packed spheres (CPS), body centred cubic spheres (*Im3m*), hexagonally packed cylinders, bicontinuous gyroid structure (*Ia3d*) and lamellae should be obtainable [40]. Closed packed sphere structures have yet to be demonstrated experimentally and other phases beyond those identified by SCMF theory have been reported, e.g. perforated lamellae [41], as shown in figure 2(b). Frederickson & Bates provide additional reviews which cover topics on thermodynamics and kinetics aspects of block copolymer films [42].

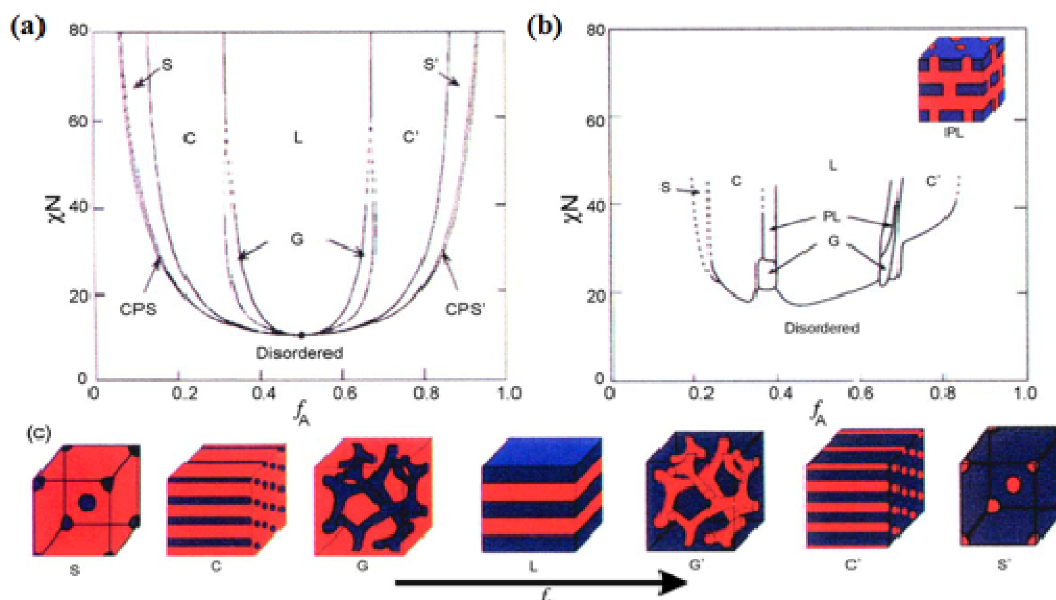

FIGURE 2: (a) SMCF phase diagram for an A-B diblock copolymer, microdomain structures such as packed spheres (CPS), body centred cubic spheres (Im3m), hexagonally packed cylinders, bicontinuous gyroid structure (Ia3d) and lamellae are predicted to exist as a function of the molar fraction. (b) Experimental A-B diblock copolymer, deviation between theoretical and experimental phase behaviour for the PS-PI diblock system (reproduced with permission from reference [40]).

In thin films, their surfaces are in close proximity to two very different interfaces; typically a substrate (silicon) and air [43]. Therefore upon confinement of a polymer to a thin film, structural orientation of the polymer becomes extremely important, especially for nano-lithographic applications. The film thickness is critical in controlling the nanostructures formed from block copolymers and as a result, the thickness of the polymer film satisfies one of two regimes known as symmetric wetting or

ACCEPTED MANUSCRIPT

ACCEPTED MANUSCRIPT

asymmetric wetting to be commensurate with the natural periodicity of block copolymer. In the symmetric case for a lamellar forming block copolymer, given a natural periodicity of L_o, a thin film with a thickness of integer value of L_o (i.e. nL_o) will dominate provided one of the blocks favours both the silicon and air interface. The asymmetric case considers polymer films where one block only wets one interface. Consequently, the preferred thickness of these films can be written as an integer value of L_o +0.5 (i.e. nL_o+0.5). A lamellar PS-*b*-PMMA copolymer when deposited on silicon will undergo microphase separation, with the PMMA segment preferentially wetting the native oxide and as a result the PMMA and PS form alternating layers normal to the substrate. PMMA has a greater affinity for the native oxide interface and as a result, the vertical orientation of lamellar structure is not accessible. Mansky *et al.* first demonstrated that by grafting a random copolymer of PS-*r*-PMMA to the silicon interface; the affinity of the both PS and PMMA to this interface was equivalent [44]. Consequently, by controlling the film thickness it was possible to tune the final orientation of the PS-*b*-PMMA films, whereby PS and PMMA adopt vertical orientations. Figure 3(a) displays a 70° tilt cross section SEM image of a symmetric PS-*b*-PMMA (37 k-37 k) block copolymer which was self-assembled on a 4 nm PS-*r*-PMMA brush layer. The PMMA portion of the lamellae structure was removed by a brief oxygen/fluorocarbon etch to yield a PS nanoresist pattern.

Although, thermal annealing has been shown to work well for a range of polymer films, the temperature window between the T_g and the order-disorder transition temperature (ODT) for some polymer films is too narrow to achieve thermodynamic equilibrium [45]. A technique known as solvent annealing or swelling, first demonstrated by Kim *et al.* [39] with polystyrene-polybutadiene-polystyrene (SBS) triblock copolymer, has received considerable attention over the last decade as an alternative to thermal annealing as it can not only induce microphase separation (orientation ordering) but also improve translational ordering [46]. Such an improvement in translational ordering is prompted by the uptake of the solvent, *e.g.* toluene, into one or both blocks, resulting in a lowering of T_g and easier diffusion of the polymer chains. This process occurs quicker at the air interface and combined with solvent evaporation, an order front is created which propagates in the direction of the silicon interface.

ACCEPTED MANUSCRIPT

Figure 3(b) displays a 70° tilt cross section SEM image of an asymmetric PS-*b*-PEO (19 k-6.5 k) block copolymer, post PEO selective removal, which was self-assembled onto a silicon wafer with a native oxide. PEO cylinders are oriented perpendicular to the substrate surface. Many other polymer systems (PS-*b*-P2VP-*b*-PtBMA [45], PS-*b*-PMMA [47], PS-*b*-PI-*b*-PS [48], PS-*b*-P4VP [49], PS-*b*-PDMS [50], PMS-*b*-PHOST [37], PS-*b*-PB-*b*-PS [51]) have been prepared *via* similar solvent swelling techniques [50].

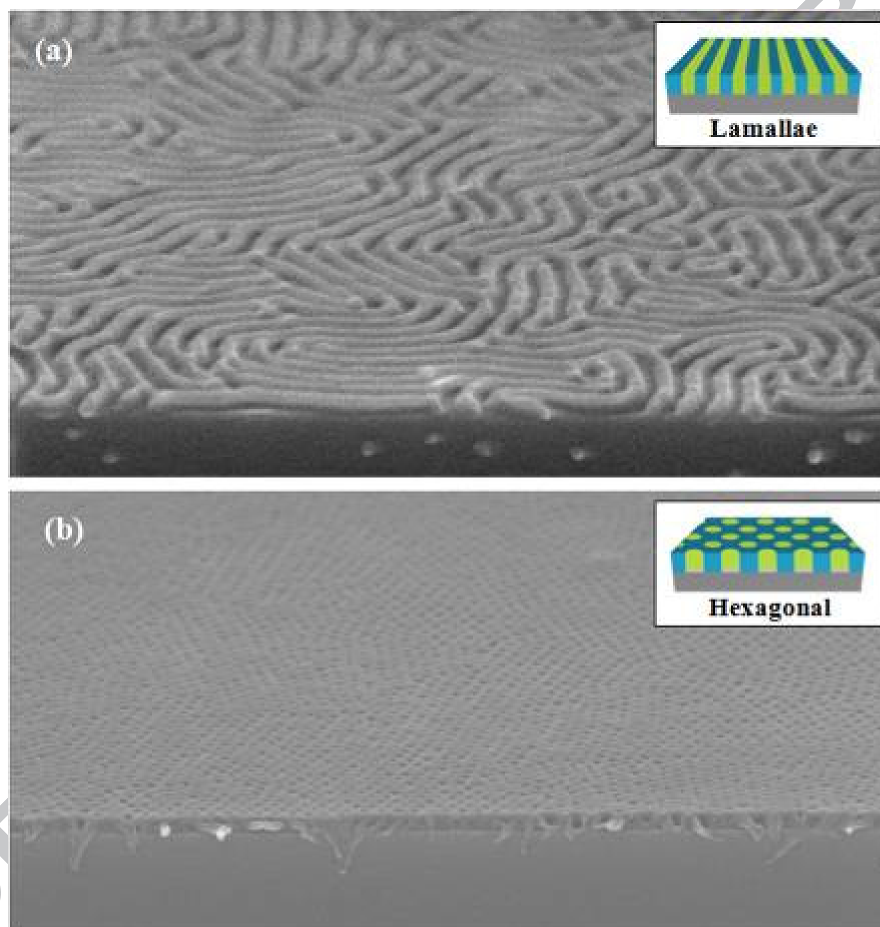

FIGURE 3: Polystyrene lines and membranes, 70° tilt SEM image of a (a) perpendicular lamellae PS-*b*-PMMA films and (reproduced with permission from reference [52]) (b) perpendicular hexagonal PS-*b*-PEO where the oxygen containing block (PEO & PMMA) was removed by an RIE etch (unpublished work). Films have orientational structure but lack translational ordering. (Inset) diagrams representing the internal structure within the films. Such nanopatterns can be used as masks for creating a wide range of nanostructures.

ACCEPTED MANUSCRIPT

New innovative synthetic polymer strategies, *e.g.* controlled/living polymerisation reactions, are rapidly emerging and consequently allowing researchers to tailor the functionality within each block [53]. For example, it is thought that ABC triblocks offer unique opportunities [54] for future technologies as they can adopt many more segregation patterns than simple diblock copolymers as outlined by Wei *et al.* in 1995 [55]. Furthermore, the addition of copolymer units increases the number of segregation pathways towards infinity. Recently, Tang *et al.* were able to mix block copolymers and limit their macrophase separation by carefully tuning the hydrogen-bonding interactions of the constituent block copolymers to create square patterns rather than then the traditionally hexagonal patterns observed in thin films [56].

With advances in synthetic approaches, a careful balance of their interfacial properties and improved characterisation techniques (spectroscopic and microscopy), block copolymers will find use in numerous applications, including catalysis, drug delivery, nanoelectronics and photonics [57].

1.3. Porous Anodic Aluminas (PAA)

The transformation of aluminium to alumina under anodic bias in different electrolytes (referred to as anodisation) has been studied extensively for the past 50 years. Typically porous anodic alumina systems (PAAs) are obtained as self-supported membranes or as layers on substrates, with nanometre sized, 1 D channels with quasi-hexagonal order and vertical orientation. However PAAs prepared by conventional methods show relatively poor ordering, dispersed size distributions and non-uniform interpore spacings from channel to channel. Recently, PAAs have been prepared with well ordered channels on large areas by applying pre-patterning or “hard anodisation” conditions. Such control makes PAAs ideal one-dimensional host materials for separations, as catalysis supports and as templates for growing one-dimensional nanostructures. In this section we present a general description of the anodisation processes and formation mechanisms under various anodisation conditions. Fundamentally the self-organisation process for PAAs is much different from the formation mechanism of the ordered mesoporous and block copolymer thin films.

ACCEPTED MANUSCRIPT

ACCEPTED MANUSCRIPT

O'Sullivan and Wood proposed a model describing the self-regulating pore growth of PAAs in 1970 [58]. The authors suggested that pore formation was driven by the difference in the electric field distribution at the tips of the pores. This suggestion was followed by a more detailed model by Masuda *et al.* [59], and later by Jessensky *et al.* [60], who elucidated the self-organisation process for the formation of hexagonally ordered anodic alumina channels. Briefly, oxide channels form orthogonal to the Al surface, due to the equilibrium between the field enhanced oxide dissolution at the oxide/electrode interface and oxide growth at the metal/oxide interface (figure 4(a)). Expansion of the material can only occur in the vertical direction because oxidation takes place at the bottom of a pore; hence the existing channel walls are pushed upwards. The authors also suggested that self-organised pore formation is caused by the mechanical stress associated with the volume expansion during oxide formation at the metal/oxide interface. The channels extend downwards to a non-porous alumina barrier layer formed between the channel bottom and the underlying non-anodised aluminium foil. The barrier layer has a hemi-spherical and scalloped geometry, and normally its thickness is approximately half that of the pore wall. The dimensions of the channels and interpore distances can be easily controlled by choosing appropriate electrolytes and anodisation voltages. Under conventional "mild anodisation" conditions the self ordering phenomenon occurs only in narrow process windows, known as "self ordering regimes". Thus, the accessible channel diameters and interpore distances are limited by the self ordering requirements.

Anodisation of aluminium layers deposited by sputtering or metal evaporation onto Si wafers or metal coated substrates has opened up new possibilities for the integration of the PAAs channels in practical device architectures. A considerable impediment in contacting such layers is the presence of a thick non-porous barrier layer at the base and the need for in-situ methods for selective removal of this barrier layer. Reverse biasing and selective chemical etching are among the most commonly used approaches for reliable and controlled barrier layer perforation. In our group we have developed anodisation procedures for manufacturing PAAs layers with channel openings as small as 10 nm which showed semi-hexagonal ordering and almost full perforation of the barrier layer (see Figures 4(b) & (c)).

ACCEPTED MANUSCRIPT

ACCEPTED MANUSCRIPT

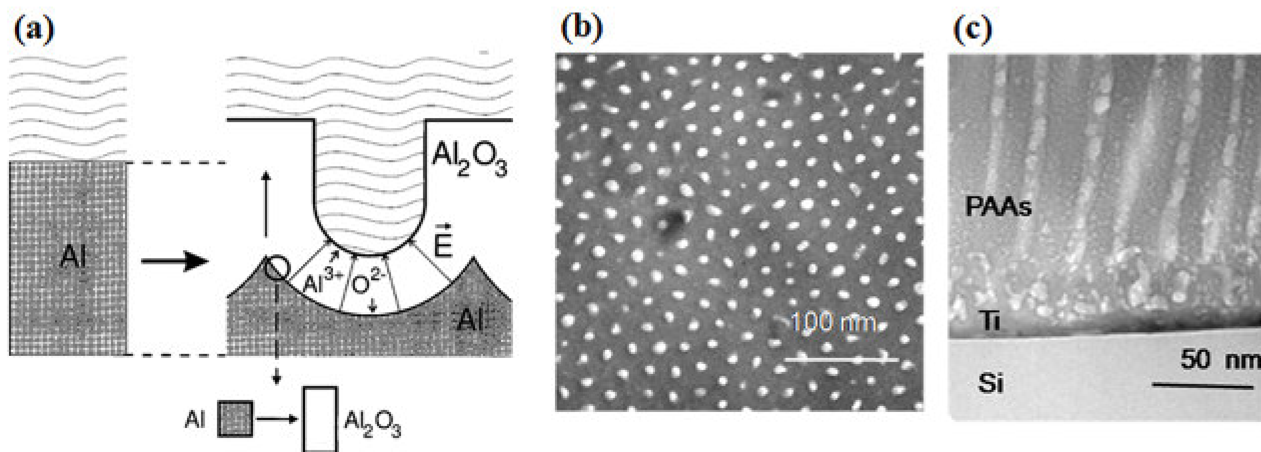

FIGURE 4: PAA films (a) Schematic of the self-organised formation of hexagonal pore structures in anodic alumina (reproduced with permission from reference [60]) where pores grow perpendicular to the surface due to the equilibrium between field enhanced oxide dissolution at the oxide/electrode interface and oxide growth at the metal/oxide interface (b) top down and (c) cross-sectional TEM images of PAAs prepared from 200 nm Al coated Si substrates by sulphuric acid anodisation of thin aluminium layers at 20 V (unpublished work). Pore diameters and pore-to-pore distances are 10-15 nm and 20-30 respectively.

Recently, there has been renewed interest in the so-called "hard anodisation" process which was invented in the early 1960's and largely used in the coating and membrane industry by taking advantage of high speed oxide growth. However until very recently it was not possible to control important structural parameters during hard anodisation. Lately, the Gosele group, and others have established new self-ordering regimes dependent on high current densities at the bottoms of the pores, which offer substantial advantages over conventional "mild anodisation" conditions, in terms of processing time and improved ordering of the channels over much larger areas [61-63]. Unfortunately the accessible channel dimensions formed in the PAAs are much bigger than those obtained under "mild anodisation" conditions. Very recently constant current and pulse anodisation process conditions have shown improved ordering of the channel system and a possibility for modulating the channel opening [64-65].

Finally it should be outlined that in contrast to MTFs and BCPs where supra-molecular interaction are responsible for the self-organisation process, the main driving force for self-organisation of PAAs is

ACCEPTED MANUSCRIPT

ACCEPTED MANUSCRIPT

the balance of the repulsive forces acting between the neighbouring channels growing from the metal oxide interface, which is controlled by the anodisation conditions and the electrolyte used. As such the size of the pore opening is governed by the equilibrium of the oxide dissolution and formation at the applied electric field for any given electrolyte. Thus the smallest reported PAAs channel diameters of about 10 to 12 nm are for anodisations accomplished with low voltages, with dilute sulphuric acid and reduced temperatures (~0 °C) [66].

The main advantages of the PAAs over other templates are that they posses highly oriented channel systems with tunable pore openings over a very wide range of diameters, *e.g.* 10 to 500 nm, by using different electrolytes or pore widening procedures. The PAAs are inferior when sub-10 nm pore openings are targeted, with nm or sub nm pore control, whereas MTFs and BCPs can be tuned. Generally all three systems under conventional preparation methods lack long range ordering and registration on the length scales that are needed for true device fabrication. Thus methods for directing the self-assembly and organisation processes are required.

SECTION 2.0. DIRECTED SELF-ASSEMBLY: ORIENTATION & PLACEMENT

Self-assembled nano-systems for the most part, have limited long range order because of the presence of defects and consequently, an external guiding force must be used to provide precision placement and registration to improve translational ordering. Although DSA is not a strict necessity for fundamental device performance, we feel it is necessary to highlight the relevance of such work as properties such as uni-directional alignment, translational ordering, registration and placement are important considerations for functioning devices. The following section provides a brief account of significant methods for improving the aforementioned DSA prerequisites for templated mesoporous silica, block copolymer and porous anodic aluminas.

2.1. Templated mesoporous films

ACCEPTED MANUSCRIPT

ACCEPTED MANUSCRIPT

Order within mesoporous silica films is mostly confined to local regions known as domains, as defects such as grain boundaries interfere with maintaining the long range (global) order. Maintaining in-plane translational ordering on a macro (> 1 micron) level requires external guiding forces to induce long range ordering/directionality of the mesopores. Furthermore, fabrication of uni-directional channels, either perpendicular or parallel to a substrate, would also be extremely advantageous for applications such as host-guest chemistry [67], nano-fluidics [68] and molecular separations [69]. In this section, we focus on techniques which are more CMOS compatible. Fan *et al.* [70] provide an excellent and detailed review on aligning mesoporous materials using electric, magnetic and mechanical methods.

2.1.1. Magnetic fields

Early reports on aligning mesoporous materials in the presence of magnetic fields were performed on powder systems. Firouzi *et al.* demonstrated that it was possible to improve the translational ordering for condensed hexagonal mesoporous silica (MCM-41) powders when heated above its anisotropic-to-isotropic phase transition temperature and allowed to cool in the presence of a 11.7 Tesla magnetic field [71]. Tolbert *et al.* extended this method for CTAB-templated silicates by using acid and base treatments to crosslink the silica matrix whilst retaining the periodic structure and macroscale alignment [72]. The mesochannels were found to orient parallel to the magnetic field direction. Lately, dip-coating in conjunction with a 12 Tesla magnetic field positioned parallel to a substrate has resulted in mesoporous silica films with uniaxially oriented mesochannels [73-74]. The authors highlighted the importance of the template molecules in achieving uni-directional mesochannels of 2 D-hexagonal nanostructures. Films templated with CTAB displayed minor improvements in the unidirectional alignment whilst those templated with P123 polymers showed a considerable improvement owing to the greater molecular weight of the Pluronic copolymer.

ACCEPTED MANUSCRIPT

2.2.2. Chemical epitaxy

One of the most successful techniques to date for aligning mesochannels on a global scale (centimetre) has originated from a technique known as 'rubbing', pioneered by researchers at Cannon and Waseda University, and initially demonstrated for mesoporous particles in 1999 and for films in 2000 [5, 75-80]. The technique entails using a 10 nm thin polyimide coating to induce preferred unidirectional alignment and orientation of the mesochannels in the overlaying film. The direction of the polyimide chains is governed by rubbing the polyimide film with a nylon-covered cylindrical roller (buffing wheel). The chains become oriented in the rubbing direction. The hexamethylene group essentially acts as a nucleation site and aligns the initial surfactant molecules orthogonal to the original rubbing direction. The silicon dioxide precursors surround this hemi-micelle structure and this initial aligned hemisphere acts to guide the next layers. The authors claim that the preferred orientation of the channels is driven by the interaction of hydrophobic hexamethylene groups and the head group of the surfactant molecules. Consequently this epitaxy is transferred to the additional mesoporous layers within the film and results in an extremely well-aligned film.

In 2005, the authors extended this rubbing technique in order to fabricate films with a three-dimensional hexagonal cage-like porous structure (space group $P6_3/mmc$), that also encompassed centimetre scale alignment of the channels, enabling the formation of single-crystalline films [5]. Figure 5(a) displays in-plane TEM images of the Brij 56-templated 3 D-hexagonal porous structure with the spherical micelles, stacked in the [001] direction when viewed orthogonal to the rubbing direction. Figure 5(b) is an image of the pores when viewed orthogonal to the rubbing direction. As TEM is a localised tool, the authors used x-ray analysis to ascertain the alignment of the structure on a global scale. The films initially formed a metastable phase consisting of aligned tube-like micelles (2 D hexagonal) perpendicular to the rubbing direction, which transform into spherical shaped micelles and essentially acted as a scaffold for the preceding layers to grow and ultimately progress into a mesostructured silica film with a 3 D-hexagonal structure.

ACCEPTED MANUSCRIPT

ACCEPTED MANUSCRIPT

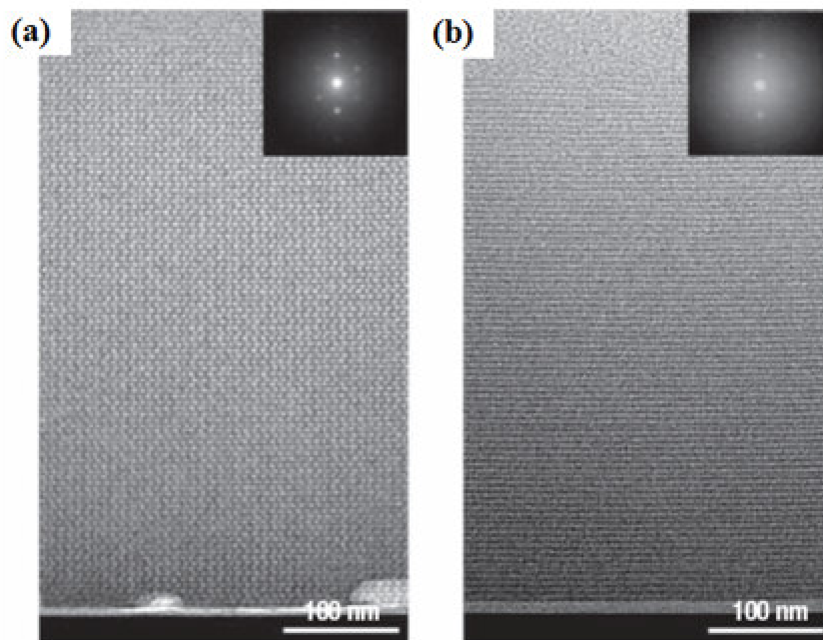

FIGURE 5: Chemical epitaxy; cross sectional TEM images of the as-grown film with a single-crystalline porous structure where (a) represents the film viewed along the rubbing direction and (b) perpendicular to the rubbing direction (reproduced with permission from reference [75]) templated with the surfactant Brij 56. The mean pore diameter is approximately 4 nm with a pore wall of 4 nm. The correlation length of the porous architecture is maintained across the substrate, over distances on the cm length scale.

One example of the importance of introducing global alignment of nano-channels was documented by Martini *et al.* [23] By confining a semiconductor polymer in a well-aligned 2 D hexagonal mesoporous film (using the rubbing technique) the polymer chains became aligned and exhibited polarised, low-threshold amplified spontaneous emission. In addition, the confined chains behaved as natural waveguides that could be utilised for optical gain requirements.

2.2.3. Physical epitaxy

Physical epitaxy (graphoepitaxy) has become a successful approach for tailoring the macroscopic alignment of colloidal spheres and recently, block copolymer films. As a result of the precision placement and registration imposed, devices such as field-effect transistors (FETs) and magnetic media have benefited [81-82]. Briefly, a physical pattern in a substrate imparts registration and alignment on a

ACCEPTED MANUSCRIPT

ACCEPTED MANUSCRIPT

self-assembled poly-domain system, and ultimately corrects defects, resulting in a film with a single domain. We have previously shown for a 2 D hexagonal mesoporous silica system, templated from the F127 triblock copolymer, that it is possible to achieve well structured films within patterned silicon and silicon nitride substrates using a dip-coating technique [83]. The mesochannels with a *P6mm* structure registered with the side wall of the topographic templates resulting in well-ordered domains; different pore orientations were found to be present across the patterned regions as confirmed by x-ray analysis and electron microscopy.

Wu *et. al* have also shown the benefits of using physical epitaxy methods for improving the translational ordering of mesoporous silicates, with a *P6mm* structure, using polymeric resist patterns [84]. The authors highlighted the need for confinement of the channels to lateral dimensions of 500 nm to minimise the growth of poly-domains originating from the presence of more than one surface (2 sidewalls must be accounted for). Under extreme confinement, the orientation of the system was perturbed with a partial re-orientation of the cylinders orthogonal (with the (10) plane perpendicular to the substrate) to the trench base of the channels. It should be noted that the resist patterns were used for topography. Consequently, the resist could also be removed to fabricate isolated arrays of channels by removing the over layer with a reactive ion etch (RIE) process and subsequently removing the polymeric resist with an ashing step. Su and co-workers have also shown that SBA-15 type mesoporous silica films can show preferred orientation when deposited on laser patterned polyimide mirco-grooves [85].

Thus far, the techniques used to evaluate the alignment of ordered mesoporous silica films have been limited to localised electron microscopy techniques or global macroscale x-ray analysis. Building on the previous alignment studies [83-84], we investigated the directionality, defect densities and correlation lengths of the mesopores aligned by physical epitaxy methods; using high resolution serial focused ion beam (FIB)-milling/SEM sectioning to characterise the c-axis of mesopores deposited within the channels of patterned substrates [15]. The mesochannels arranged in a single domain, following the sidewalls of the channels provided the aspect ratio of the channel remained close to a 1:1 configuration when combined with a controlled dip-coating process.

ACCEPTED MANUSCRIPT

ACCEPTED MANUSCRIPT

Furthermore, precision tuning of the over layer on the mesa can be accomplished to essentially collapse the mesostructure as a result of high stress (during calcination), thereby making it redundant. Pore correlation lengths beyond several microns were observed but significant delamination owing to the calcination step hampered precise 3 D reconstruction of the pore network. Figure 6 highlights some of the microscopy research carried out by our group. TEM and FIB sectioning revealed that the hexagonal porous channels registered and aligned themselves with the trench sidewalls, with correlation lengths extending well beyond the micrometre threshold. This was possible due to the careful selection of the right trench dimensions, coating mixture and deposition technique.

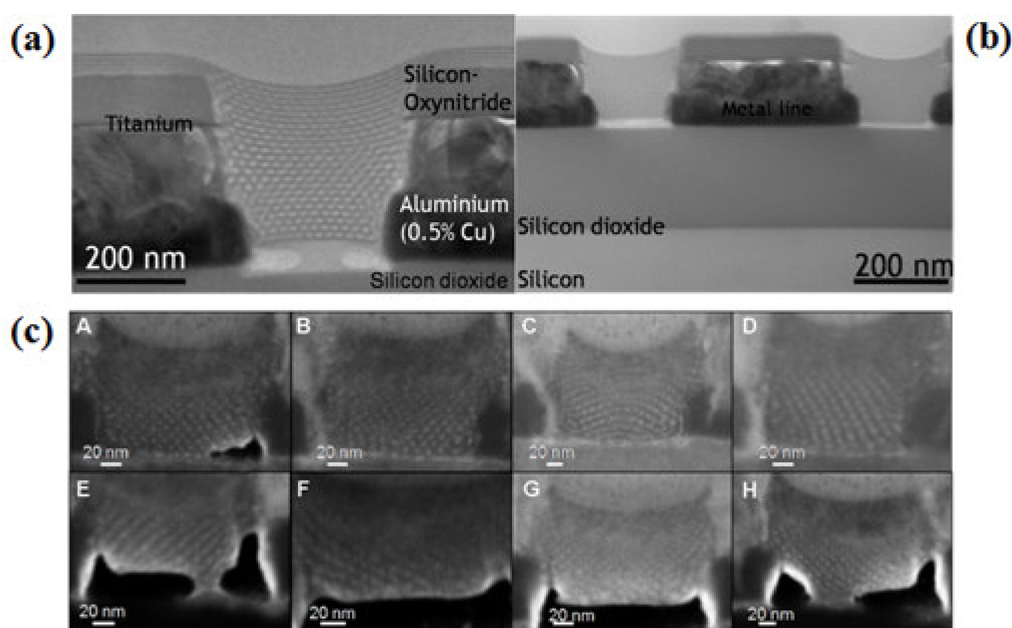

FIGURE 6: FIB sectioning & Physical epitaxy of aligned mesoporous silica channels (a) and (b) cross sectional TEM micrographs of mesoporous silica confined with a patterned metal/oxide stack with an aspect ratio of 3:2. (c) SEM micrographs of the 'front-on' sections taken through the mesoporous silica thin film within the channels, each showing the pore ordering of the eight separate channels (A-H) (reproduced with permission from reference [15]). The hexagonal pore structure is maintained but delamination of the mesoporous segments is evident; due to the annealing step required to remove the organic template and cross-link the silica network.

ACCEPTED MANUSCRIPT

2.2.4. Vertical orientation

Orientating the channels of ordered mesoporous silica films orthogonal to a substrate surface has also received significant attention in the last decade. Regrettably, the 2 D hexagonal channels in the mesoporous films have the tendency to arrange with their c-axis parallel to the substrate surface, limiting their applications; most notably as accessible arrays of nanowires. Freer and co-workers were the first to show that mesoporous channels could be oriented with their c-axis perpendicular to a silicon substrate by using a mixture of polystyrene-*block*-polyethylene oxide and poly-methyl-silsesquioxane (PMSQ) in a saturated solvent environment [86]. Figure 7(a), displays a cross sectional TEM image of the perpendicular orientation of cylindrical pores after solvent annealing for 48 hour in a chloroform and octane vapour at 20 °C. Another viable approach to vertical arrays involves using electrochemical methods to apply a bias to an electrode in the presence of the silica oligomers and CTAB surfactants, thereby generating hydroxyl ions which promote poly-condensation of the precursors and initiate self-assembly of hexagonally packed one-dimensional channels [87]. Figure 7(b) displays a cross section TEM image of an 80 nm film which has been assembled with a vertical morphology by electrochemical techniques on a gold substrate, although other substrates such as Pt, C, ITO and Cu are also possible. Richman and colleagues have used nanoscale epitaxy to promote vertical morphologies in F127 films by carefully selecting a cubic titania structure as the epitaxial under layer [88]. The surface of the templated cubic (111) titania films have a hexagonal arrangement of pores on their outermost surface (figure 7(c)) which can be used to provide vertical alignment for a 2D hexagonal F127 templated mesoporous silica. Two criteria were identified for establishing vertical films; the pore of the cubic film should be commensurate with the pore of the F127 2D-hexagonal film and the rate of self-assembly be sufficient slow (controlled by dip-coating) to help promote this vertical alignment.

Recently we and others have shown that mesoporous silica channels can be successfully aligned using highly oriented nature of the PAAs membranes [89] shown in figure 8. Samples with a columnar hexagonal 2D structure along the vertical channels of the AAM can be produced with ionic CTAB as template. However, when non-ionic surfactants (Pluronic P123 and Brij 56) are used, samples with a

ACCEPTED MANUSCRIPT

ACCEPTED MANUSCRIPT

circular hexagonal 2D structure perpendicular to the channels or phase mixtures of circular and columnar orientations are obtained. The behaviour of ionic CTAB can be mimicked by adding inorganic salt to the non-ionic template precursor solution, thus leading to a phase transformation toward columnar orientation. The distribution between the orientations was determined by means of small-angle X-ray scattering (SAXS) experiments.

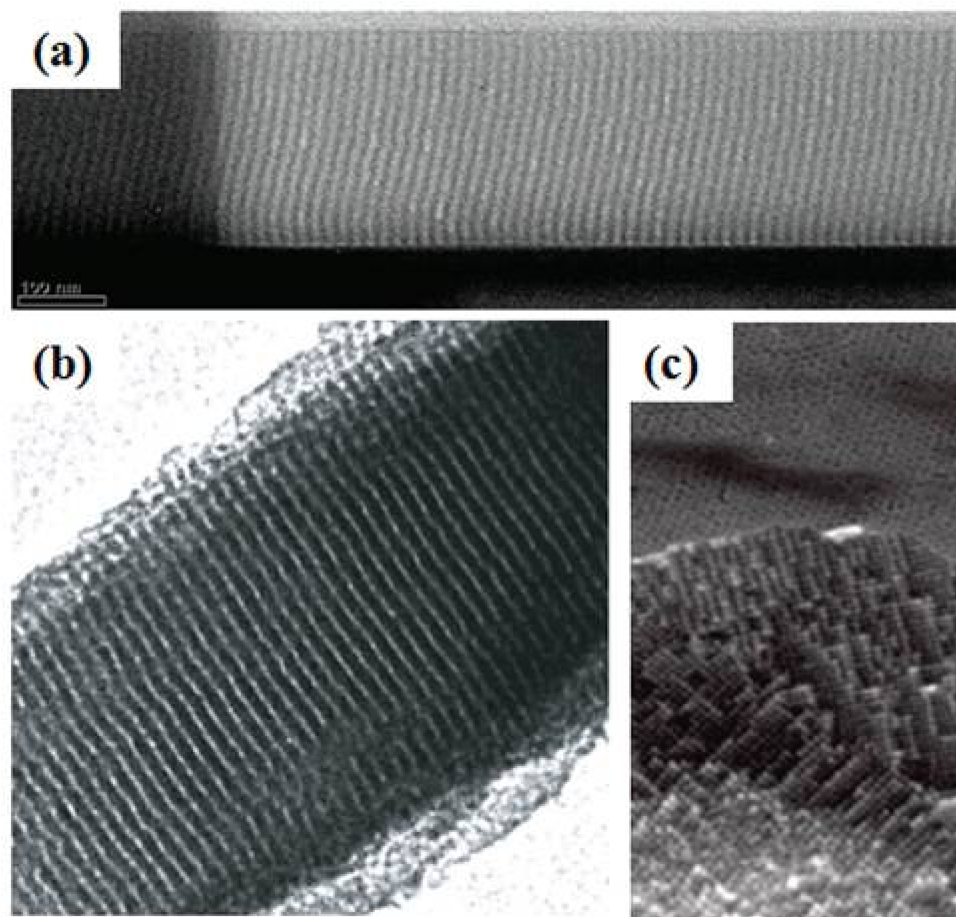

FIGURE 7: Vertical channel formation using various techniques: (a) *Solvent annealing*; TEM cross-sectional micrograph of the porous SSQ film shown with pores oriented vertically to the substrate surface templated by a PS-*b*-PEO diblock coploymer grown on a Au substrate (reproduced with permission from reference [86]) (b) *Cathodic Electrodepositon*; TEM cross section image of the electrodeposited surfactant-templated mesoporous silica films on a gold substrate (scale bar 20 nm) (reproduced with permission from reference [87]), (c) *Epitaxial Growth*; SEM image of a cut in a (111)-oriented cubic mesoporous titania film used as seed layer for oriented 2D mesoporous channels orthogonal to the substrate (reproduced with permission from reference [88]). The pores on the top surface of the titania seed layer are commensurate with the vertical pores in the P123 surfactant film, having similar periodicities and enabling effective epitaxial growth.

ACCEPTED MANUSCRIPT

ACCEPTED MANUSCRIPT

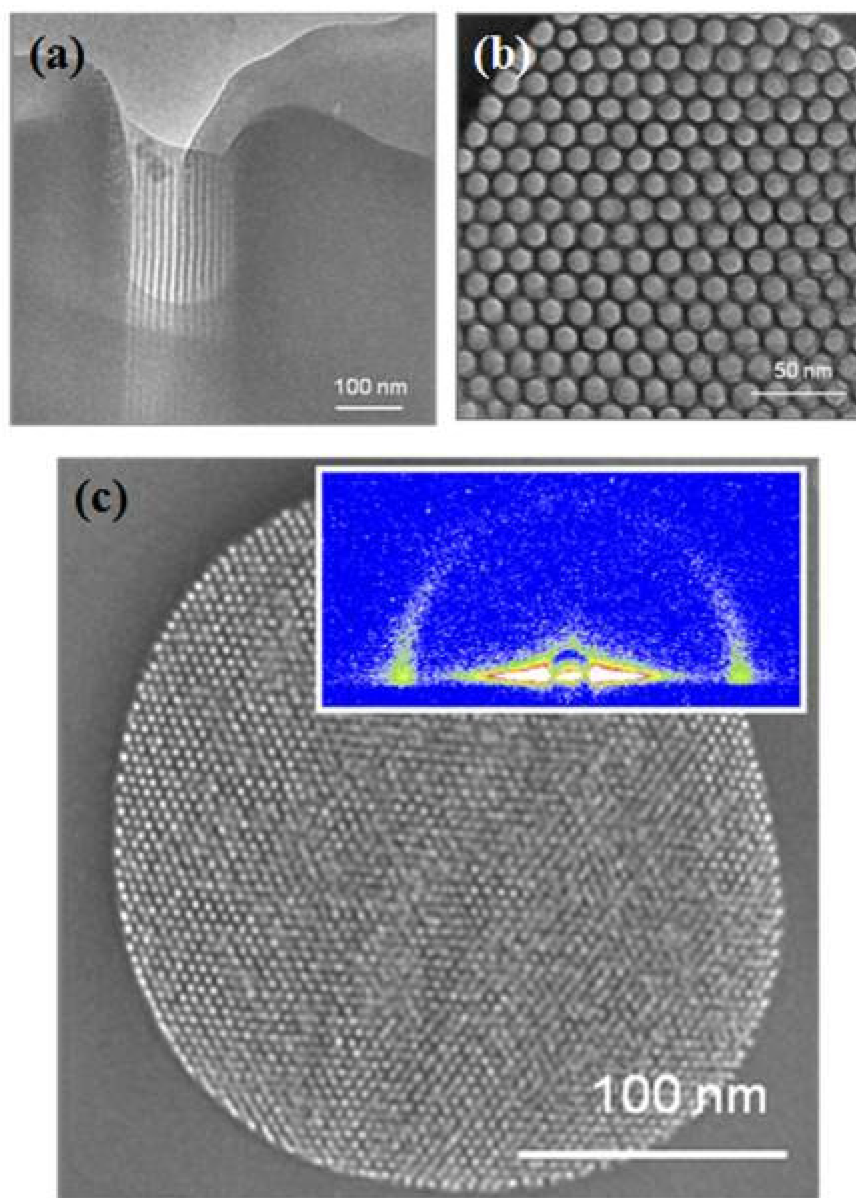

FIGURE 8: Mesoporous silica deposited within vertical channels of PAA membranes (a) Cross-sectional TEM image of P123 templated material with columnar orientation of the pores, (b) top down TEM image of the same specimen showing the perfect hexagonal order of the channels, (c) top down TEM image of CTAB-templated mesoporous silica with columnar orientation of the channels and 2 nm pore diameters, (inset) corresponding 2D SAXS pattern (reproduced with permission from [89]).

ACCEPTED MANUSCRIPT

2.2. Block copolymer thin films

Aligning microdomains within block copolymers is perhaps one of the most active areas in combined macromolecule and nano-lithography research. Block copolymer lithography alone cannot fulfil the requirements for future lithographic patterning as it lacks long-range order. Consequently, it is envisioned that block copolymers will require a top down pattern to guide the nanostructure, ultimately a compromise between top down and bottom up methods.

Techniques for aligning block copolymer include solvent evaporation fields [46], physical epitaxy/graphoepitaxy [90], chemical epitaxy [4], optical (holographic) radiation [91], droplet pinning [92], shear forces [93], nanoimprint lithography [94], e-beam lithography [95], zone annealing [96] and casting [97]. We concentrate in this section on graphoepitaxy (including nanoimprint lithography) and chemical pre-patterning as these techniques represent the most practical methods for device integration.

2.2.1. Graphoepitaxy

Graphoepitaxy is the most widely used method for aligning block copolymers for nanoelectronic applications [36, 50, 81, 98-105]. This ‘multiscale lithographic’ technique relies on using a ‘top-down’ lithographically defined template which imposes self-alignment (registration) and improves translational order on the ‘bottom-up’ self assembled polymer system; subdividing the feature size (resolution enhancement technique) of the overall process (figure 9). Many reviews have been written on the graphoepitaxy of block copolymers [26-33, 106], so we have focused below on the major milestones since Segalman *et al.* [90] first demonstrated this approach as a viable method in 2001.

Segalman’s seminal work demonstrated that it was possible to achieve well ordered block copolymer systems with long range order greater than the intrinsic poly-domain length, *i.e.* > 400 nm [90]. The authors focused on aligning polyvinyl-pyridine (PVP) spheres in a polystyrene (PS) matrix with a natural periodicity (L_0) of 27 nm, deposited within channels and mesas ranging from 1 to 10 microns (depths of 3 to 300 nm). The authors noted that the dimensions of the substrate were crucial in achieving well-ordered systems, and that BCPs deposited in trenches with widths > 5 µm tended to lose

ACCEPTED MANUSCRIPT

ACCEPTED MANUSCRIPT

order and registration. Above 5 µm, spheres located closer to the sidewall registered with the sidewall but spheres within the centre of the trench displayed poor registration to the nearest sidewall.

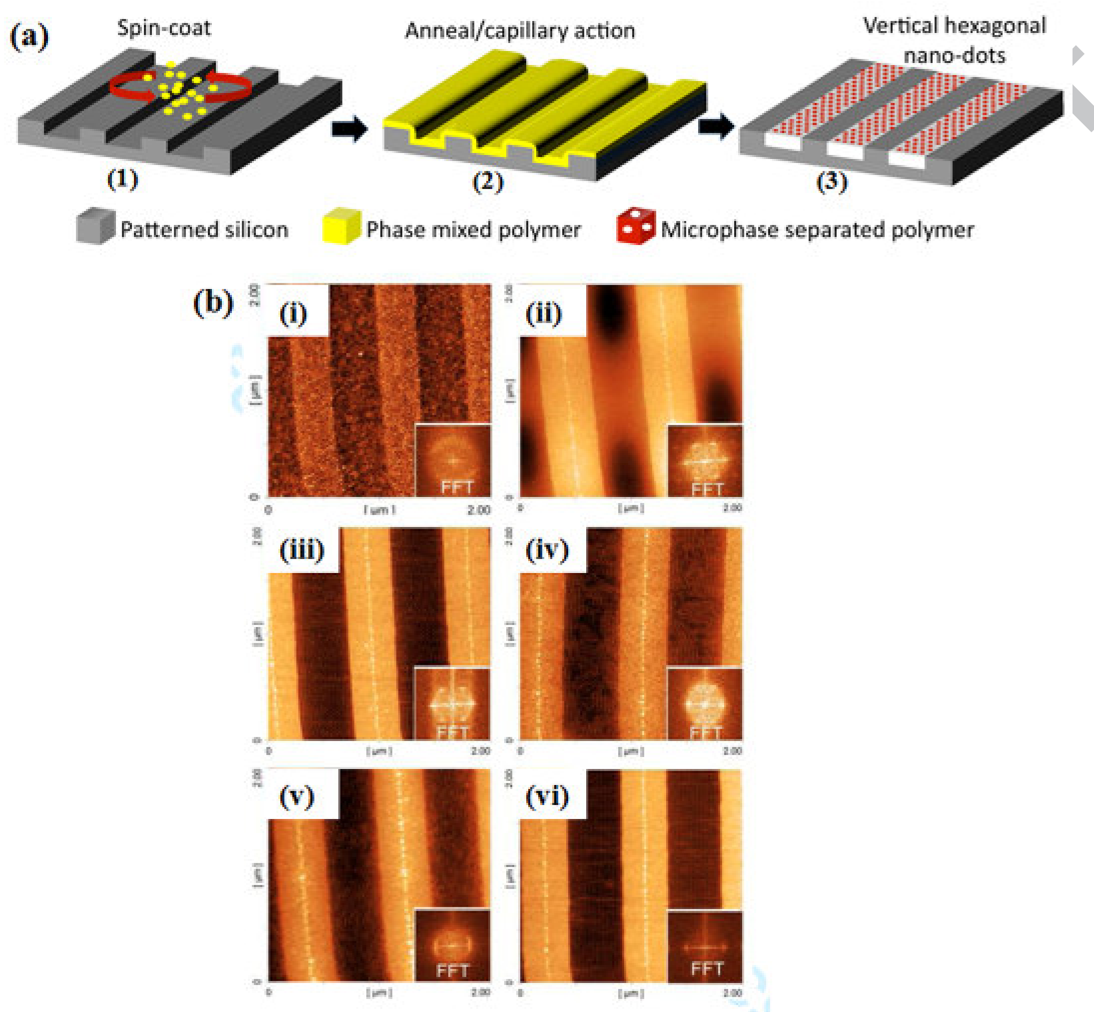

FIGURE 9: (a) Graphoepitaxy schematic for perpendicular hexagonal (1) deposition of BCP on patterned topography (2) thermal or solvent annealing induces microphase separation whilst capillary action pulls the polymer in the trenches and (3) registration and alignment of the nanopattern to the fabricated micron-sized channels. (b) Time resolved study of polymer flow and cylinder orientation for parallel hexagonal 2D Tapping mode AFM phase images of triblock PS-*b*-PI-*b*-PS thin films prepared from 0.7 wt% solutions of block copolymer in toluene on topographically patterned substrates (430 nm channel) (i) prior to thermal annealing and upon annealing at 120 °C for (ii) 1 h, (iii) 1.5 h, (iv) 2.5 h, (v) 4 h and (vi) 6 h. Insets are the corresponding FFT image (reproduced with permission from reference [107]). After 3 hr the nanopattern displays well aligned cylinders within the PS matrix.

ACCEPTED MANUSCRIPT

Cheng and co-workers later revealed using a sphere-forming polystyrene-*block*-polyferrocenyldimethysilane (PS-*b*-PFS) block copolymer, with a periodicity of 28 nm, that extreme channel confinement (1 to 12 rows/~60 to 300 nm trench width) is required to precisely position PFS spheres in a PS matrix, whilst maintaining perfect hexagonal close packing arrangements [103, 108-109]. Prior to this report, the authors had also highlighted that a polymers' row spacing will conform to fit the trench (term known as commensurability) by either expanding or contracting. Modelling of the polymeric systems by free energy models tied in well with the experimental data. Channels beyond 12/13 rows of spheres were found to have significant amounts of defects within the hexagonal lattice and overall resulted in a breakdown of the long range order of the block copolymer nanopattern.

Subsequently, Sundrani *et al.* reported the alignment of PS-*b*-PEP (modified from PS-*b*-PI) with 27 wt% PS, where hexagonally packed cylinders oriented parallel to the channel base. Precision control of the trench width and accurate polymer deposition resulted in alignment of PS-*b*-PEP cylindrical domains, either in-channel only (single layers) or by propagation onto the mesa from the channel (multi-layers) with a significant reduction of defects [101-102]. Our group has also shown that the tri-block copolymer PS-*b*-PI-*b*-PS, where the PS cylinders are oriented in a 2 D hexagonal arrangement within a PI matrix, adopts highly regular and periodic linear arrays with excellent registration to the topographic channels [107, 110]. Precision control of the polymer thickness within the topographic pattern (200 – 500 nm wide) allowed us to control the orientation (arrays of lines versus arrays of vertical cylinders) of the final nanostructures. Figure 9(b) highlights some of our work on time-resolved studies of the PS cylinders re-orientating in a PI matrix when confined in 500 nm channels and thermally annealed for 6 hour at 120 °C. Film thickness, polymer flow and solvent evaporation have profound affects on the evolution of the nanostructured polymer film over a 6 hour period, with cylinders finally orientating parallel to the substrate. Unfortunately, although the polymer system can be stained using ruthenium or osmium to provide etch contrast [25, 111], owing to the lack of oxygen in either backbone, reactive ion etching of either block to yield a suitable etch mask was not possible.

ACCEPTED MANUSCRIPT

Workers at IBM have focused on developing strategies for aligning primarily PS-*b*-PMMA block copolymers by graphoepitaxy [26, 104, 112]. The authors have shown that process parameters such as polymer film thickness across the trench, confinement/commensurability of the nanostructure within the trench, annealing time/temperature all play a pivotal role in the outcome of the final orientation, defect density and registration of the final nanostructures. Figure 10(a) displays SEM micrographs of linear arrays of nanostructures for an asymmetric PS-*b*-PMMA system with 5 aligned polystyrene strips, post PMMA removal, in a ~ 220 nm SiO_x trench and (b) a porous polystyrene matrix six rows wide, post PMMA removal, in a ~ 260 nm trench coated in a neutral PS-*r*-PMMA polymer. Aligning symmetric PS-*b*-PMMA (lamellae) has proven much more difficult when substrate topography is introduced as the PMMA components tend to wet the SiO_x mesa sidewall and trench base interfaces. To this end, researchers have devised elaborate schemes for balancing the interfacial energies by using gold strips evaporated onto PS-*r*-PMMA brush layers [99] or the actual resist pattern for mesa structures [113]; using the alignment properties of a commensurate asymmetric PS-*b*-PMMA system to create a chemical pre-pattern for directing the lamellae structure [112] or evaporating amorphous silicon onto a PS-*r*-PMMA combined with tapered trench designs for local defect density minimisation [114]. Figure 10(b) shows a schematic top down and cross sectional lay-out of the tapered substrate approach used to limit defect formation within the channel. By precisely tuning the interfacial interactions between the sidewall and base of the trench, ensuring commensurability is ideal, and providing a substrate which facilitates polymer shear flow can produce aligned defect-free lamellar striped nanopatterns.

The complexity of achieving alignment in PS-*b*-PMMA systems, along with their limited etch contrast and an ultimate resolution limit of ~14 nm [81], has brought about a surge in research on other polymer systems for directed self-assembly. Other polymer systems have availed of topographic alignment techniques including PS-*b*-PVP [115-117], PS-*b*-PDMS [50, 82, 118], PMeS-*b*-P4OHS [37], PS-*b*-PEO [38, 46] to improve translational ordering. Moreover, these polymers were investigated as they can provide improved etch contrast, or have feature sizes below 10 nm, without the need for extensive substrate design and interface engineering. Figure 11 highlights some of our work on the

ACCEPTED MANUSCRIPT

ACCEPTED MANUSCRIPT

DSA of vertical arrays of PS-*b*-PEO block copolymers confined within topographic templates. Well aligned defect-free nanostructures with rows of 13 PEO cylinders in a PS matrix (where the PEO block has been removed) were fabricated using a solvent swelling technique. In addition, Sundstrom [119] *et al.* have created hybrid PS-*b*-PEO- silsesquioxane (SSQ) hybrid films with half-pitch dimensions of 20 nm using solvent swelling methods by sequestering SSQ molecules into the PEO block of the PS-*b*-PEO film during solvent swelling. Subsequently, Cheng [120] *et al.* were able to direct the self-assembly of the hybrid structures using graphoepitaxy techniques [49].

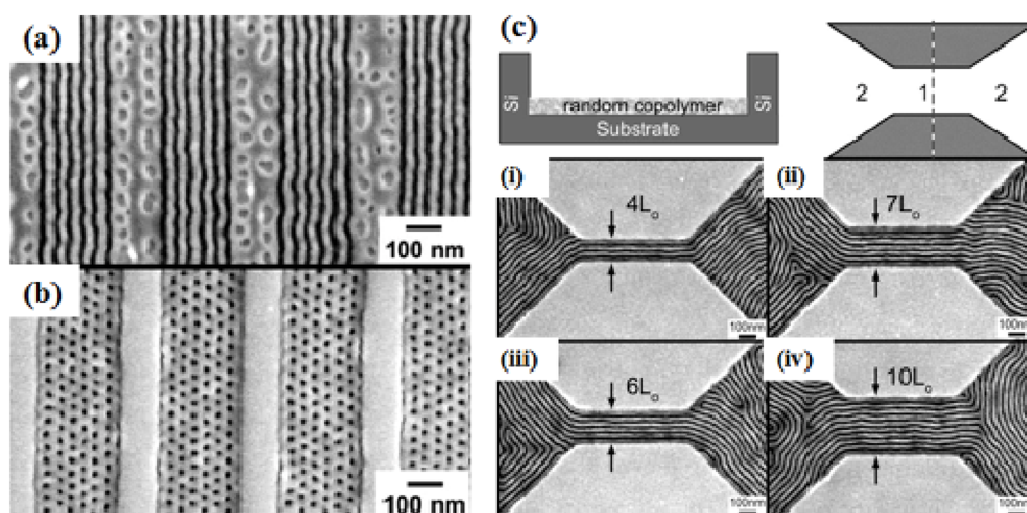

FIGURE 10: Aligned asymmetric PS-*b*-PMMA films with (a) controlled orientation: 5 aligned polystyrene strips (post PMMA removal) in a ~ 220 nm wide SiO_x trench and (b) a porous polystyrene matrix six rows wide (post PMMA removal) in a ~ 260 nm trench coated on a PS-*r*-PMMA polymer. By introducing different wetting layers on the base and side walls of the channels, using random copolymer brushes, orientational control is achieved. Defect density control for symmetric PS-*b*-PMMA films (c) using a series of tapered trenches with varying trench widths (i) to (iv) $4L_o$ to $10L_o$ (L_o – equilibrium distance), where defects are observed outside channels in the tapered zones (reproduced with permission from reference [104, 114]). By ensuring that the channel width is an integer number of the natural polymer periodicity, and creating tapered regions in close proximity, defects within the narrow regions can be minimised to ensure excellent alignment of the nanopattern.

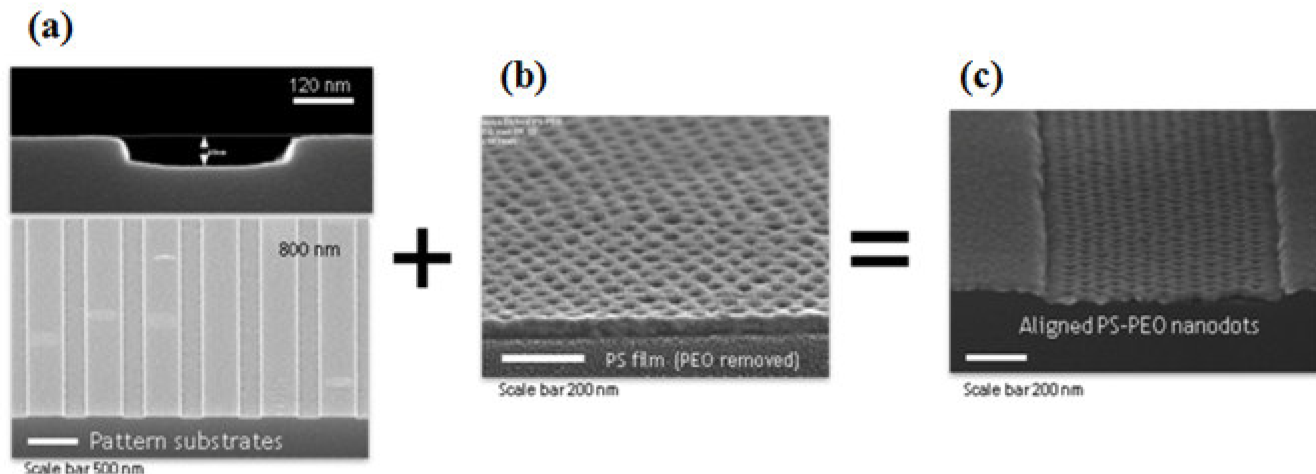

FIGURE 11: Aligned asymmetric PS-*b*-PEO films (a) cross sectional and 70° tilt SEM images of topographic patterns (b) 70° tilt SEM image of PS-*b*-PEO films (PEO removed) on a planar silicon substrate (c) and 70° tilt SEM image of PS-*b*-PEO films (PEO removed) on a topographic substrate. 13 rows of PEO nanodots are observed to register with the sidewall of the channel (unpublished work). The films were annealed in a solvent vapour for 6 hr at room temperature.

Nanoimprint lithography can also be considered a graphoepitaxy technique, as a patterned substrate is used to guide a block copolymer nanostructure [94, 121]. Li *et al.* have shown that PS-*b*-PMMA can be directed into linear arrays of parallel PMMA cylinders or hexagonal packed vertically cylinders by subtle film thickness changes using nano-imprinting on a random copolymer brush [94]

Graphoepitaxy is undoubtedly a valuable and effective resolution enhancement technique for creating sub 10 nm nanoscale devices. Although graphoepitaxy is a viable approach to realising nanoscale devices, certain challenges must be overcome for the technique to be accepted for future 'complimentary' lithographic technologies, such as channel width and confinement [26, 99, 110, 112, 122], mesa to trench dimension [98, 122], effect of trench wall and base chemistry [112-113, 123] and importantly inhibit defect formation within both the top-down template pattern and bottom-up polymer self-assembled nanopattern [114].

ACCEPTED MANUSCRIPT

ACCEPTED MANUSCRIPT

2.2.2. Chemical pre-patterning

Orientation in thin films of diblock copolymers is determined by their interfacial energies and for the most part, one copolymer block tends to wet the substrate interface in preference to the other block. To this end, researchers have developed methods whereby substrates can be pre-patterned with different chemical functionalities (heterogeneous surfaces via reconstruction and gold [124], chemical epitaxy [4]) at precise locations and more importantly, commensurate with the natural periodicity of the block copolymer, to overcome these preferential wetting tendencies. Over the past decade, this technique has progressed from its early development to become a genuine contender for future lithographic processing [4, 125-127]. This section covers the major milestones over the last decade on aligning block copolymers (PS-*b*-PMMA) using chemical pre-patterns.

Nealey and co-workers were the first to effectively demonstrate that it was possible to direct the self-assembly of a block copolymer over large areas with precision placement and registration using symmetric PS-*b*-PMMA. Briefly, a series of patterns (pitch of 45 – 55 nm) were created in a resist layer using x-ray interference (XIL) lithography on a thin brush layer of polystyrene (~3-7 nm). The pattern was developed and the underlying polystyrene (PS) layer exposed to a short oxygen plasma to oxidise the open PS. Following a resist strip, an array with different chemical functionalities of alternating polystyrene and oxidised polystyrene was created. Deposition of a lamellae forming PS-*b*-PMMA film with a natural period of 48 nm resulted in the formation of well-aligned PS-*b*-PMMA block copolymer films with low defect densities and excellent registration to the underlying chemical pattern, where the pattern is commensurate with the chemical pre-pattern. The polystyrene wetted the polystyrene portion whilst the polymethylacrylate segments favoured the plasma damaged/oxygenated polystyrene strip. In their work, the authors showed that, provided the underlying chemical pattern differed by no more than 10 % with the periodicity of the BCP film, alignment was unaffected as demonstrated in figures 12(a) and (b). The authors extended on their initial work by establishing that block copolymer/homopolymer ternary blends could indeed be directed into non-linear (bends of 45°, 90° and 135°) device-oriented arrays on chemical pre-patterned substrates [128]. The addition of PS and PMMA homopolymer and

ACCEPTED MANUSCRIPT

more importantly the redistribution of homopolymer to certain locations (bends), allowed for the domain dimensions to diverge from those formed in the bulk. Using chemical nanopatterns with periodicities of between 50 to 70 nm, it was possible to direct the self-assembly at bends of 45°, 90° and 135° for the most part except at high angles and large grating periodicity. Wilmes *et al* [128] later confirmed that the addition of homopolymer was not a prerequisite to bending block copolymer nanopatterns. In their work, the authors fabricated the concentric patterns with electron beam lithography and were able to effectively self-assembly a PS-*b*-PMMA nanopattern over a 1000 nm diameter circle and show that the lamellar block copolymer adopts the radii of curvature equal to the equilibrium domain spacing. The authors concluded that the energetic cost of lamellae curvature was relatively small and as such it was possible to form a PS centre spot with a diameter of 24 nm. In 2007, Stoykovich *et al.* further increased the repertoire of device oriented geometries and demonstrated the capability to effectively pattern a range of required arbitrary geometries as outlined by the ITRS roadmap, including single device line geometries and arrays of lines, segments, jogs, and T-junctions [126].

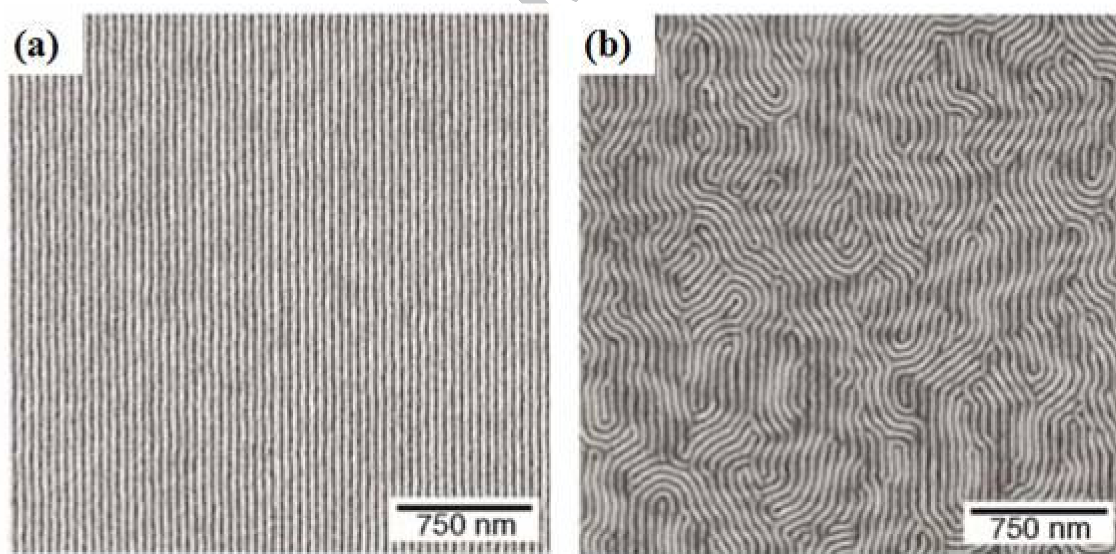

FIGURE 12: BCP aligned on chemical pre-patterns top down SEM micrographs of (a) PS-*b*-PMMA with excellent alignment on a 47.5 nm grating and (b) with herringbone (defect) formation on a 55 nm grating (reproduced with permission from reference [4]). Chemical patterns are effective for aligning block copolymers.

ACCEPTED MANUSCRIPT

Thus far, we have only considered non-resolution enhancement chemical pre-patterns, *i.e.* where a high resolution lithographic step is required, to write the features with a 1:1 scale (written top down feature is commensurate with the bottom up self-assembled line). Researchers at IBM, recently demonstrated a method for resolution enhancement by a factor of 2 by using sparse ultra thin hydrogen silsesquioxane films (~ 2 nm) by direct write resist methods [129]. All aforementioned strategies for directing the self-assembly of block copolymers have restricted themselves to lamellae PS-*b*-PMMA patterns. Researchers at the University of Wisconsin-Madison and Hitachi Global Storage have recently shown that chemical epitaxy is not restricted to symmetric lamellar structures but also has the ability to align and orient asymmetric (cylindrical) PS-*b*-PMMA on chemical pre-patterns generated by electron beam lithography on polystrene brush layers. Moreover, the authors demonstrated density multiplication on sparse chemical pre-patterns highlighting that defect-free nanopatterns were possible. This technique has merits especially when one considers that by combining this technique with electron beam lithography, one can reduce the time taken to write patterns for high throughput nanoimprint lithography (NIL) mask fabrication [130].

2.3. Porous anodic alumina thin films

The regularity of perfectly arranged hexagonal pores in PAA films and membranes is limited to areas of only a few square microns without guided anodisation. Here we focus on different methods for guiding the anodisation process to obtain necessary registration, pore regularity and ordering for PAA films and membranes. These are based on using pre-patterned aluminium substrates obtained by nano-imprint lithography, FIB patterning or BCP pattern transfer.

2.3.1. Imprint lithography

Imprint lithography uses an array of shallow concave features formed on the aluminium surface by indentation using a pre-patterned mold (stamp). The cavities obtained serve as initiation sites for the formation of channels in PAA during the initial stage of anodisation. Using appropriate anodisation

ACCEPTED MANUSCRIPT

ACCEPTED MANUSCRIPT

conditions, hexagonal long-range order can be extended to single domain over millimetre square areas, limited only to the area of the pre-textured mold. In particular, Masuda *et al.* [131-133] used a SiC stamp, prepared by electron beam lithography (EBL), to pre-pattern the surface of aluminium foils to generate PAA membranes with a hexagonal pore arrangement under mild anodisation conditions, *i.e.* 40 V using oxalic acid. However, direct writing of large area stamps by EBL is expensive and has hindered, to a large extend, the application of this approach for obtaining well ordered PAAs. Recently an inexpensive, high throughput method for preparing recyclable Ni stamps was developed by MacManus-Driscoll *et al.* [134] based on laser interference lithography (LIL) (figure 13(a) and (b)) Nevertheless both EBL and LIL are limited to producing stamps with imprinting feature sizes and densities that match the anodisation conditions for oxalic or phosphoric acids only.

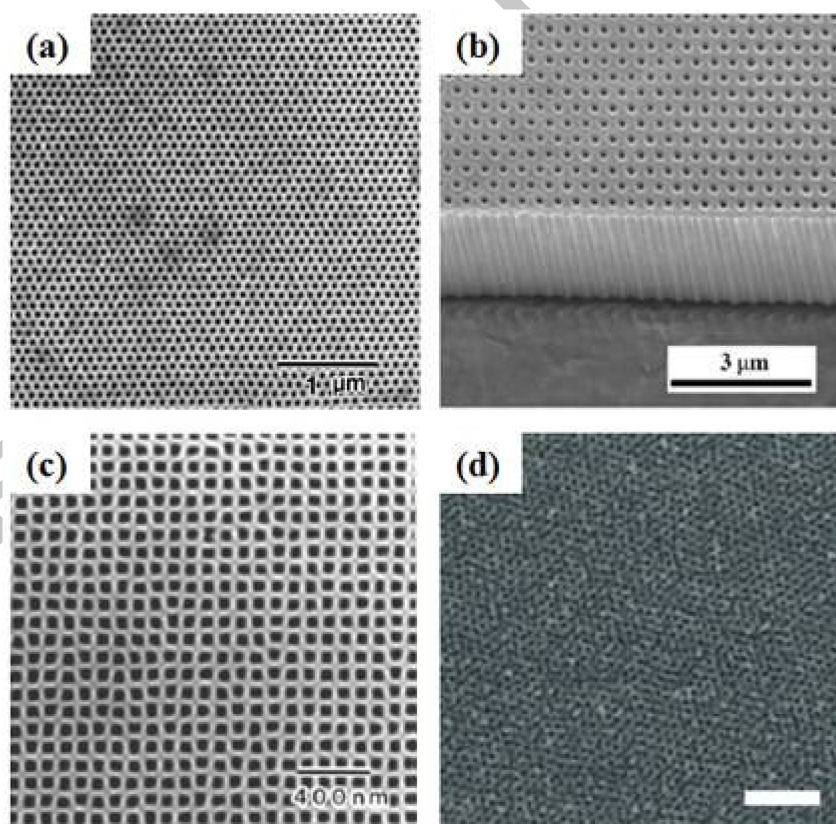

FIGURE 13: Directed self assembly of PAA films (a) and (b) shows an example of an array of about 100 nm PAAs channels perfectly organised in hexagonal arrangement after using indentations obtained by stamping with SiC and Ni imprint stamps manufactured by EBL and LIL, and (c) square arrangements of the pores was also demonstrated by using imprint

ACCEPTED MANUSCRIPT

stamps but also FIB patterning and (d) hexagonal arrangement of 30 nm PAA channels guided by concaves obtained by BCP lithography (reproduced with permission from reference[134-136]) (Scale bar = 300 nm).

2.3.2 Focused Ion Beam (FIB)

A relatively straightforward approach to create well ordered arrays of concave structures that can guide the anodisation process in aluminium membranes is based on using focus-ion beam (FIB) milling. Several reports have shown that optimised serial FIB milling procedures (Ga-ion dose, dwell time *etc*.) can produce hexagonal or square lattices of concaves on the surface of aluminium membranes which subsequently guide the anodisation process [135-136] (figure 13(c)). The automation of FIB systems, in so-called "auto-FIB" mode, and the ever increasing resolution of the Ga-ion columns, well below a threshold of 50 nm, makes this approach highly promising for the preparation of very large and dense areas of concaves. Nevertheless, the preparation of well ordered arrays of sub-20 nm concaves by FIB milling, to guide the anodisation process has still to be demonstrated. Similarly to the EBL technique, an apparent limitation of FIB milling is the time required to write very large patterned areas; as the technique is a serial rather than parallel patterning method.

2.3.2 BCPs guided anodisation

A conceptually new approach for obtaining ordered channels in PAA membranes has been to use self-assembled BCPs as lithographic masks to guide the anodisation process. Briefly, poly-styrene-*block*-4-vinlpyridine (PS-*b*-P4VP) was phase separated on an aluminium substrate, by solvent-induced reconstruction, to form a hexagonally ordered BCPs film with vertical cylindrical microdomains. Using reactive ion etching (RIE), the BCP pattern was transferred to the underlying aluminium substrate where it was used to define the initial concaves for the ensuing channel growth in the PAA membrane. Subsequently, sulphuric acid anodisation was used to obtain well ordered PAA channels with sub-20 nm openings, as shown in figure 13(d). This is a potentially valuable approach as it provides a low cost alternative to the conventional lithography methods used to create arrays of well ordered concaves over

ACCEPTED MANUSCRIPT

large areas that can direct the anodisation process. Additionally, this BCP approach provides control over the pore periodicity and centre-to-centre pore distance between the PAAs channels, simply by changing the molecular weight of the BCP used [137].

2.3.4. Parallel porous anodic alumina films

Shortly after establishing the process for the fabrication of vertical PAAs channels, Masuda *et al*., proposed that the channels of PAA films could be grown in a parallel orientation with respect to the substrate by sandwiching the aluminium between two non-conductive layers [138]. Such an approach has not received much attention in the past until it was demonstrated that a 1 D array of PAA channels could be obtained [6] (figure 14).

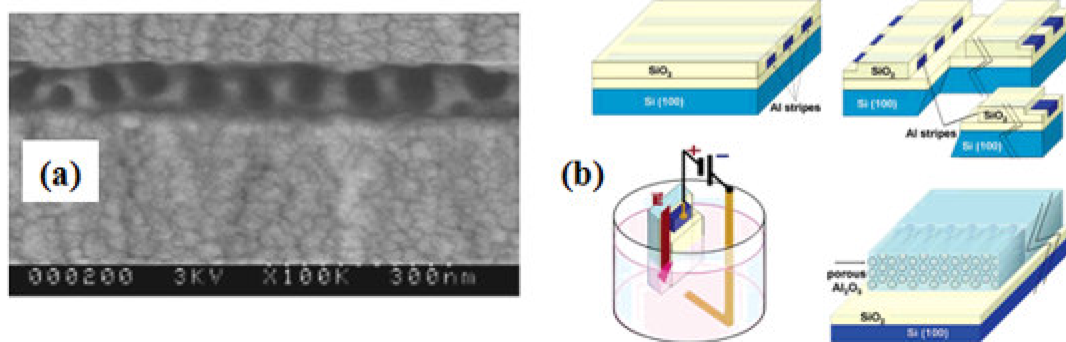

FIGURE 14: Crossbar PAA films (a) Single layer of parallel PAA channels sandwiched between thick silica layers and reproduced with permission from reference [6]). (b) schematics of array SiO_2/Al/SiO_2 structures that were used to prepare patterned parallel PAA channels (reproduced with permission from reference[139]).

Briefly, the direction of the electric field determines the direction of the nanopores; by placing the electric field in parallel with aluminum substrate, the porous structure may be form on the side of aluminum as shown in figure 14(a). By selecting the thickness of the aluminum film close to the PAAs cell size, it is possible to form a single array of nanopores. As mentioned above, at a steady state the oxide formation and dissolution is balanced, depending on the electric field at an applied fixed voltage. Theoretically there is no reason why a single cell and a single PAA channel cannot be formed in a fin of

ACCEPTED MANUSCRIPT
aluminum sandwiched by two layers of SiO_2. One may argue that it might be possible to have two half-cells formed instead of a single cell. It is shown theoretically that this case is not realistic in the steady state due to the self-adjusting effect [6].

Section 2 addressed several of the strategic advances of DSA, enabled by top-down pre-patterns, and highlighted that careful consideration must be given to achieving the desired orientation without perturbing the local nanostructure. It has become evident that future nanodevices will be constructed in a mutual and co-operative manner, whereby a 'top-down' technique will guide a 'bottom-up' nanopattern.

SECTION 3.0: NANOSCALE DEVICES ENABLED BY SELF-ASSEMBLED TEMPLATES

After designing the templates for generating one-dimensional nanostructures with the desired orientation, registration, feature size and density, the next step is to develop suitable methods for the preparation of the nanostructures themselves. As we will show in this part of the review, the production of self-assembled templates and the methods for manufacturing nanoscale structures should always be considered as one process, guided by the aim of achieving a desired functional device. With this in mind, the final section of this review focuses on devices created within or by self-assembled templates. Rather than focusing on individual templates, we have approached this section from a growth technique perspective; **additive growth** whereby a template is back filled or **subtractive fabrication** whereby a template pattern is transferred to another functional layer. As we shall see, additive growth is associated more with PAA and MTF templates, whilst subtractive fabrication is associated with block copolymer films. Additionally, we contrast the usage of different templates and exemplify several cases where both the host materials and the encapsulated nanostructures are obtained on a silicon platform. We centre our discussion on methods for the generation of conductive nanostructures, *e.g.* semiconductors (Si and Ge) and metals, with applications as interconnects or memory storage devices, and some oxides that are deposited by different growth methods. Regrettably, we should note that although significant progress

ACCEPTED MANUSCRIPT

ACCEPTED MANUSCRIPT

has been achieved to date with respect to tailoring the templates as membranes, films or masks for fabricating devices, actual device characteristics, most notably with mesoporous silica films are limited.

3.1. Additive growth schemes

Herein the nanostructured materials are deposited by additive methods within an ordered channel matrix of insulating material where the structures are encapsulated and therefore isolated from each other. The template-assisted methods for depositing one-dimensional nanostructured materials have been extensively studied and resulted in numerous publications and several reviews [140-143]. Various approaches, including electrochemical [144] and electroless deposition [145], sol-gel [146], chemical vapour deposition [143], and supercritical fluid deposition [147] have been exploited to deposit a range of 1 D nanostructures with single crystalline [148-149], polycrystalline [146] or amorphous [143] structure within these templates. Notably these methods are characterised by specific growth mechanisms and inclusion pathways, governed by the type of template support and deposition procedure. When one-dimensional nanostructures are deposited within channelled substrates with ordered porosity, important characteristics such as loading/filling factors, number density, spatial distribution, crystal structure, orientation and composition of the embedded materials needs to be determined. These together with the traditional aspects of a material's structural characteristics can give information on the encapsulation process and provide directions for controlling the deposition conditions. Almost all of these characteristics are easily accessed by electron microscopy and spectroscopy methods, not only because of the additional high spatial resolution but also because of the ability to analyse materials deposited within channels and not on the periphery of the template. This is of great importance since the crystal structure, morphology, surface states and defects can be altered considerably when nanostructures are encapsulated within porous channel supports.

ACCEPTED MANUSCRIPT

3.1.1. Silicon and germanium nanostructures within PAA, MTFs and BCP templates

In the Emerging Research Devices (ERD) section of the International Technology Roadmap for Semiconductors (ITRS) 2007, Si and Ge nanowires are specified as realistic and practicable post-CMOS elements below the 22 nm node [150]. Electrochemical deposition within PAA membranes is the most commonly used approach for generating 1 D nanostructures, because of the highly oriented nature of the support and the ease of depositing a bottom contact for electroplating. Nevertheless valuable semiconductor nanowires such as Si and Ge are difficult to obtain by electrochemical deposition. Recently, the first reports demonstrating electrochemical deposition of Si in ionic-liquids have been shown [151]. Unfortunately, the published reports did not present detailed information on the crystal structure and continuity of the deposited materials within the porous channels, nor any detailed mechanism explaining the crystal growth of the 1D nanostructure.

Redwing and co-workers, were the first to explore the possibility of combining the principles of vapour-liquid-solid (VLS) growth and encapsulated to deposit Si nanowires within PAA channels [152-153]. Briefly, Au segments that served as nucleation seeds were deposited by electrochemical means for the subsequent CVD silane (SiH_4) at 650 °C. Regrettably, limited details describing the inclusion process were presented, including direct observation of the nanowire arrays within the channel supports and their interface to the metal seeds at the base of the porous template. Gösele *et al.* demonstrated an alternative route for the preparation of arrays of epitaxial Si (100) nanowires grown by CVD using PAA membranes deposited on Si wafers with Au seeds precisely positioned at the bottom of the channels by electroless deposition [154]. Very recently, this approach was extended to the deposition of segmented Si/Ge nanowires within PAA membranes by growing heteroepitaxial Ge segments using the embedded Si nanowires (figures 15(a) and (b)) [155]. Nevertheless, nanowire loading factors, continuity and homogeneity of the deposited nanostructures within the channels was not favourable for precision device fabrication (see figure 15(a)). In addition, the approach requires a pre-annealing step of the PAA membrane above 800 °C prior to seeding of catalytic gold nanoparticles and an ultrahigh vacuum

ACCEPTED MANUSCRIPT

ACCEPTED MANUSCRIPT

(UHV) system for subsequent VLS growth of the nanowires. A significant drawback of this technique is that nanowires with diameters below 60 nm have yet to be generated. Nevertheless these examples show that potentially, the combination of VLS growth combined with the highly anisotropic structure of PAA membranes can be utilised to yield extremely high density arrays of semiconductor nanostructures with controlled diameters and ordered arrangements.

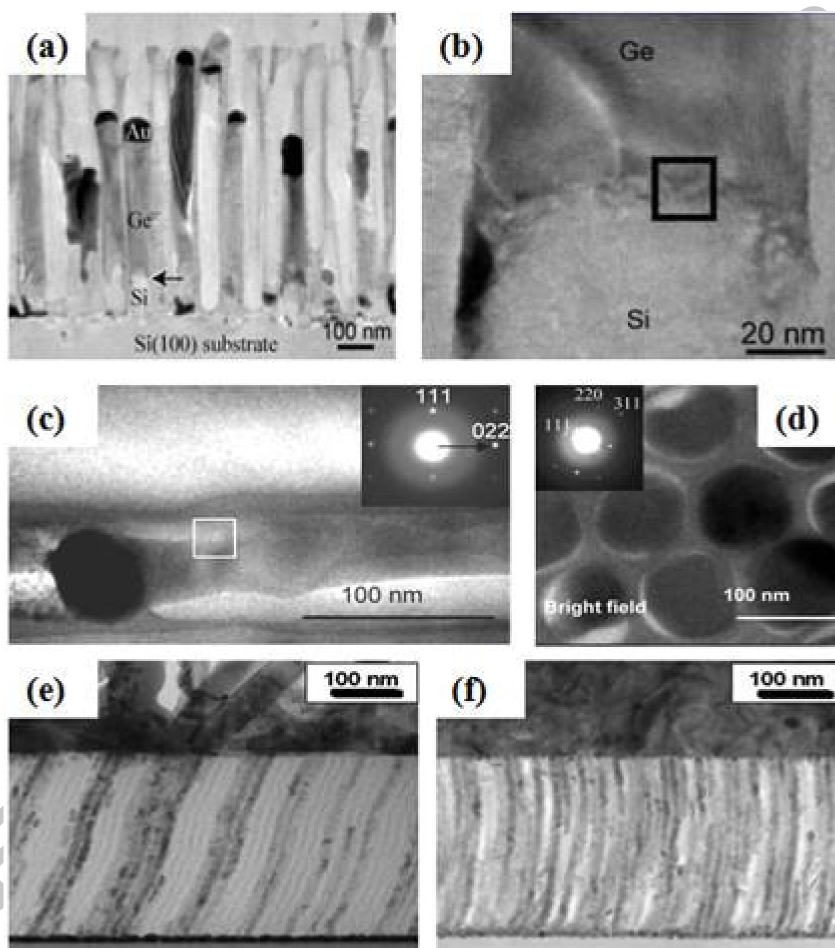

FIGURE 15: Nanowire in porous templates (a) and (b) Cross-sectional TEM images of Ge/Si nanowires grown by VLS technique within PAAs deposited on Si substrate (reproduced with permission from reference [155]) (c) and Ge nanowires grown by the SFLS technique with PAA membranes (reproduced with permission from reference [147]), d) Ge nanowires deposited within MTFs with vertical orientation of the pores. Cross-section TEM image of (e) nanowires grown at 340 °C showing a small number of pores filled with nanowires and (f) nanowires grown at 380 °C showing nearly 100% of the pores filled with germanium nanowires (reproduced with permission from reference [156])

ACCEPTED MANUSCRIPT

Complimenting these approaches, our group has developed a supercritical fluid (SCF) method for growing embedded semiconductor (Ge and Si) nanostructures within PAA membranes. The SCF method for growing nanostructures is an inexpensive solution-based growth technique utilising liquid precursors dissolved in supercritical carbon dioxide and/or organic solvents, for producing large quantities of a variety of semiconductor nanowires [151]. This method utilises equipment that can be easily integrated into a laboratory environment with no need to use extremely pyrolitic gases such as silane (SiH_4) or germane (GeH_4) and dedicated CVD equipment. Moreover the same equipment can be used to synthesise not only Si and Ge nanowires but also III-V nanowires [157-158], carbon nanotubes [159], *etc*. by choosing the appropriate metal seeds, *e.g.* Au, Ni, Co, Cu, *etc*. and suitable organometalic precursors. Additionally, the SCF technique allows precise control of the deposition parameters by controlling the pressure and temperature conditions, fluid flow rates, *etc*. [157-158, 160-161]. SCF deposition of semiconductor nanowires into porous templates can also be highly effective due to the low viscosity, negligible surface tension and good wetability of the fluid phase [162]. We have reported the Au seeded growth of Ge nanostructures, with controlled crystallinities, within the channels of PAA membranes [147]. Supercritical flow-through conditions were used to obtain single-crystalline Ge nanowires within the PAA templates (see figure 15(c) and (d)). However the Au seeds were deposited by electroless reduction and were randomly distributed along the PAAs channels, circumventing any possibility for the integration of the deposited nanowires into functional device architectures. Additionally, we used a combination of electrochemical plating and SFLS growth techniques under constant flow-through conditions to obtain segmented Au/Ge nanowire structures. On account of the increased wetability and diffusivity of the precursors under supercritical conditions, we were able to attain reasonably good loading (70 %) and uniformity of Ge nanostructures even within sub-20 nm PAAs channels. Unfortunately the crystallinity of the deposited Ge nanowires was largely perturbed by the confining environment of the sub-20 nm PAAs channels. We shall see in other parts of the chapter that this is typical for the encapsulated growth of nanowires at these dimensions; not only Si and Ge

ACCEPTED MANUSCRIPT

ACCEPTED MANUSCRIPT

nanowires but also other materials, a major disadvantage for device fabrication at very small dimensions (approaching 10 nm).

For a number of years many groups have endeavoured to achieve grow a variety of nanostructures within MTFs, with high channel loadings and uniformity for device manufacture, but without any real success. As mentioned previously in section 2.4.4, oriented mesoporous inorganic thin films templated with the PS-*b*-PEO block copolymer by solvent swelling methods are ideal candidates for growing vertical arrays of nanowires. Consequently, polycrystalline germanium nanowires (figures 15(e) and (f)) have been grown in 12 nm vertical pores orthogonal to the surface using a gold seed layer (which also serves to orient the hybrid inorganic-organic film). The authors noted that 100 % loading could be achieved when the growth temperature was raised from 275 °C (50 % efficient loading) to 380 °C for nanowire growth. Significantly this work highlights that a template system should be fully accessible so that precursors can infiltrate readily and participate in the growth process within the porous system. Unfortunately even with such highly oriented supports the deposited Ge nanostructures possessed far from optimal uniformity and crystallinity; the Ge nanostructures were polycrystalline and the deposition was non-uniform across the MTF channels. Nevertheless this is truly the first example of strictly 12 nm one-dimensional semiconductor nanostructures obtained by encapsulated growth within channel substrates.

Thus far, there is little research on using BCPs templates for the encapsulated growth of Si or Ge nanostructures. This is not surprising since the growth temperatures for Si and Ge, even when using metal seeds as catalysts, far exceeds the melt transition temperature of the BCP templates. However, other growth techniques can be used to create Si and Ge nanostructures provided the growth takes place closer to room temperature and more importantly, below the T_g of the polymer template. Figure 16 is a proof of concept process flow for growing polycrystalline Ge nanostructures at room temperature using electron beam evaporation on 'fingerprint' patterns of a PS-*b*-PMMA template (figure 16(a)). Briefly, a symmetric PS-*b*-PMMA block copolymer is self-assembled onto a random PS-*r*-PMMA copolymer to

ACCEPTED MANUSCRIPT

induce preferential orientation, orthogonal to the substrate. The PMMA component of the PS-*b*-PMMA lamellae structure is removed with a fluorocarbon based selective etch to generate a polystyrene (resist) profile. The resulting polystyrene profile is then transferred into the underlying bulk silicon substrate using another fluorocarbon etch. Finally, poly-crystalline germanium is evaporated by e-beam to achieve a non-conformal coating of germanium on the surface (figure 16(b) & (c)) and the additional recess created by the initial silicon etch, helps to achieve lift-off of the germanium to create germanium nanowires entrenched in a silicon substrate (figure 16(d)). Although, the germanium is again polycrystalline, techniques such as CVD epitaxial growth [163] in combination with precision etch and clean controls (removal of the native oxide) and subsequent post deposition annealing (to generate crystalline nanostructures), may provide an alternative route for low temperature growth of single crystalline materials.

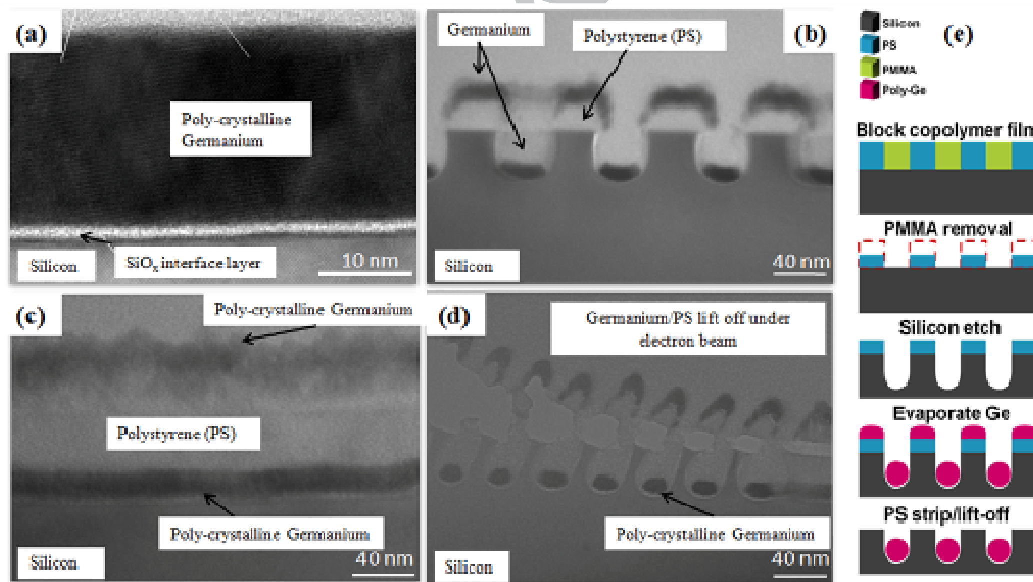

FIGURE 16: Polycrystalline Germanium nanowires using an additive technique for a block copolymer template. (a) HRTEM cross section of a germanium film deposited on a silicon substrate by e-beam evaporation, (b) front-on TEM view of Ge deposited an 80 nm pitch PS template etched into silicon, (c) side-view TEM image of Ge deposited on a 40 nm pitch PS template etched into silicon, (d) front-on TEM view of Ge deposited on a 40 nm pitch PS template undergoing lift-off in TEM and (e) process flow (unpublished work). Using other deposition techniques it may be possible to generate arrays of single crystalline Ge nanowires.

Besides Si and Ge there are a variety of other semiconductor materials that have been targeted for encapsulated growth within PAA membranes [146] and MTFs [164]. It is beyond the scope of this review to embark on an extensive review of exotic compositions and deposition methods that fall under this definition. Hence we will examine methods that resulted in single crystalline and oriented structures with very small diameters. For example, we have demonstrated the use of a pressure-injection solvent-less approach, without the use of a catalyst or complexing agent, to synthesise single crystalline and oriented Bi_2S_3, CdS and SnS_x nanostructures within PAA membranes [165] (figure 17). Using electron microscopy, we were able to identify a variety of 1 D nanostructures ranging from well faceted nanowires to nanotubes and nanobelts with diameters as small as 20 nm. All of the nanostructures exhibited preferential growth directions imposed by the confining environment of the PAA channels. Consequently, these structures may find use in such applications as thermoelectrics, optoelectronics and photovoltaic devices [166-168].

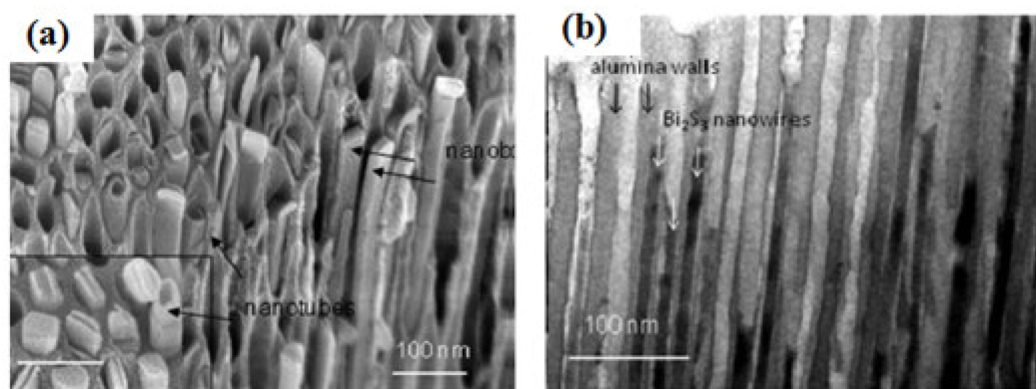

FIGURE 17: SnS_x nanostructures deposited within 80 nm PAAs membrane and Bi_2S_3 nanowires deposited in 20 nm PAAs channels by solventless growth. Note that structures are not only single crystalline but they are also grown with the same growth direction across different PAA channels, thus giving preferentially oriented arrays of one-dimensional nanostructures (reproduced with permission from reference [169]).

ACCEPTED MANUSCRIPT

ACCEPTED MANUSCRIPT

3.1.2. Metals within PAA, MTFs and BCPs templates

One-dimensional metal nanostructures show great potential as future electrical interconnects or functional units in memory storage devices. Electrochemical deposition of metals within PAA membranes is by far the most studied method of templated growth of one-dimensional nanostructures. There is an abundant amount of published papers relating to deposition of metallic nanowires within PAA with targeted applications ranging from arrays of interconnects [170], magnetic and memory devices [171-172], bio-and chemical sensing based on surface enhanced Raman scattering (SERS) [173] and wave guides [174] to thermoelectric and superconductive devices [175].

The electrochemical deposition of metallic nanowires is relatively straightforward and frequently achieved by potentiostatic techniques (depositions at constant current are also well investigated). The technique is reliant upon a suitable plating bath (for some of the metals there are commercially available plating baths), a proper backside electrode (deposited by metal sputtering on one side of the PAA membrane) and suitable deposition times. Thus, based on the pioneering work of Martin and Searson [142], and later by Mallouk [141] and Gösele [144], a vast variety of metal nanowires have been successfully deposited in PAA templates including: Pt [176], Ag [177], Au [178], Co [179], Cu [180], Ni [144, 178, 181], Pb [182], and Pd [183]. In addition multi-segment nanowires including; Au/Ni/Au [184] and Co/Cu [172] have been reported. Both binary and ternary alloy nanowire arrays of; CoCr [185], CoPt [186], FePt [186], FePd [187], NiCo [188], Ni_5Zn_{21} [171], and FeCoNi [189] have also been fabricated. The metal nanowires deposited by electrodeposition usually adopt polycrystalline structures but single crystal nanowires have also been obtained. One of the ways to control the crystallinity and the loading of the nanostructure during the electrochemical deposition process is to introduce surface active additives such as surfactants or gelatine into the plating bath [171, 188-189]. This is particularly important when depositing within sub-20 nm PAA channels. Recently, much effort has been devoted to the deposition of metallic tubes within PAA because of the intriguing magnetic and sensor properties of the structures [190]. Pulsed electrochemical deposition [191-192], plating within PAA membranes modified with reactive organic groups [193-194] and seeded electrochemical depositions [195] have

ACCEPTED MANUSCRIPT

ACCEPTED MANUSCRIPT

shown promise for obtaining metal tubes with various dimensions, composition and structure. Lately, atomic layer deposition (ALD) [196] and electron beam induced shadow evaporation [197] methods have been utilised for the precise and controlled deposition of conformal metal and metal oxide nanotubes within PAA membranes with various channel dimensions.

Much more complex is the inclusion of metal nanostructures by electrochemical deposition within MTFs. The major obstacle here is the lack of highly oriented template structures with accessible channels deposited on conductive supports. Stucky and colleagues utilised mesoporous silica with oriented mesoporous channels prepared within PAA membranes, that were coated with metal, to electrodeposit Ag nanostructures that fully replicated the mesoporous channel system [198]. The structures were investigated solely after dissolving the templating matrix and showed unique spiral, donut and chain-type shapes, dependent on the confinement imposed by the PAAs channels (see figure 18). Our group investigated the electroless depositions of Pt, Pd, Au within comparable templates. Notably, we were able to deposit aligned metal nanostructures oriented along the long axis of the confining mesoporous fibres encapsulated in the PAA channel (refer to figure 18(b) and (c)) [199]. Unfortunately the growth of one-dimensional metal nanostructures by electroless deposition within such sub-10 nm templates resulted in particulate morphologies with poor uniformity that hindered any realistic contacting strategies. Moreover electrical contacting of such extremely high density and small diameter one-dimensional nanostructures presents a considerable challenge on its own.

The fabrication of metallic nanowires and nano-dots *via* block copolymer templates has received considerably interest, most notably from the magnetic memory perspective [100, 200]. Under direct current electrodeposition conditions, high density arrays of 14 nm diameter ferromagnetic cobalt nanowires ($> 1.9 \times 10^{11}$ nanowires per cm^2) have been fabricated in one micron thick porous polystyrene films. The final ferromagnetic cobalt nanowires were approximately 14 nm in diameter and 500 nm in length (aspect ratio of 36) and as a result of this 1 D confinement showed higher coercivity compared to thin cobalt films, due to the presence of shape anisotropy. The ability to create high density arrays of

ACCEPTED MANUSCRIPT

ferromagnetic nanowires with large coercive and saturation fields whilst preventing superparamagnetism effects are advantageous for high density magnetic storage industry requirements.

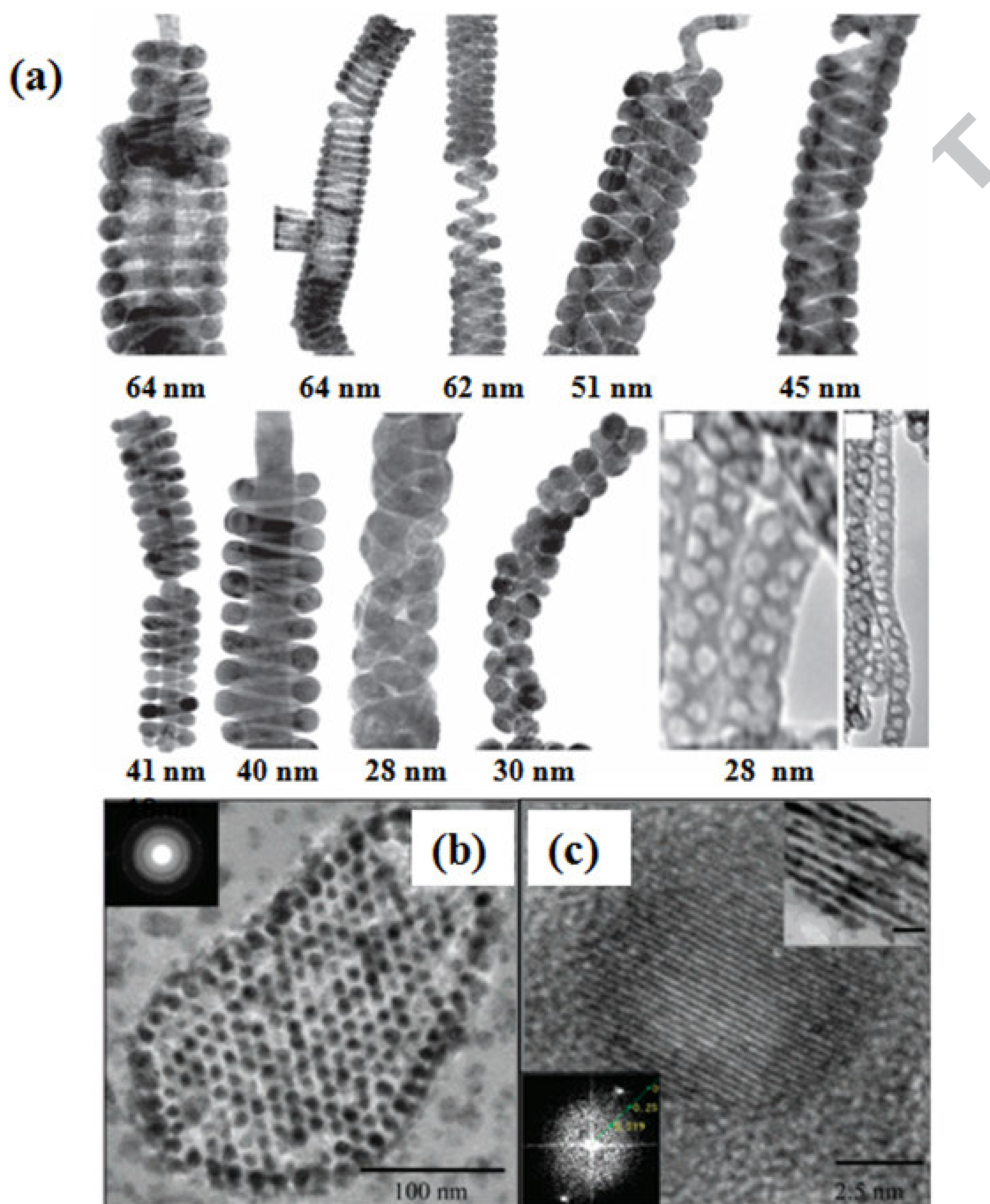

FIGURE 18: Metal nanostructures templated by mesoporous silica (a) various shapes of one-dimensional Ag nanostructures after dissolving the templating mesoporous silica and PAAS channels (the size of the confining PAAs channels is given below the images), reproduced with permission from ref. 46, B) and C) cross-sectional views of aligned Pd nanostructures deposited by electroless reduction within mesoporous channels encapsulated and oriented parallel to the long axis of the PAA channels (reproduced with permission from reference [198]).

ACCEPTED MANUSCRIPT

The authors also showed that the cobalt nanowire arrays could be extended to other systems such as giant-magneto-resistance devices [202]. Cobalt hexagonal arrays of nanodots with long range order have been created using an asymmetric PS-*b*-PMMA copolymer in combination with a topographic guide (graphoepitaxy), where the surface was chemically modified with the PS-*r*-PMMA brush layer to induce preferential ordering. Cobalt was sputtered into the porous PS matrix and lifted-off with a dry etch (mild ion beam) to realise individual discrete nanodots [100].

Chai and co-workers were successful in loading the PVP domain of an aligned PS-*b*-PVP block copolymer with anionic metal complexes to form metallic polycrystalline nanowires [115-116]. By immersing the aligned PS-*b*-P2VP film *via* graphoepitaxy methods in a concentrated acid, the protonated PVP complexed with the anionic metallic species. After a brief oxygen plasma treatment to remove the underlying block copolymer, well-aligned 10 nm wide metallic nanowires were produced which could be directed into many different pre-pattern shapes: linear (figure 19(a)), triangular and circular trenches. The technique is extremely versatile and efficient and the authors were able to generate a wide range of metallic nanowires: gold, nickel, platinum, palladium, copper, iron and cobalt [115]. Resistance of the nickel nanowires was determined by fabricating a macroscale contact at one end and rastering a conductive platinum AFM tip across an array of platinum nanowires with dimensions of 7.2 nm wide by 9.2 nm high [116]. Upon increased loading with a platinum salt, the nanowire dimensions grew to a final width of 11.6 nm and 13.5 nm in height. As a result, electrical resistivity increased from 3.0 kΩ per nm to 1.2 kΩ per nm and scaled linearly as a function of contact distance to the AFM tip (200 nm to 1000 nm), suggesting that grain boundaries limited the flow of current within the wire. Hence the resistance of the nanowires increased with their decreasing diameters, owing to the reduced pathways for current flow [203].

Concentric circular ferromagnetic cobalt rings with L_o dimensions of ~ 34 nm (depending on confining template, *i.e.* commensurability) have been fabricated using a PS-*b*-PDMS based template which provided a significant etch contrast enhancement with respect to other BCPs [82]. The researchers investigated the effects of confinement diameter and commensurability as a function of

ACCEPTED MANUSCRIPT

increasing concentric rings (1-5 rings) for the block copolymer system (figure 19(b)). Ferromagnetic cobalt nano-rings were subsequently created from the PDMS template using a series of reactive-ion etching, metal sputter and physical ion-beam etch steps. Magnetisation reversal between double ferromagnetic rings showed that magnetic switching between the onion and vortex states was present; however the vortex had a non-zero moment because the majority of the ring material was magnetised in the direction of the reverse field. Ferromagnetic ring structures have received considerable interest recently as they have stable magnetic states (onion and vortex) at remanence and as a result, may find uses in magnetic RAM applications [204].

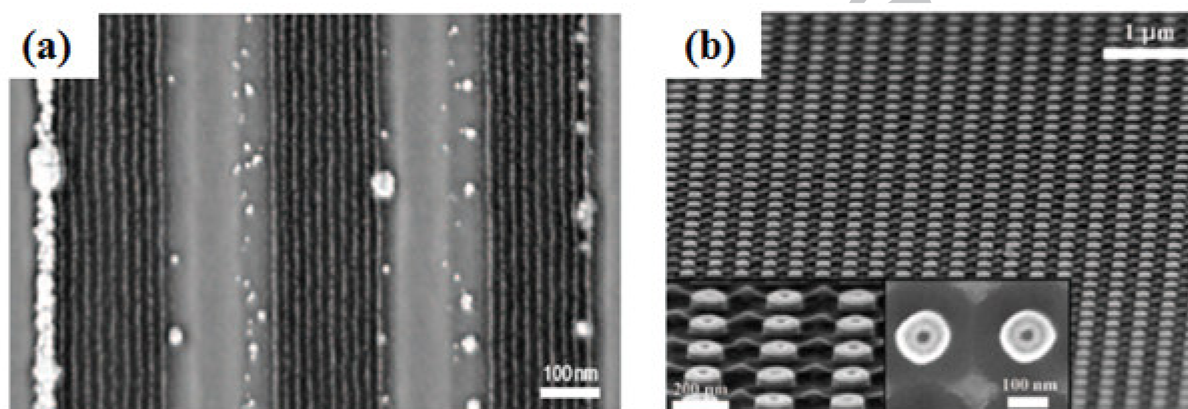

FIGURE 19: Metal nanostructures produced using block copolymers and graphoepitaxy methods: (a) SEM image of aligned gold nanowires using PS-*b*-PVP and graphoepitaxy (reproduced with permission from reference [116]). Metal salts are reduced by the PVP domains to generate nanostructures such as nanowires and nanorings. (b) SEM image of an array of 100 nm Co ferromagnetic double rings (reproduced with permission from reference [82]), using PS-PDMS as the initial template.

ACCEPTED MANUSCRIPT

ACCEPTED MANUSCRIPT

3.2. Subtractive nanopattern transfer

Subtractive pattern transfer is analogous to lithographic processing whereby a profile is created using a self-assembled template and transferred to an underlying film or substrate *via* wet or dry etch techniques. Such an approach permits researchers to control the doping, substrate orientation and purity of the underlying layers prior to template deposition. Templates must meet the following criteria, such as stability during etching, good pore accessibility and pore orientation, to allow high fidelity pattern transfer.

3.2.1. Nanowire arrays

Nanowires grown exclusively *via* bottom-up methods have fallen short of one specific requirement; they cannot be positioned/aligned on selected regions of silicon substrates with great accuracy. Significant attempts have been highlighted in the literature (Langmuir Blodgett [205], dielectrophoresis [206], fluidic alignment [207]) to align nanowires but these techniques never match the nanometre tolerances required for precision placement and overlay within semiconductor high volume manufacturing. Apart from the obvious benefits of using semiconductor nanowires in microelectronic devises, such as resolution enhancement and density, other advantages include the ability to generate cross-bar arrays of nanowires [208], reduced power consumption and increased electrostatic control through the use of a wrap-around gate dielectrics [209].

N-type field-effect transistors (FETs) based on arrays of Si nanowires have been generated from block copolymer lithography; whereby a PS-*b*-PMMA cylindrical forming polymer was aligned (6 to 16 lateral PMMA cylinders, 14 nm diameter) using pre-patterned channels (graphoepitaxy) in silicon-on-insulator substrates to create lines of polystyrene (resist) after a PMMA removal step [81]. Transferring the polystyrene pattern to the underlying silicon device layer, using a reactive ion etch and the buried oxide as an etch stop, ensured isolation of the nanowire array (figures 20(a)-(d)). Device on/off current

ACCEPTED MANUSCRIPT

ACCEPTED MANUSCRIPT

(I_{on}/I_{off}) ratios of 10^5 at V_{ds} of 1 V were achieved for an 8 nanowire array owing to full depletion of charge within the channel, as a result of the dimensions of the nanowire (15 nm by 15 nm cross sectional diameter post etching). Creating arrays of nanowires is extremely favourable as it is believed that such arrangements can result in increased drive currents at lower voltages. The authors also demonstrated that drive current (I_d) scales with the number of nanowires (6, 8 and 16), which suggest that each nanowire transfers equivalent amounts of current with a value close to 5 µA per nanowire (figure 20(e)). The nanowire array was gated through the silicon wafer and experienced short channel effects (SCE) as a result. Consequently the authors envisioned that the introduction of a top gate dielectric/gate stack would help to alleviate these effects and moreover, provide better electrostatic control. In comparison to other bottom nanowire fabrication techniques, BCP lithography offers clear advantages over its other counterparts in areas such ease-of-manufacture, alignment and registration, overlay and high resolution/critical dimensions.

Researchers at MIT have recently used PS-*b*-PDMS block copolymers for improving directed self-assembly in a topographic template (alignment of 15 nm PDMS cylinders in near micron sized channels) but more importantly to utilise the PDMS as a high etch resistant mask layer for high fidelity pattern transfer [50]. The authors employed this graphoepitaxy technique to fabricate nanowires of poly(3,4-ethylenedi-oxythiophene)-poly(styrenesulfonate) for ethanol vapour detection without any discernable loss in the gas sensing properties of the aforementioned nanowires when a BCP lithographic step was introduced [118]. Indeed, the poly(3,4-ethylenedi-oxythiophene)-poly(styrenesulfonate) nanowires were more sensitive to ethanol vapour when compared to their bulk thin film analogues as a result of increased surface-to-volume ratio of the nanowire arrays.

Jeong *et al.* have recently shown that symmetric PS-*b*-PMMA can assemble into well-aligned linear arrays of alternating PS and PMMA using a soft lithography approach [113]. Consequently, the authors used this approach to construct both metallic aluminium (additive) and silicon semiconductor (subtractive) nanowires. Aluminium nanowires were prepared by first removing the PMMA copolymer portion, by employing reactive ion etching with oxygen, proceeded by thermal evaporation of

ACCEPTED MANUSCRIPT

ACCEPTED MANUSCRIPT

aluminium. The current-voltage (*I-V*) characteristics of the 24 aluminium nanowires of 15 nm width with lengths of 224 microns exhibited ohmic behaviour at room temperature with a resistivity's of 17.6 μΩ cm. The authors attributed this higher resistivity value when compared to its bulk derivative due to the presence of grain boundaries within the nanowires as previously highlighted by Chai *et al* [116]. This soft lithography approach represents an extremely effective method for arranging linear arrays of block copolymer patterns and is likely to find use in front end microelectronic applications.

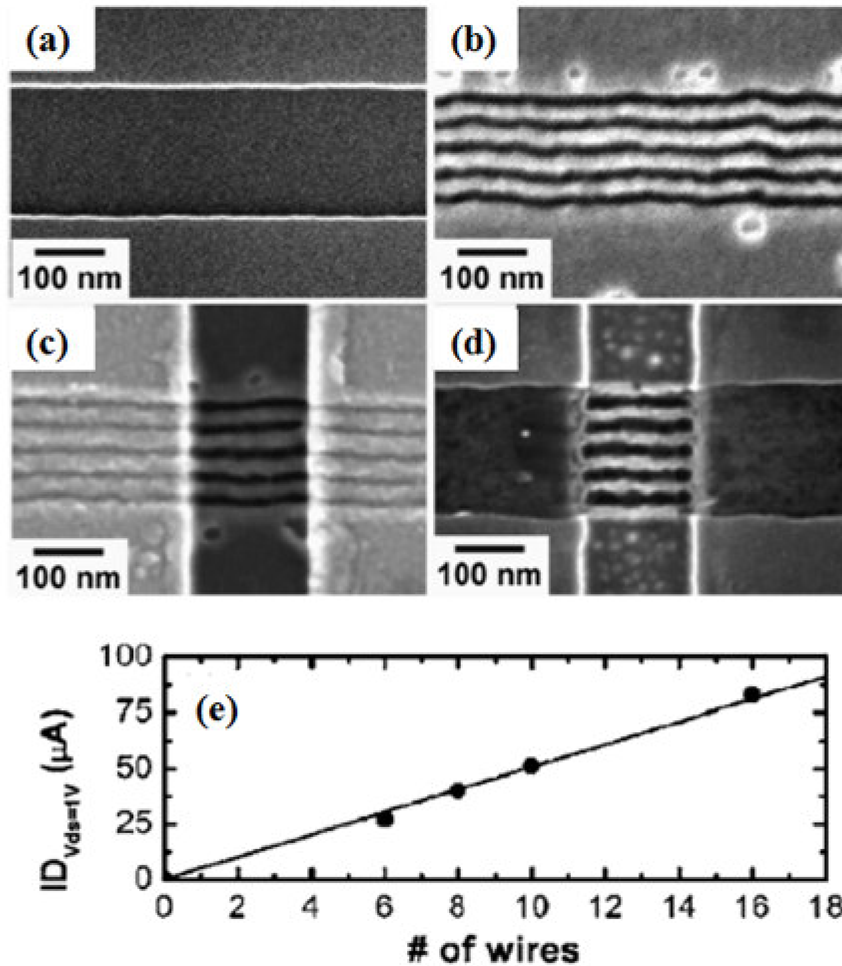

FIGURE 20: Step by step nanowire fabrication using block copolymers and graphoepitaxy: (a) blank trench prior to polymer deposition, (b) self-aligned PS-*b*-PMMA block copolymer with PMMA removed and silicon nanowire etch completed, (c) definition of titanium silicide source and drain contacts to form a 145 nm channel and the (d) completed 6 wire silicon nanowire array. I_D scaling with number of silicon nanowires Plot of current (I_D) at V_{ds}=1 V, V_g–V_T=25 V versus the number of wires in nanowire-array devices. Solid line is the best linear fit to the data, with slope equal to 5 μA/wire (reproduced with permission from reference [81]).

ACCEPTED MANUSCRIPT

One prominent difference for planar nanowires in comparison to vertical nanowires templated by block copolymers is film thickness. In the former, film thickness (t ~ 1-2 L_0) tends to be thin as precision orientation requires thin films rather than thick ($t > 3\ L_0$) films where orientation and pattern transfer can be difficult to control. A balance in thin film thickness must be achieved as too thin provides little etch contrast and too thick can disrupt the orientation.

3.2.1. Nano-pillars and anti-dot arrays

As outlined in the previous section, nanowire arrays fabricated *via* block copolymer lithography routes are viable alternatives for creating front end transistors. Similarly, nano-pillars, nano-rings and anti-dot arrays can find use in many devices and applications such as photovoltaics, light-emitting diodes and most importantly bit-patterned magnetic and DRAM memory storage applications [130]

One of the first demonstrations of patterned (cobalt) magnetic nanodot arrays was published in 2003 by Ross and co-workers using a PS-*b*-PFS sphere-forming system with a natural periodicity of 55 nm and a PFS sphere size of 35 nm [200]. The process was quite detailed and required 3 pattern transfers after the PS removal: (a) PFS profile transferred into SiO_2, (b) SiO_2 profile transferred into tungsten and finally (c) tungsten profile transferred into the magnetic cobalt film using a series of RIE processes and a final ion-beam etch of the cobalt. The authors revealed that the coercivity of the Co nanodots could be tuned with the final physical ion beam etch process, which caused obstruction of domain wall motion owing to corrugations created in the as-deposited sputter cobalt film. CoCrPt [210] and FePt [211] films have also been created using a similar approach with PS-*b*-PMMA as the principal polymer template.

Non-magnetic memory devices have also benefited from the resolution of block copolymer systems. Shallow-trench array capacitor (decaps) were fabricated using a 40 nm pitch hexagonal array of PMMA cylinders in a PS matrix oriented perpendicular to the substrate [123]. The template was first transferred into a silicon dioxide hard mask. This hard mask allowed for a deep etch into the bulk

ACCEPTED MANUSCRIPT

ACCEPTED MANUSCRIPT

silicon wafer (~ 50 nm) to create an array of shallow-trench capacitors (figures 21(a)-(c)). To complete the devices, a 4.5 nm silicon dioxide layer was thermally grown and followed a conformal tantalum nitride (TaN) top gate grown by ALD. Although a capacitance enhancement of ~ 400-500 % was achieved, lateral leakage currents from device to device (trench to trench) increased by 2 orders of magnitude (figures 21(e) and (f)).

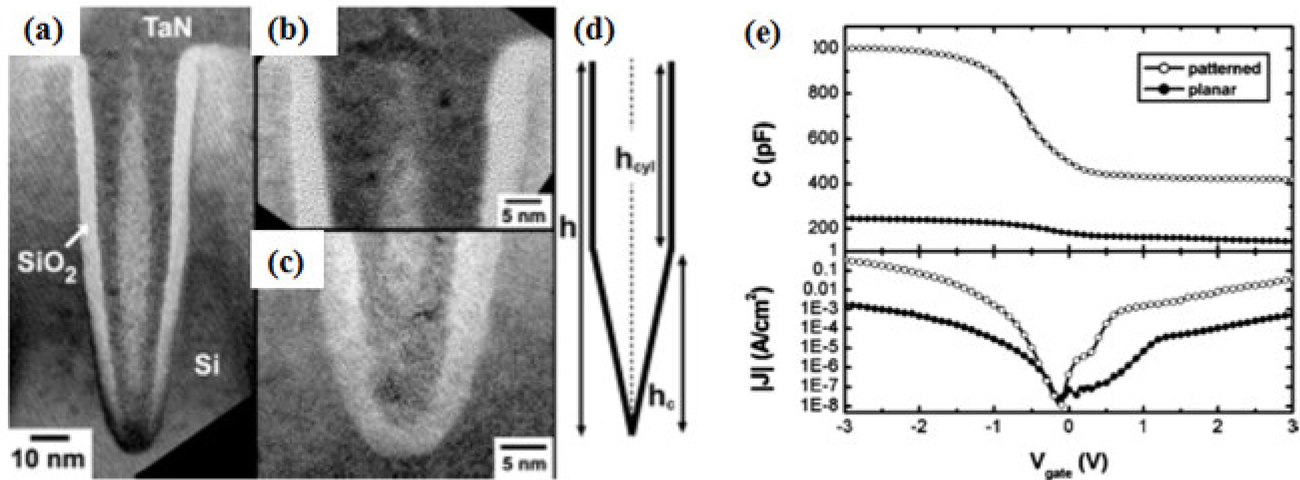

FIGURE 21: (a) Metal–Oxide–Semiconductor Decoupling Capacitors (a)–(c) Cross section TEM images of completed MOS decoupling capacitor. The mask was a porous polystyrene film created from a PS-*b*-PMMA film with PMMA cylinders oriented vertically to the substrate surface, (d) Schematic device cross section showing etch profile. (e) Capacitance versus voltage for planar (solid circles) and patterned (open circles) devices of the same lateral area (measured at 100 kHz). (f) Leakage current per lateral device area for planar (solid circles) and patterned (open circles) devices (reproduced with permission from reference [212]). Although the capacitance increased by 400-500 %, current leakage also increased.

Relatively less explored is the possibility of using PAA materials as hard masks for subtractive transferring. Ultra-thin alumina masks (UTAMs) have been described for such applications; a special type of anodic alumina membrane with a thickness of several hundred nanometres [213]. UTAMs can be placed (attached) post synthetically or fabricated directly on a substrate, and as such are independent of the type of substrate used. However, as placed UTAMs are maintained on substrates *via* weak Van der Waals surface attachment, *e.g.* a quick drying process of acetone, they are not typically in good

ACCEPTED MANUSCRIPT

contact with the underlying substrate. A subsequent wet-chemical process may cause the detachment of the UTAM from the substrate. Therefore, placed UTAMs can only be used in vapour-phase deposition (additive) processes for fabricating ordered nanoparticles or nanoholes. UTAMs fabricated directly onto substrates can be used for the generation of nanostructures by both vapour-phase deposition and wet-chemical processes, as the membrane remains in intimate contact with the substrate. Nevertheless UTAMs placed onto a substrate can still be explored for subtractive transferring if one uses metal or oxide evaporation to deposit semi-spherical nanoparticles; using the UTAM as a mask and after removing the UTAM utilising the deposited features as etch an mask. Si nano pillar arrays were obtained on Si-on-insulator substrates using this approach (see figure 22) [214]. Similarly, Gösele *et al.* used attached UTAMs to deposit a perforated metal layer with ordered holes and used this for metal assisted chemical etching of Si to obtain ordered arrangements of Si nano-pillars [215].

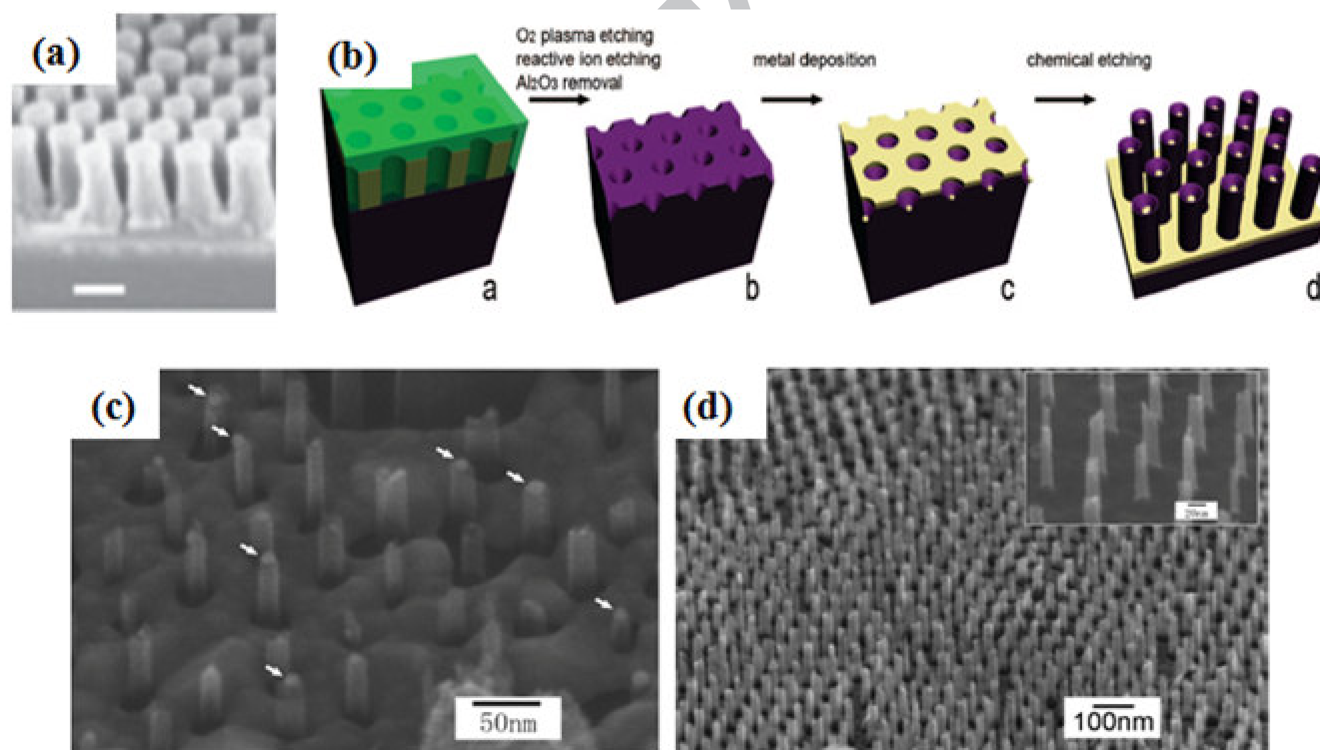

FIGURE 22: (a) Si nano-pillars obtained by using metal semi-spheres as mask for dry Si etch, reproduced with permission from reference [214]). (b) schematics of the process flow for pattern transfer into Si through metal assisted chemical etch of Si, and (c) and (d) corresponding nano-pillar structures showing pillars with different diameters (reproduced with permission from [215]).

ACCEPTED MANUSCRIPT

Block copolymer lithography is a significantly developed and advanced process, capable of meeting the challenges for future semiconducting and memory storage applications, and is considerably ahead of the other two templates in areas such as integration and development [26, 130]. Notably, the use of mesoporous materials as nano-lithographic etch masks is limited mainly due the thickness of the mesoporous films where both PAA membranes and BCP films can tune their thickness/orientation in the thin film format, but most importantly they have accessible porous templates.

3.3. Intrinsic device properties of MPS films

Block copolymers (and in some cases PAA membranes) are sacrificial templates, meaning that the polymer self-assembly is only an intermediate step within the process and is completely removed for device operation. Thus far, we have neglected to consider the template itself as a device or more importantly as part of a device.

3.3.1. Low-*k* dielectrics/proton gated devices

Templated mesoporous films represent a unique material set within nanoelectronics, as they can serve as a host matrix for aligning, separating and confining nanoscale device materials and also function as the low-*k* dielectric within device architectures as a result of their inherent nanoscale porosity. Since the 1970s the semiconductor community has witnessed a persistent struggle to sustain Moore’s law [216] with recent advances such as strained silicon [217-218] and copper interconnects [219] helping to extend device scaling. Nevertheless, even with all of the recent research breakthroughs, low-*k* dielectrics have remained a constant impediment to the ITRS roadmap and ultimately threaten to restrict future device speeds (and dimensional scaling) [150]. The interruption in the low-*k* dielectric roadmap can be directly associated with their incompatibility with current and future CMOS integration schemes. Porous dielectrics suffer from inferior mechanical (elastic modulus, prone to cracking) and electrical properties, *e.g.* water uptake, and as a result, integration with present CMOS based

ACCEPTED MANUSCRIPT

technologies is exceptionally complex [220-221]. Conversely, the advent of templated mesoporous silica films has allowed for the fabrication of low-*k* films with organised porosity [9]. By controlling the pore size, pore size distribution and porous architectures, the dielectric film properties can be tailored to suit the needs of the manufacturer. The general consensus is that to attain films which have dielectric constants of 2.5 and below, the inclusion of pores (air) is unavoidable. The addition of pores within an oxide has significant implications; reduced capacitance per unit area, increase in adsorption properties, low modulus and low crack resistance.

We have also characterised in detail the electrical behaviour of self assembled mesoporous materials and microporous dielectric films [24, 222]. Dielectric constants ranging from 1.6 to 2.8 were achieved without any significant observed frequency effects depending on the block copolymer template. The leakage currents and breakdown electric fields of the films, with *k*-values of ~2.8, were comparable to those commonly found for CVD grown silica films, but significant deterioration of electrical performance was observed as the dielectric constant was reduced. The films contained large amounts of charge, not as a product of inappropriate deposition environments, but primarily as a result of the high content of surface silanol groups (both at interface and within bulk) relating to the large surface areas of the mesoporous films. The resistance of the films and any low-*k* material to water remains the foremost problem for successful and swift integration of low-*k* materials (figure 23(b)). The films mesostructural ordering and dielectric properties are severely affected by physisorbed water. The effective passivation or suppression of these active sites will certainly quicken the integration times of mesoporous and other dielectric films [223].

Proton generation within silica and mesoporous silica films is well known to arise upon exposure to a humid environment as shown by the flat band voltage shift in figure 23 [24]. Fan and co-workers have successfully used an aligned SBA type-15 mesoporous silica framework as a channel material, where the protons behave as the carriers between the HCl reservoirs (source and drain) [16]. An aligned film was achieved by dip-coating thin films (100-200 nm) followed by a controlled calcination step to yield uni-directional films. The authors concluded that such alignment was possible due to the

ACCEPTED MANUSCRIPT

ACCEPTED MANUSCRIPT

interfacial shear at reduced dimension. Next, the mesoporous films were patterned into 2 mm wide strips using a series of photolithography and reactive ion etching steps. Rather than strip the resist, the authors used this layer (which was hardened by baking) to act as a hydrophobic barrier to separate the HCl reservoirs on each side of the mesoporous strip. The insertion of two Ag/AgCl electrodes completed the electrochemical cell and facilitated extraction of the proton conductivity characteristics of the system. The dominant mechanism of current transport within the channels was found to be surface-charge-mediated at low proton concentrations but above the isolectronic point of the silica surfaces, bulk behaviour became the prevailing mechanism. Modulation of the proton conduction was achieved by positioning a gate above the mesoporous channels and applying a bias. The mesoporous/microfluidic device was analogous to a p-type transistor, whereby applying a positive voltage at the gate, the ionic current was observed to decrease. Interestingly, gate voltages as low as 1 V were able to modulate the proton conduction within the mesoporous channels.

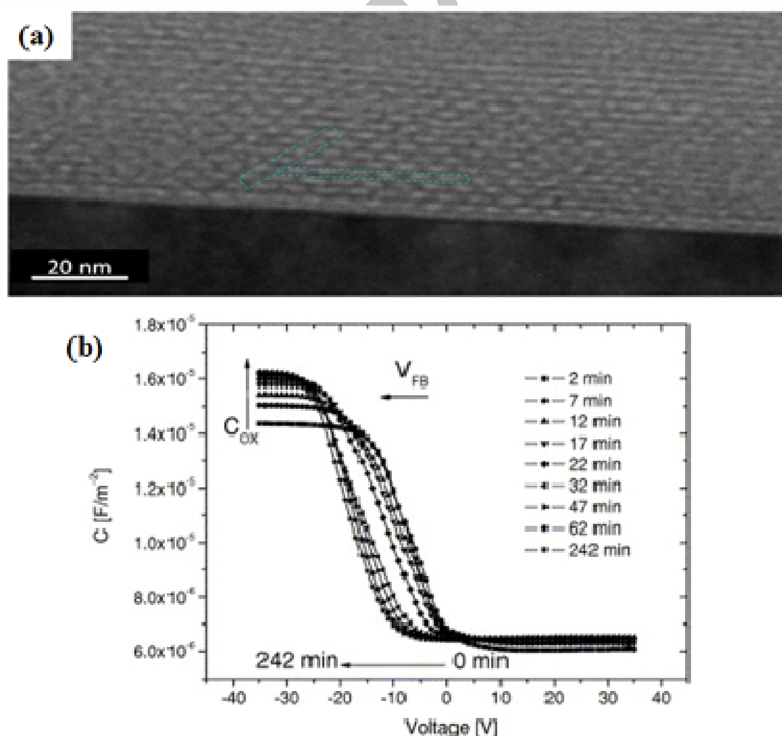

FIGURE 23 (a) TEM cross sections of a self-assembled mesoporous film with 2D hexagonal ordering and a pore diameter of 3-4 nm templated from a Brij 56 block copolymer, (b) Capacitance-voltage (CV) characteristics recorded at 1 MHz *CV* curves for a low-*k* film when exposed to a humid environment of 6 0% relative humidity over a 4 hr interval highlighting proton generation at the interface as evidenced by the V_{fb} shift (reproduced with permission from [24]).

ACCEPTED MANUSCRIPT

Mesoporous silica films are susceptible to water uptake and consequently methods of pore sealing or molecular capping must be employed.

SECTION 4.0: PERSPECTIVES

Self-assembly is a powerful and effective method for creating and manipulating nanoscale templates and patterns. Predominantly, such structures have allowed researchers to grow and confine 1 D nanostructures in specific geometries, which has subsequently provided important information on the size-dependent properties of materials. Although these experiments have served as excellent test structures, further manipulation (directed self-assembly) of templates beyond their use as channels for controlling growth is required. The long range order of templates and nanopatterns is still currently limited to the local scale (< 1 μm^2) and as a result top-down patterning is likely to play a key role in creating large scale global arrays (< 1 μm^2) in the future.

Indubitably, the advances in directed self-assembly pertaining to block copolymers are significantly ahead of initial demonstrations for PAA membranes and MTFs, with a dedicated section addressing their integration into future lithographic process flows in the emerging materials section of the ITRS 2007 roadmap. Nonetheless, challenges such as reduced line edge roughness, scalability over several process generations, the ability to self-assemble into a range of non-arbitrary patterns (single line and dot, circular openings) and most critically, an understanding of defect minimisation in the nanostructures generated still needs to be addressed. Block copolymers have already been integrated into fabrication process flows with semiconductor and memory manufactures actively pursuing this technology (IBM, Hitachi Global Storage and Seagate). PAA membranes and MTFs have yet to be utilised within the semiconductor community.

Encapsulated growth in PAA membranes and MTFs films does allow the production of high density ordered arrays of nanostructures with controllable dimensions, orientation and alignment which

ACCEPTED MANUSCRIPT

ACCEPTED MANUSCRIPT

are extremely important for future device applications. However, the crystallinity, defect density, and surface states of arrays of 1 D nanostructures obtained within these confining templates have to date been far inferior to those produced by template-free CVD, SCF or hydrothermal growth methods. Additionally, only limited electrical data has been collected for arrays of high density 1 D nanostructures, primarily due to limited nanoscale electrical contacting strategies. This fact emphasises the need for the directed deposition of templating structures, by fusing top-down and bottom-up approaches, and the development of improved growth methods and contacting strategies so that practicable device architectures can be realised.

In conclusion, self-assembled templates are exceptional systems for creating and tuning arrays of nanowires, nanopillars and nanodots and will, in some format, play a pivotal role in future nanoscale devices. With continuous advances in template design, feature size and orientation/structure, novel and functional templates will be readily available to researchers to extend current technologies into future nanotechnologies.

ACKNOWLEDGMENTS

We acknowledge financial support from the Centre for Research on Adaptive Nanostructures and Nanodevices (CRANN) and Science Foundation Ireland (Proposal 08-CE-I1432). This research was also enabled by the Higher Education Authority Program for Research in Third Level Institutions (2007-2011) via the INSPIRE programme.

ACCEPTED MANUSCRIPT

ACCEPTED MANUSCRIPT

FIGURE CAPTIONS

FIGURE 1: (a) Schematic of evaporation induced self-assembly (EISA), cartoon represents 4 stages of film formation – initial sol, evaporation driven self-assembly, equilibrium with environment and condensation of silica network (reproduced with permission from reference [12]). (b) TEM cross section of a film formed by the EISA methods, film of ~700 nm with a p6m 2D hexagonal structure was fabricated through a dip-coating process where Pluronic F127 was the template used (unpublished work). Careful control during deposition (humidity and precursor concentrations) ensures the formation of well-ordered periodic nanostructures.

FIGURE 2: (a) SMCF phase diagram for an A-B diblock copolymer, microdomain structures such as packed spheres (CPS), body centred cubic spheres (Im3m), hexagonally packed cylinders, bicontinuous gyroid structure (Ia3d) and lamellae are predicted to exist as a function of the molar fraction. (b) Experimental A-B diblock copolymer, deviation between theoretical and experimental phase behaviour for the PS-PI diblock system (reproduced with permission from reference [40]).

FIGURE 3: Polystyrene lines and membranes, 70° tilt SEM image of a (a) perpendicular lamellae PS-*b*-PMMA films and (reproduced with permission from reference [52]) (b) perpendicular hexagonal PS-*b*-PEO where the oxygen containing block (PEO & PMMA) was removed by an RIE etch (unpublished work). Films have orientational structure but lack translational ordering. (Inset) diagrams representing the internal structure within the films. Such nanopatterns can be used as masks for creating a wide range of nanostructures.

FIGURE 4: PAA films (a) Schematic of the self-organised formation of hexagonal pore structures in anodic alumina (reproduced with permission from reference [60]) where pores grow perpendicular to the

ACCEPTED MANUSCRIPT

ACCEPTED MANUSCRIPT

surface due to the equilibrium between field enhanced oxide dissolution at the oxide/electrode interface and oxide growth at the metal/oxide interface (b) top down and (c) cross-sectional TEM images of PAAs prepared from 200 nm Al coated Si substrates by sulphuric acid anodisation of thin aluminium layers at 20 V (unpublished work). Pore diameters and pore-to-pore distances are 10-15 nm and 20-30 respectively.

FIGURE 5: Chemical epitaxy; cross sectional TEM images of the as-grown film with a single-crystalline porous structure where (a) represents the film viewed along the rubbing direction and (b) perpendicular to the rubbing direction (reproduced with permission from reference [75]) templated with the surfactant Brij 56. The mean pore diameter is approximately 4 nm with a pore wall of 4 nm. The correlation length of the porous architecture is maintained across the substrate, over distances on the cm length scale.

FIGURE 6: FIB sectioning & Physical epitaxy of aligned mesoporous silica channels (a) and (b) cross sectional TEM micrographs of mesoporous silica confined with a patterned metal/oxide stack with an aspect ratio of 3:2. (c) SEM micrographs of the 'front-on' sections taken through the mesoporous silica thin film within the channels, each showing the pore ordering of the eight separate channels (A-H) (reproduced with permission from reference [15]). The hexagonal pore structure is maintained but delamination of the mesoporous segments is evident; due to the annealing step required to remove the organic template and cross-link the silica network.

FIGURE 7: Vertical channel formation using various techniques: (a) *Solvent annealing*; TEM cross-sectional micrograph of the porous SSQ film shown with pores oriented vertically to the substrate

ACCEPTED MANUSCRIPT

ACCEPTED MANUSCRIPT

surface templated by a PS-*b*-PEO diblock coploymer grown on a Au substrate (reproduced with permission from reference [86]) (b) *Cathodic Electrodepositon*; TEM cross section image of the electrodeposited surfactant-templated mesoporous silica films on a gold substrate (scale bar 20 nm) (reproduced with permission from reference [87]), (c) *Epitaxial Growth*; SEM image of a cut in a (111)-oriented cubic mesoporous titania film used as seed layer for oriented 2D mesoporous channels orthogonal to the substrate (reproduced with permission from reference [88]). The pores on the top surface of the titania seed layer are commensurate with the vertical pores in the P123 surfactant film, having similar periodicities and enabling effective epitaxial growth.

FIGURE 8: Mesoporous silica deposited within vertical channels of PAA membranes (a) Cross-sectional TEM image of P123 templated material with columnar orientation of the pores, (b) top down TEM image of the same specimen showing the perfect hexagonal order of the channels, (c) top down TEM image of CTAB-templated mesoporous silica with columnar orientation of the channels and 2 nm pore diameters, (inset) corresponding 2D SAXS pattern (reproduced with permission from [89]).

FIGURE 9: (a) Graphoepitaxy schematic for perpendicular hexagonal (1) deposition of BCP on patterned topography (2) thermal or solvent annealing induces microphase separation whilst capillary action pulls the polymer in the trenches and (3) registration and alignment of the nanopattern to the fabricated micron-sized channels. (b) Time resolved study of polymer flow and cylinder orientation for parallel hexagonal 2D Tapping mode AFM phase images of triblock PS-*b*-PI-*b*-PS thin films prepared from 0.7 wt% solutions of block copolymer in toluene on topographically patterned substrates (430 nm channel) (i) prior to thermal annealing and upon annealing at 120 °C for (ii) 1 h, (iii) 1.5 h, (iv) 2.5 h, (v) 4 h and (vi) 6 h. Insets are the corresponding FFT image (reproduced with permission from reference [107]). After 3 hr the nanopattern displays well aligned cylinders within the PS matrix.

ACCEPTED MANUSCRIPT

ACCEPTED MANUSCRIPT

FIGURE 10: Aligned asymmetric PS-*b*-PMMA films with (a) controlled orientation: 5 aligned polystyrene strips (post PMMA removal) in a ~ 220 nm wide SiO_x trench and (b) a porous polystyrene matrix six rows wide (post PMMA removal) in a ~ 260 nm trench coated on a PS-*r*-PMMA polymer. By introducing different wetting layers on the base and side walls of the channels, using random copolymer brushes, orientational control is achieved. Defect density control for symmetric PS-*b*-PMMA films (c) using a series of tapered trenches with varying trench widths (i) to (iv) $4L_o$ to $10L_o$ (L_o – equilibrium distance), where defects are observed outside channels in the tapered zones (reproduced with permission from reference [104, 114]). By ensuring that the channel width is an integer number of the natural polymer periodicity, and creating tapered regions in close proximity, defects within the narrow regions can be minimised to ensure excellent alignment of the nanopattern.

FIGURE 11: Aligned asymmetric PS-*b*-PEO films (a) cross sectional and 70° tilt SEM images of topographic patterns (b) 70° tilt SEM image of PS-*b*-PEO films (PEO removed) on a planar silicon substrate (c) and 70° tilt SEM image of PS-*b*-PEO films (PEO removed) on a topographic substrate. 13 rows of PEO nanodots are observed to register with the sidewall of the channel (unpublished work). The films were annealed in a solvent vapour for 6 hr at room temperature.

FIGURE 12: BCP aligned on chemical pre-patterns top down SEM micrographs of (a) PS-*b*-PMMA with excellent alignment on a 47.5 nm grating and (b) with herringbone (defect) formation on a 55 nm grating (reproduced with permission from reference [4]). Chemical patterns are effective for aligning block copolymers.

ACCEPTED MANUSCRIPT

ACCEPTED MANUSCRIPT

FIGURE 13: Directed self assembly of PAA films (a) and (b) shows an example of an array of about 100 nm PAAs channels perfectly organised in hexagonal arrangement after using indentations obtained by stamping with SiC and Ni imprint stamps manufactured by EBL and LIL, and (c) square arrangements of the pores was also demonstrated by using imprint stamps but also FIB patterning and (d) hexagonal arrangement of 30 nm PAA channels guided by concaves obtained by BCP lithography (reproduced with permission from reference[134-136]) (Scale bar = 300 nm).

FIGURE 14: Crossbar PAA films (a) Single layer of parallel PAA channels sandwiched between thick silica layers and reproduced with permission from reference [6]). (b) schematics of array $SiO_2/Al/SiO_2$ structures that were used to prepare patterned parallel PAA channels (reproduced with permission from reference[139]).

FIGURE 15: Nanowire in porous templates (a) and (b) Cross-sectional TEM images of Ge/Si nanowires grown by VLS technique within PAAs deposited on Si substrate (reproduced with permission from reference [155]) (c) and Ge nanowires grown by the SFLS technique with PAA membranes (reproduced with permission from reference [147]), d) Ge nanowires deposited within MTFs with vertical orientation of the pores. Cross-section TEM image of (e) nanowires grown at 340 °C showing a small number of pores filled with nanowires and (f) nanowires grown at 380 °C showing nearly 100% of the pores filled with germanium nanowires (reproduced with permission from reference [156])

FIGURE 16: Polycrystalline Germanium nanowires using an additive technique for a block copolymer template. (a) HRTEM cross section of a germanium film deposited on a silicon substrate by e-beam evaporation, (b) front-on TEM view of Ge deposited an 80 nm pitch PS template etched into silicon, (c) side-view TEM image of Ge deposited on a 40 nm pitch PS template etched into silicon, (d) front-on TEM view of Ge deposited on a 40 nm pitch PS template undergoing lift-off in TEM and (e)

ACCEPTED MANUSCRIPT

ACCEPTED MANUSCRIPT

process flow (unpublished work). Using other deposition techniques it may be possible to generate arrays of single crystalline Ge nanowires.

FIGURE 17: SnS_x nanostructures deposited within 80 nm PAAs membrane and Bi_2S_3 nanowires deposited in 20 nm PAAs channels by solventless growth. Note that structures are not only single crystalline but they are also grown with the same growth direction across different PAA channels, thus giving preferentially oriented arrays of one-dimensional nanostructures (reproduced with permission from reference [169]).

FIGURE 18: Metal nanostructures templated by mesoporous silica (a) various shapes of one-dimensional Ag nanostructures after dissolving the templating mesoporous silica and PAAS channels (the size of the confining PAAs channels is given below the images), reproduced with permission from ref. 46, B) and C) cross-sectional views of aligned Pd nanostructures deposited by electroless reduction within mesoporous channels encapsulated and oriented parallel to the long axis of the PAA channels (reproduced with permission from reference [198]).

FIGURE 19: Metal nanostructures produced using block copolymers and graphoepitaxy methods: (a) SEM image of aligned gold nanowires using PS-*b*-PVP and graphoepitaxy (reproduced with permission from reference [116]). Metal salts are reduced by the PVP domains to generate nanostructures such as nanowires and nanorings. (b) SEM image of an array of 100 nm Co ferromagnetic double rings (reproduced with permission from reference [82]), using PS-PDMS as the initial template.

ACCEPTED MANUSCRIPT

ACCEPTED MANUSCRIPT

FIGURE 20: Step by step nanowire fabrication using block copolymers and graphoepitaxy: (a) blank trench prior to polymer deposition, (b) self-aligned PS-*b*-PMMA block copolymer with PMMA removed and silicon nanowire etch completed, (c) definition of titanium silicide source and drain contacts to form a 145 nm channel and the (d) completed 6 wire silicon nanowire array. I_D scaling with number of silicon nanowires Plot of current (I_D) at V_{ds}=1 V, V_g–V_T =25 V versus the number of wires in nanowire-array devices. Solid line is the best linear fit to the data, with slope equal to 5 μA/wire (reproduced with permission from reference [81]).

FIGURE 21: (a) Metal–Oxide–Semiconductor Decoupling Capacitors (a)–(c) Cross section TEM images of completed MOS decoupling capacitor. The mask was a porous polystyrene film created from a PS-*b*-PMMA film with PMMA cylinders oriented vertically to the substrate surface, (d) Schematic device cross section showing etch profile. (e) Capacitance versus voltage for planar (solid circles) and patterned (open circles) devices of the same lateral area (measured at 100 kHz). (f) Leakage current per lateral device area for planar (solid circles) and patterned (open circles) devices (reproduced with permission from reference [212]). Although the capacitance increased by 400-500 %, current leakage also increased.

FIGURE 22: (a) Si nano-pillars obtained by using metal semi-spheres as mask for dry Si etch, reproduced with permission from reference [214]). (b) schematics of the process flow for pattern transfer into Si through metal assisted chemical etch of Si, and (c) and (d) corresponding nano-pillar structures showing pillars with different diameters (reproduced with permission from [215]).

FIGURE 23 (a) TEM cross sections of a self-assembled mesoporous film with 2D hexagonal ordering and a pore diameter of 3-4 nm templated from a Brij 56 block copolymer, (b) Capacitance-voltage (CV) characteristics recorded at 1 MHz *CV* curves for a low-*k* film when exposed to a humid

ACCEPTED MANUSCRIPT

ACCEPTED MANUSCRIPT

environment of 6 0% relative humidity over a 4 hr interval highlighting proton generation at the interface as evidenced by the V_{fb} shift (reproduced with permission from [24]). Mesoporous silica films are susceptible to water uptake and consequently methods of pore sealing or molecular capping must be employed.

ACCEPTED MANUSCRIPT

ACCEPTED MANUSCRIPT

Figures

Figure 1

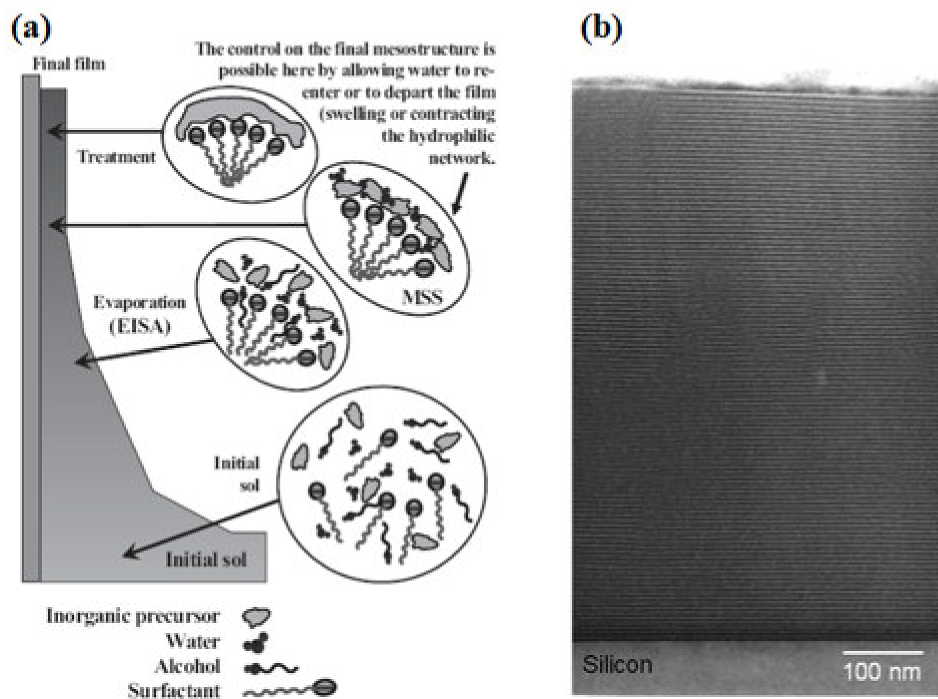

ACCEPTED MANUSCRIPT

ACCEPTED MANUSCRIPT

Figure 2

ACCEPTED MANUSCRIPT

Figure 3

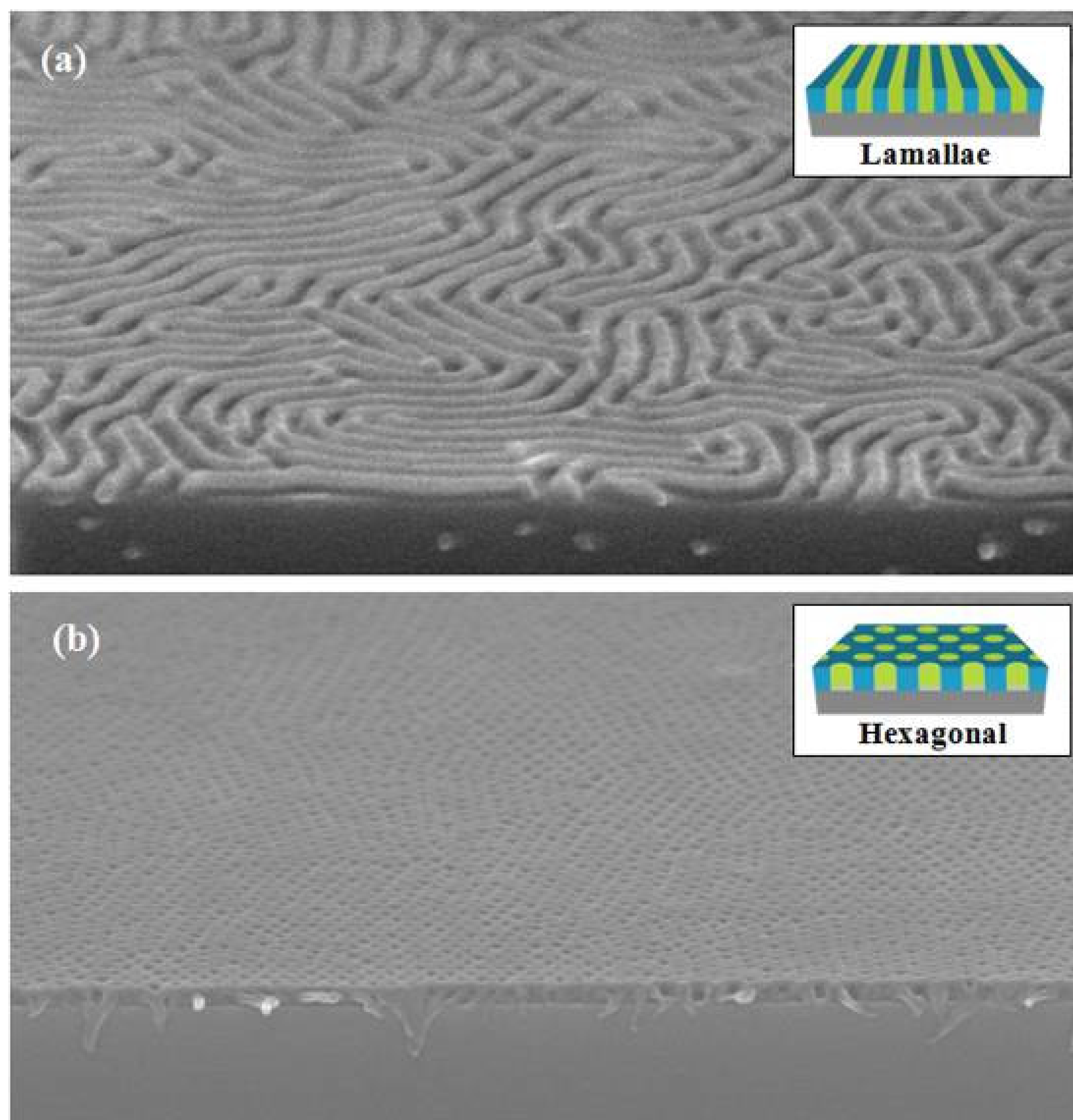

ACCEPTED MANUSCRIPT

Figure 4

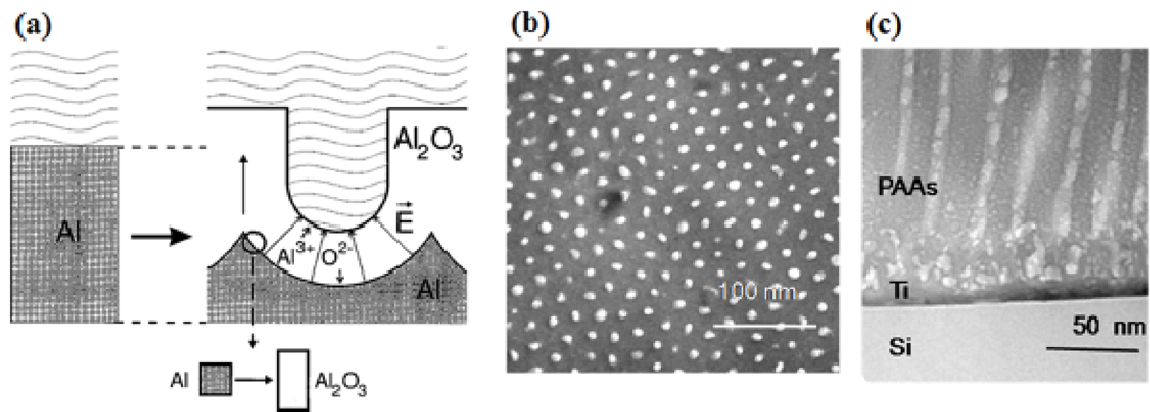

ACCEPTED MANUSCRIPT

ACCEPTED MANUSCRIPT

Figure 5

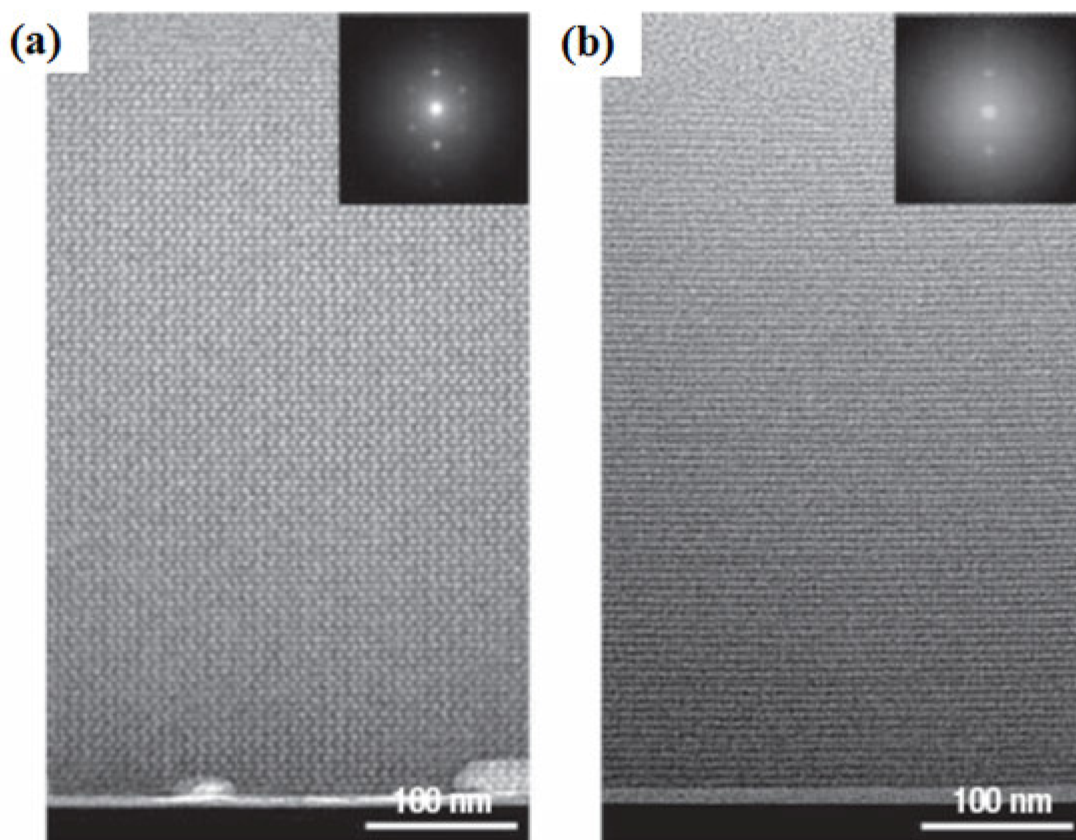

ACCEPTED MANUSCRIPT

ACCEPTED MANUSCRIPT

Figure 6

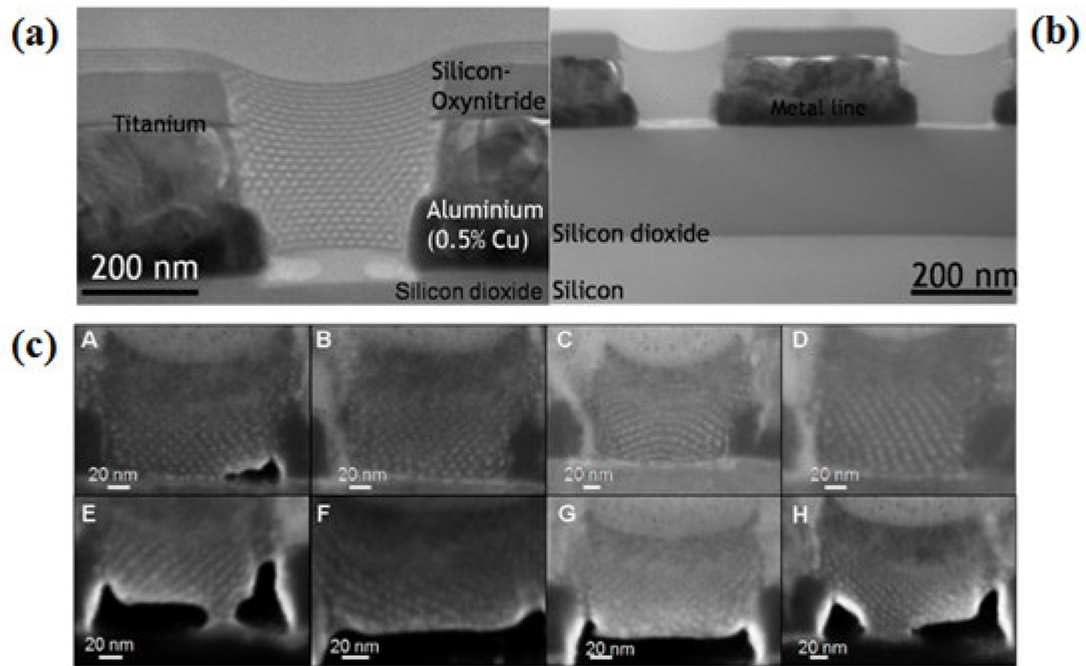

ACCEPTED MANUSCRIPT

ACCEPTED MANUSCRIPT

Figure 7

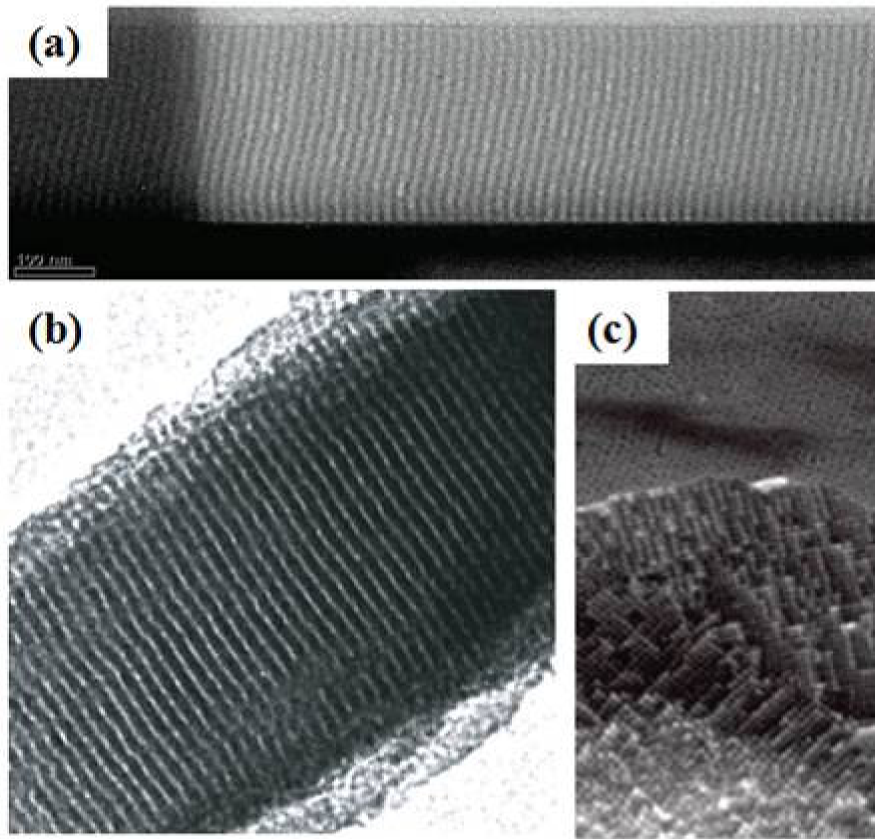

ACCEPTED MANUSCRIPT

ACCEPTED MANUSCRIPT

Figure 8

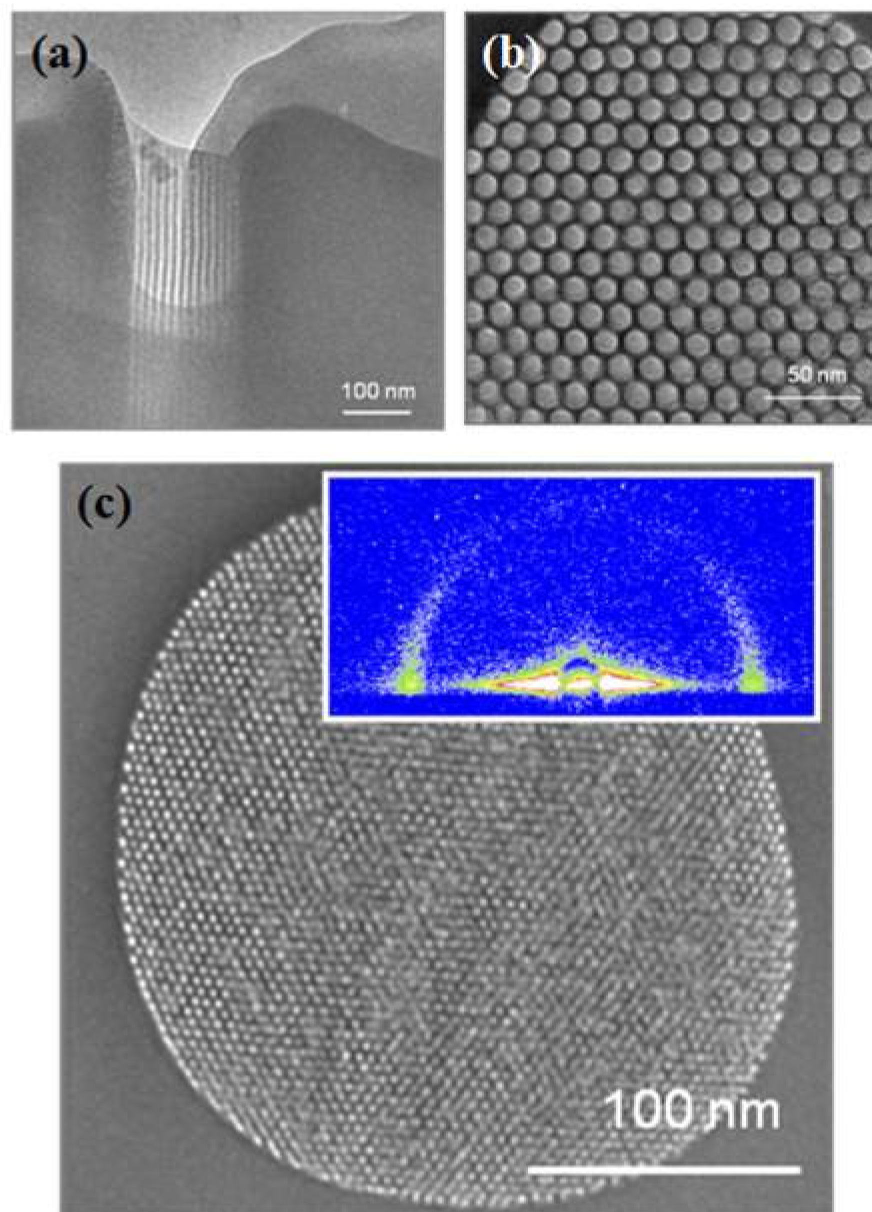

ACCEPTED MANUSCRIPT

Figure 9

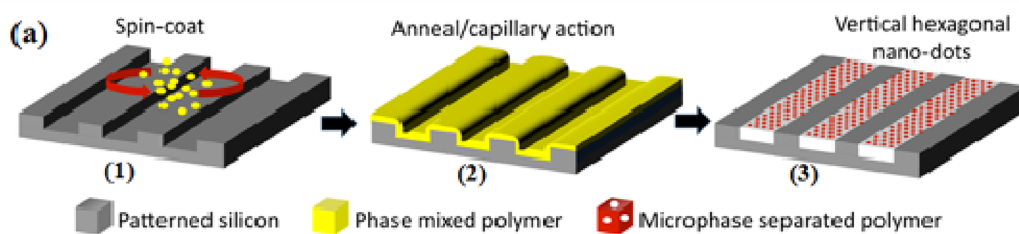

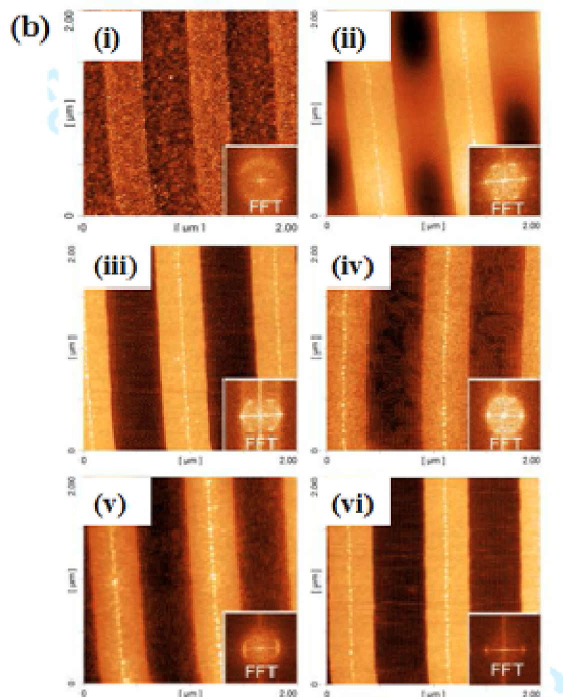

ACCEPTED MANUSCRIPT

ACCEPTED MANUSCRIPT

Figure 10

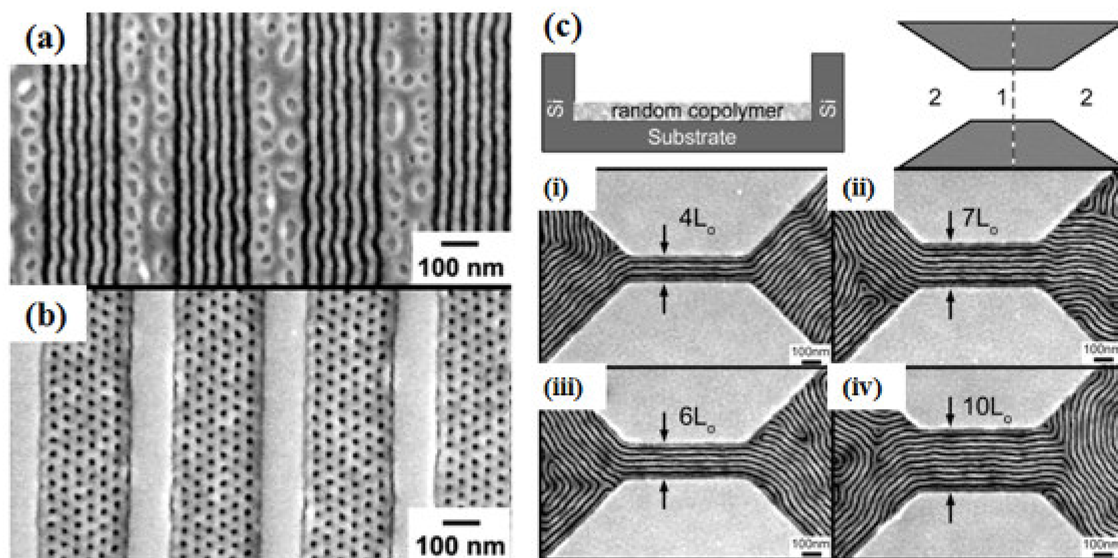

ACCEPTED MANUSCRIPT

ACCEPTED MANUSCRIPT

Figure 11

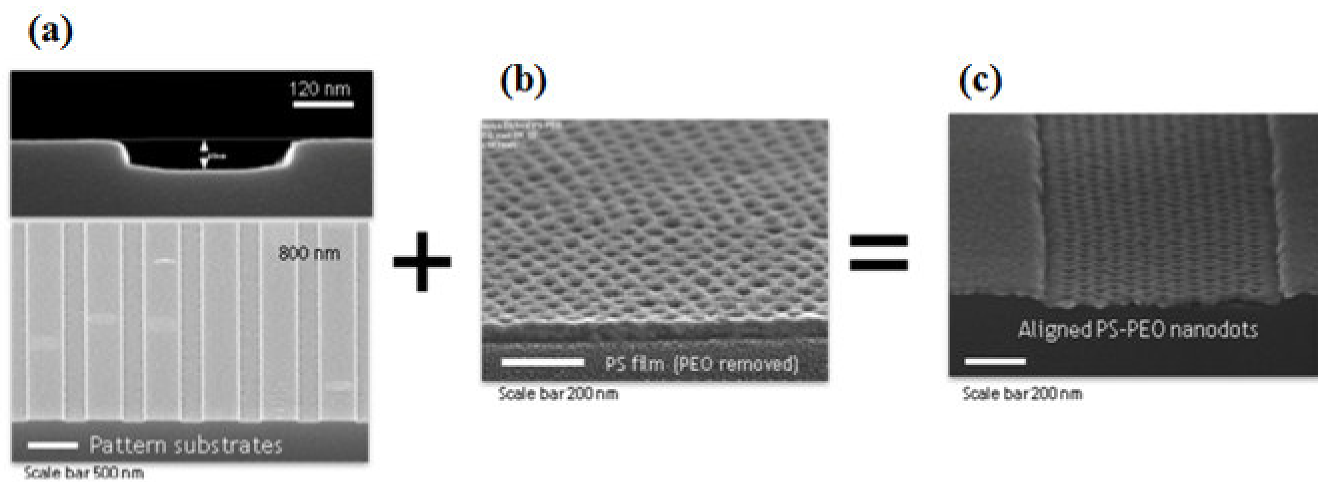

ACCEPTED MANUSCRIPT

ACCEPTED MANUSCRIPT

Figure 12

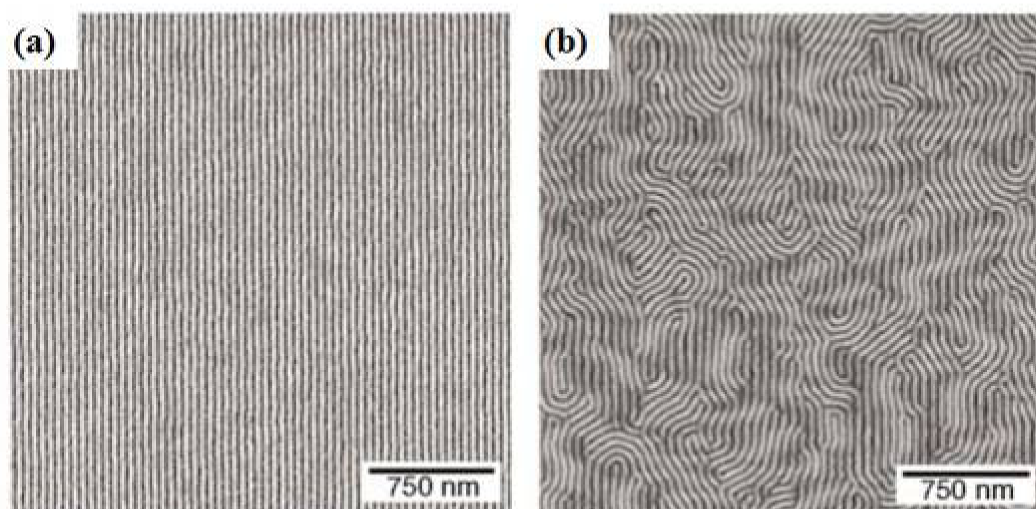

ACCEPTED MANUSCRIPT

ACCEPTED MANUSCRIPT

Figure 13

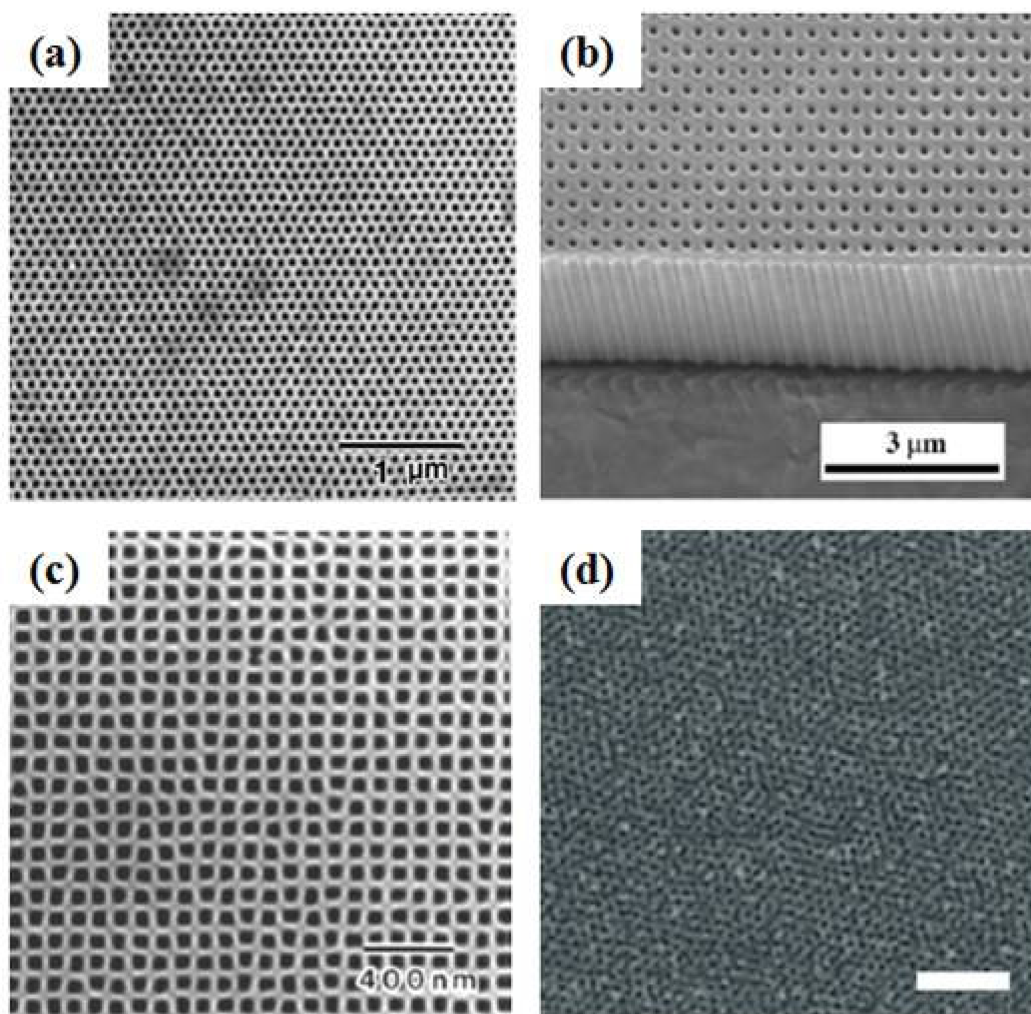

ACCEPTED MANUSCRIPT

Figure 14

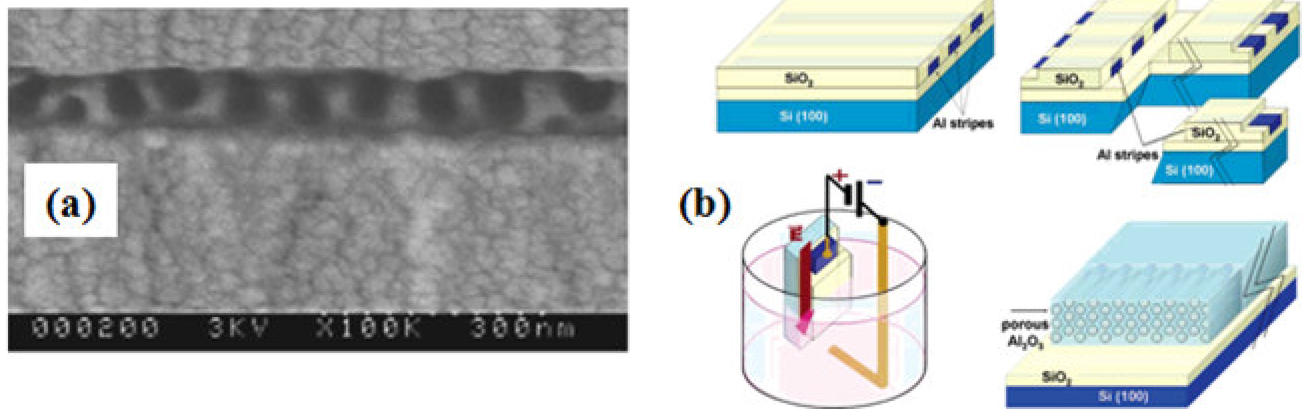

ACCEPTED MANUSCRIPT

ACCEPTED MANUSCRIPT

Figure 15

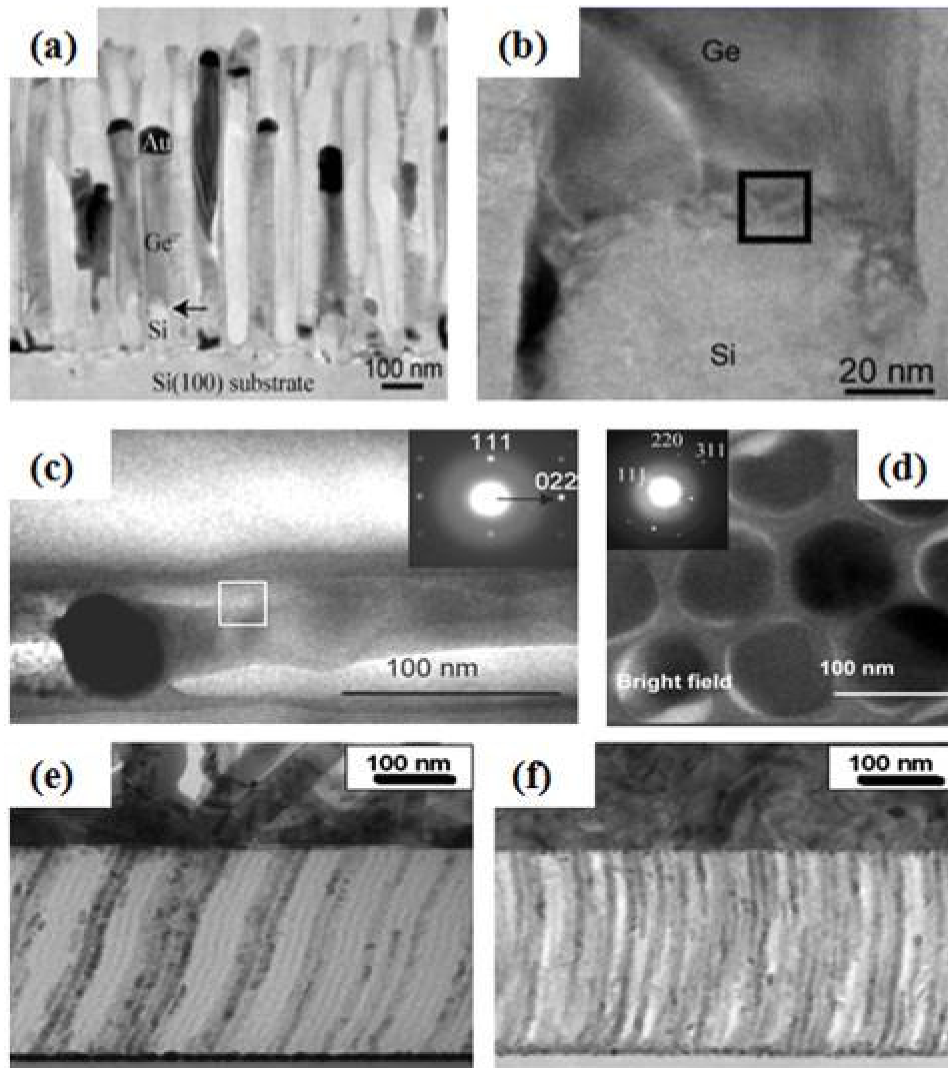

ACCEPTED MANUSCRIPT

Figure 16

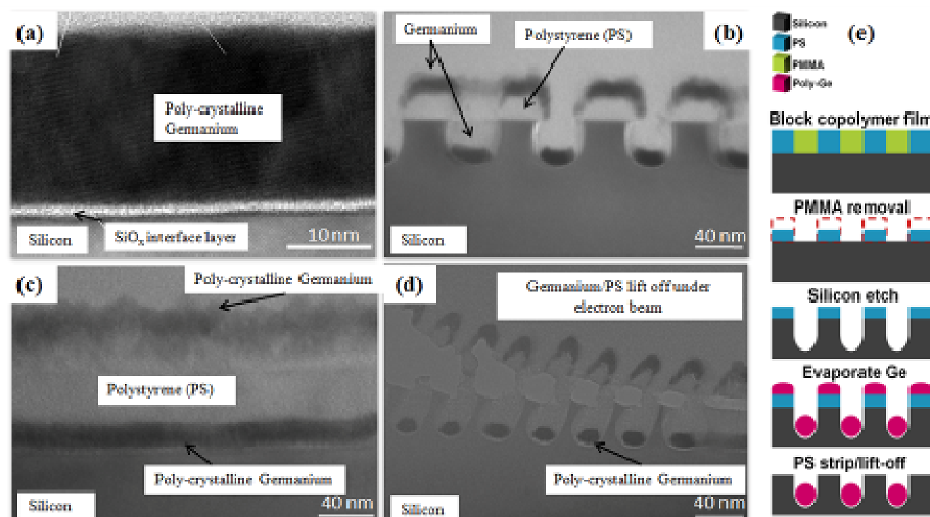

ACCEPTED MANUSCRIPT

ACCEPTED MANUSCRIPT

Figure 17

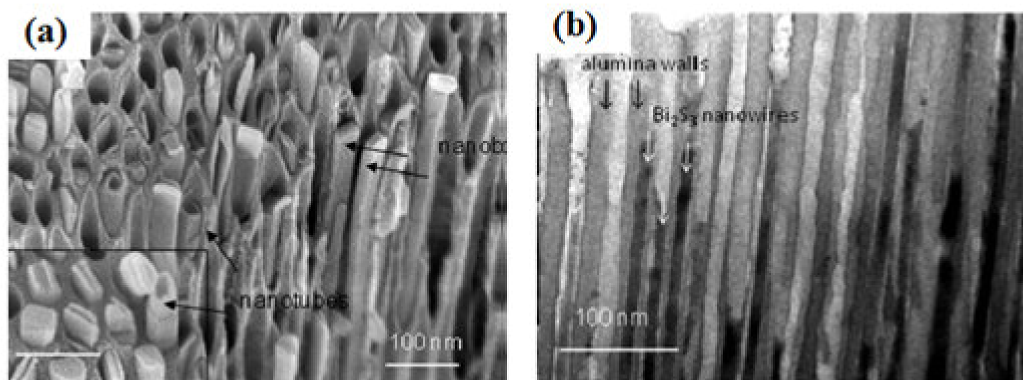

ACCEPTED MANUSCRIPT

ACCEPTED MANUSCRIPT

Figure 18

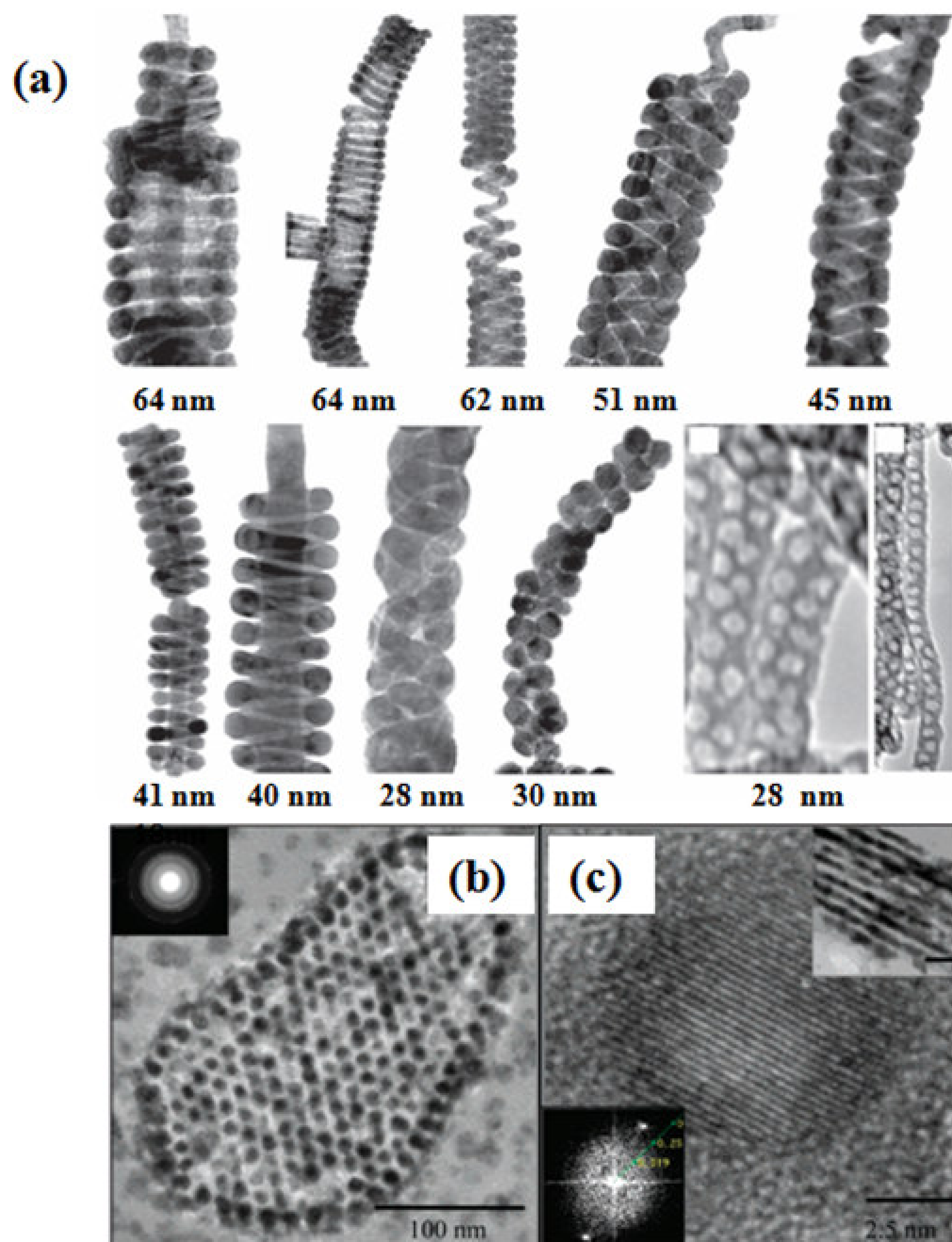

ACCEPTED MANUSCRIPT

Figure 19

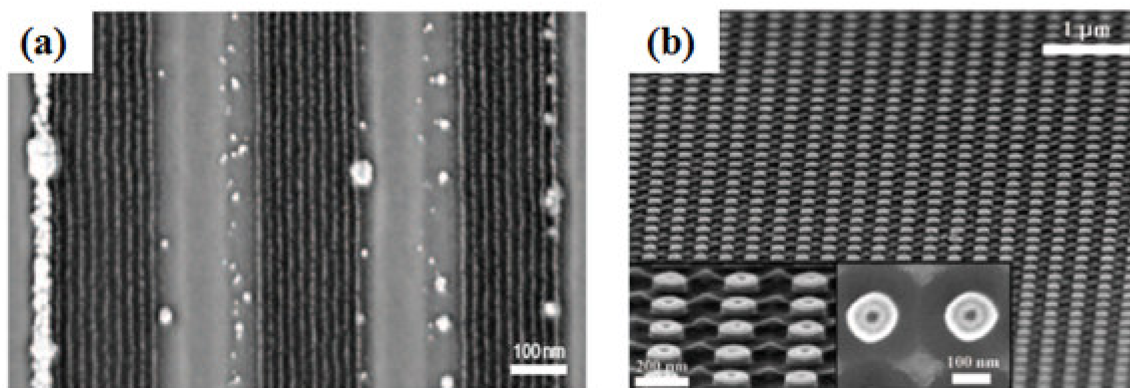

ACCEPTED MANUSCRIPT

ACCEPTED MANUSCRIPT

Figure 20

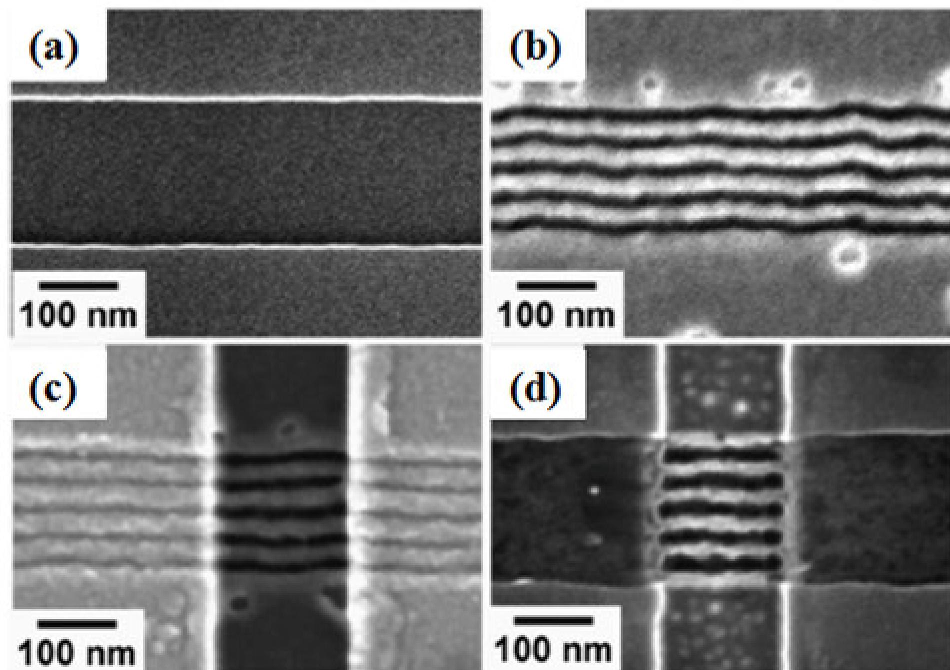

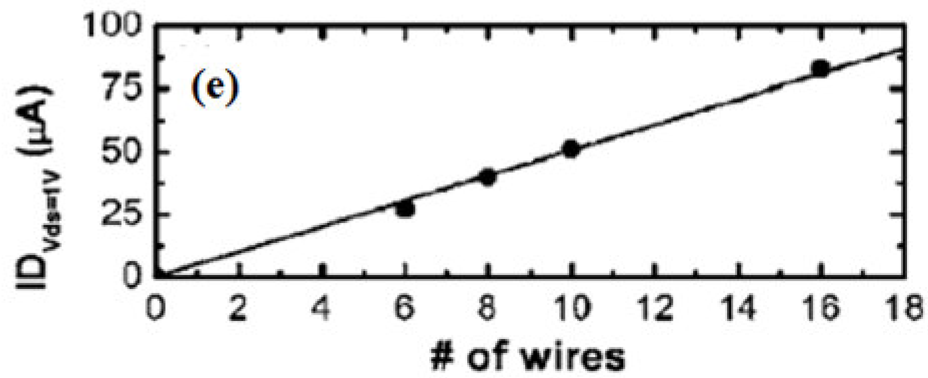

ACCEPTED MANUSCRIPT

Figure 21

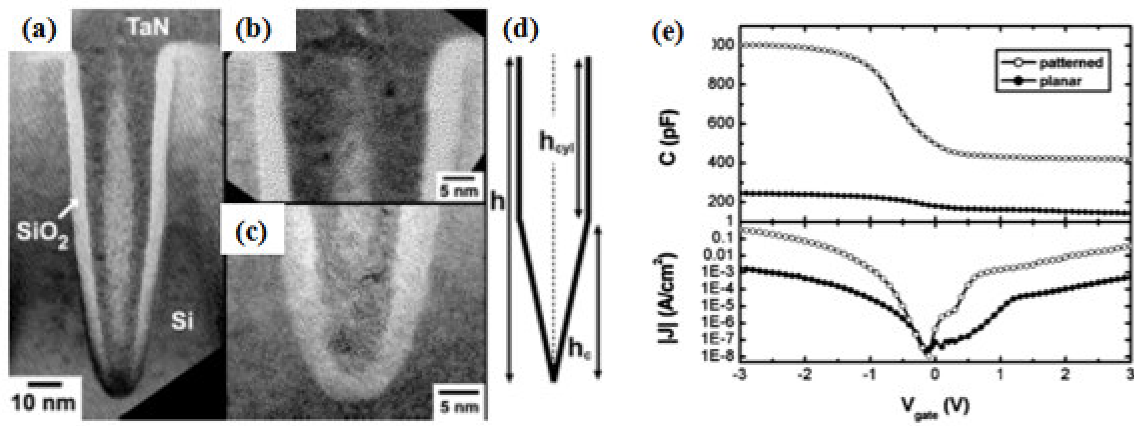

ACCEPTED MANUSCRIPT

ACCEPTED MANUSCRIPT

Figure 22

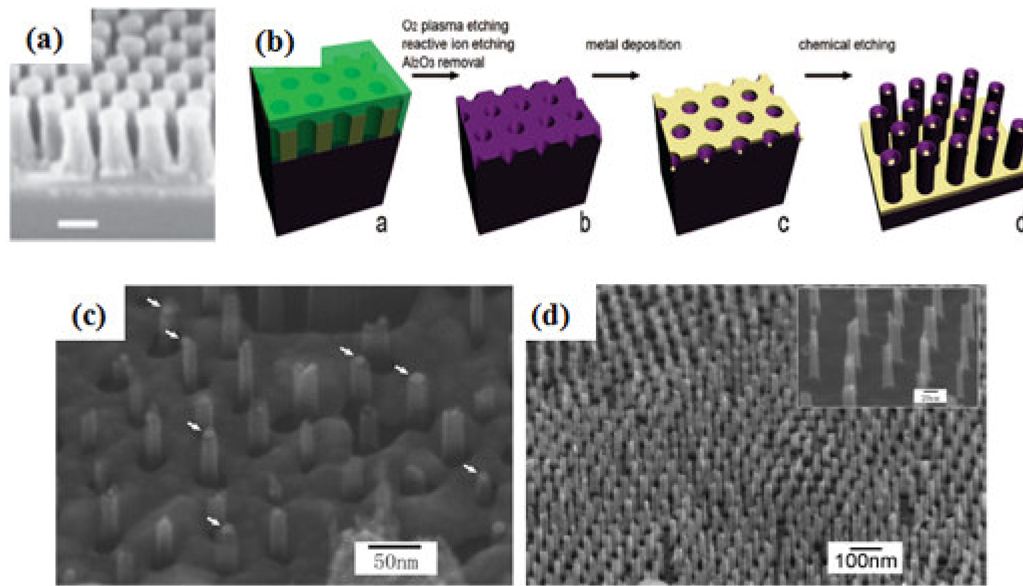

ACCEPTED MANUSCRIPT

ACCEPTED MANUSCRIPT

Figure 23

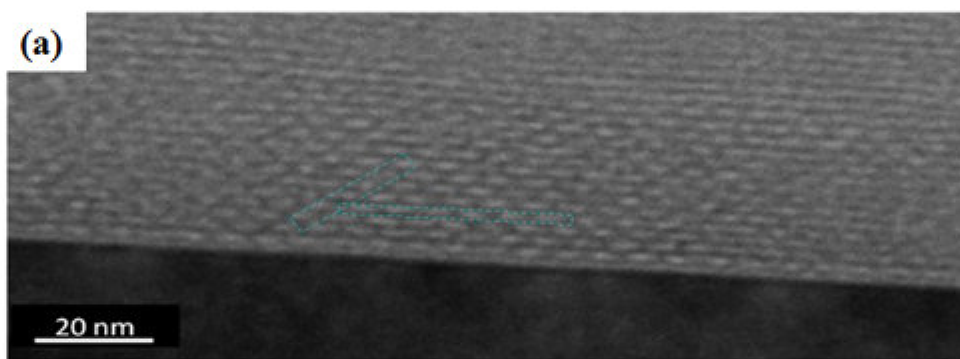

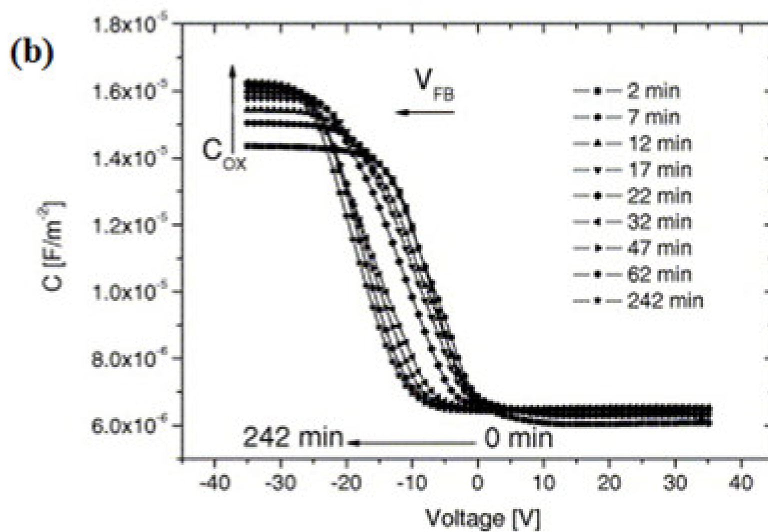

ACCEPTED MANUSCRIPT

REFERENCES

[1] C.T. Kresge, M.E. Leonowicz, W.J. Roth, J.C. Vartuli, J.S. Beck, Nature 359 (1992) 710.
[2] S.M. Park, O.H. Park, J.Y. Cheng, C.T. Rettner, H.C. Kim, Nanotechnology 19 (2008).
[3] C.Y. Peng, C.Y. Liu, N.W. Liu, H.H. Wang, A. Datta, Y.L. Wang, J. Vac. Sci. Technol. B 23 (2005) 559.
[4] S.O. Kim, H.H. Solak, M.P. Stoykovich, N.J. Ferrier, J.J. de Pablo, P.F. Nealey, Nature 424 (2003) 411.
[5] H. Miyata, T. Suzuki, A. Fukuoka, T. Sawada, M. Watanabe, T. Noma, K. Takada, T. Mukaide, K. Kuroda, Nat. Mater. 3 (2004) 651.
[6] Z. Chen, H.G. Zhang, J. Electrochem. Soc. 152 (2005) D227.
[7] J.S. Beck, J.C. Vartuli, W.J. Roth, M.E. Leonowicz, C.T. Kresge, K.D. Schmitt, C.T.W. Chu, D.H. Olson, E.W. Sheppard, S.B. McCullen, J.B. Higgins, J.L. Schlenker, J. Am. Chem. Soc. 114 (1992) 10834.
[8] H. Yang, N. Coombs, I. Sokolov, G.A. Ozin, Nature 381 (1996) 589.
[9] Y.F. Lu, R. Ganguli, C.A. Drewien, M.T. Anderson, C.J. Brinker, W.L. Gong, Y.X. Guo, H. Soyez, B. Dunn, M.H. Huang, J.I. Zink, Nature 389 (1997) 364.
[10] C.J. Brinker, MRS Bull. 29 (2004) 631.
[11] C.J. Brinker, Y.F. Lu, A. Sellinger, H.Y. Fan, Adv. Mater. 11 (1999) 579.
[12] D. Grosso, F. Cagnol, G. Soler-Illia, E.L. Crepaldi, H. Amenitsch, A. Brunet-Bruneau, A. Bourgeois, C. Sanchez, Adv. Funct. Mater. 14 (2004) 309.
[13] A. Gibaud, D. Grosso, B. Smarsly, A. Baptiste, J.F. Bardeau, F. Babonneau, D.A.Doshi, Z. Chen, C.J. Brinker, C. Sanchez, J. Phys. Chem. B. 107 (2003) 6114.
[14] D. Grosso, F. Babonneau, P.A. Albouy, H. Amenitsch, R. Balkenende, A.B. Bruneau, J. Rivory, Chem. Mater. 14 (2002) 931.
[15] C.T. Bolger, R.A. Farrell, G.M. Hughes, M.A. Morris, N. Petkov, J.D. Holmes, ACS Nano 3 (2009) 2311.
[16] F. Rong, H. Seong, Y. Ruoxue, J. Arnold, Y. Peidong, Nat. Mater. 7 (2008) 303.
[17] G. Xomeritakis, C.M. Braunbarth, B. Smarsly, N. Liu, R. Kohn, Z. Klipowicz, C.J. Brinker, Microporous and Mesoporous Materials 66 (2003) 91.
[18] R.A. Pai, R. Humayun, M.T. Schulberg, A. Sengupta, J.N. Sun, J.J. Watkins, Science 303 (2004) 507.
[19] J. Kobler, K. Moller, T. Bein, ACS Nano 2 (2008) 791.
[20] L. Mercier, T.J. Pinnavaia, Adv. Mater. 9 (1997) 500.
[21] A. Bearzotti, J.M. Bertolo, P. Innocenzi, P. Falcaro, E. Traversa, Journal of the European Ceramic Society 24 (2004) 1969.
[22] D.E. Barreca, M.P. Copley, A.E. Graham, J.D. Holmes, M.A. Morris, R. Seraglia, T.R. Spalding, E. Tondello, Appl. Cat. A: General 304 (2006) 14.
[23] I.B. Martini, I.M. Craig, W.C. Molenkamp, H. Miyata, S.H. Tolbert, B.J. Schwartz, Nat. Nanotechnol. 2 (2007) 647.
[24] R.A. Farrell, K. Cherkaoui, N. Petkov, H. Amenitsch, J.D. Holmes, P.K. Hurley, M.A. Morris, Microelectron. Reliab. 47 (2007) 759.
[25] M. Park, C. Harrison, P.M. Chaikin, R.A. Register, D.H. Adamson, Science 276 (1997) 1401.
[26] C.T. Black, R. Ruiz, G. Breyta, J.Y. Cheng, M.E. Colburn, K.W. Guarini, H.C. Kim, Y. Zhang, IBM J. Res. Dev. 51 (2007) 605.
[27] J.Y. Cheng, C.A. Ross, H.I. Smith, E.L. Thomas, Adv. Mater. 18 (2006) 2505.
[28] S.B. Darling, Prog. Polym. Sci. 32 (2007) 1152.
[29] I.W. Hamley, Nanotechnology 14 (2003) R39.
[30] C.J. Hawker, T.P. Russell, MRS Bull. 30 (2005) 952.
[31] M. Lazzari, M.A. Lopez-Quintela, Adv. Mater. 15 (2003) 1583.

ACCEPTED MANUSCRIPT

ACCEPTED MANUSCRIPT

[32] M.Q. Li, C.A. Coenjarts, C.K. Ober, in: (Ed.)^(Eds.)Block Copolymers Ii; Springer-Verlag Berlin, Berlin, 2005, p 183.
[33] M.Q. Li, C.K. Ober, Mater. Today 9 (2006) 30.
[34] C.A. Ross, J.Y. Cheng, MRS Bull. 33 (2008) 838.
[35] M.P. Stoykovich, P.F. Nealey, Mater. Today 9 (2006) 20.
[36] I.W. Hamley, Prog. Polym. Sci. 34 (2009) 1161.
[37] J.K. Bosworth, M.Y. Paik, R. Ruiz, E.L. Schwartz, J.Q. Huang, A.W. Ko, D.M. Smilgies, C.T. Black, C.K. Ober, ACS Nano 2 (2008) 1396.
[38] S. Park, D.H. Lee, J. Xu, B. Kim, S.W. Hong, U. Jeong, T. Xu, T.P. Russell, Science 323 (2009) 1030.
[39] G. Kim, M. Libera, Macromolecules 31 (1998) 2569.
[40] F.S. Bates, G.H. Fredrickson, Phys. Today 52 (1999) 32.
[41] Y.S. Jung, C.A. Ross, Adv. Mater. 21 (2009) 2540.
[42] F.S. Bates, G.H. Fredrickson, Annu. Rev. Phys. Chem. 41 (1990) 525.
[43] H.C. Kim, T.P. Russell, J. Polym. Sci. Pt. B-Polym. Phys. 39 (2001) 663.
[44] P. Mansky, Y. Liu, E. Huang, T.P. Russell, C.J. Hawker, Science 275 (1997) 1458.
[45] K. Fukunaga, H. Elbs, R. Magerle, G. Krausch, Macromolecules 33 (2000) 947.
[46] S.H. Kim, M.J. Misner, T. Xu, M. Kimura, T.P. Russell, Adv. Mater. 16 (2004) 226.
[47] Y. Xuan, J. Peng, L. Cui, H.F. Wang, B.Y. Li, Y.C. Han, Macromolecules 37 (2004) 7301.
[48] S.J. Niu, R.F. Saraf, Macromolecules 36 (2003) 2428.
[49] S. Park, B. Kim, J. Xu, T. Hofmann, B.M. Ocko, T.P. Russell, Macromolecules 42 (2009) 1278.
[50] Y.S. Jung, C.A. Ross, Nano Lett. 7 (2007) 2046.
[51] A. Knoll, R. Magerle, G. Krausch, J. Chem. Phys. 120 (2004) 1105.
[52] R.A. Farrell, N. Nikolay, M.T. Shaw, V. Djara, J.D. Holmes, M.A. Morris, submitted to Chem. Mater. (2010).
[53] Block Copolymers in Nanoscience. Wiley-VCH Verlag GmbH & Co. KGaA, Weinheim, 2006.
[54] S. Ludwigs, A. Boker, A. Voronov, N. Rehse, R. Magerle, G. Krausch, Nat. Mater. 2 (2003) 744.
[55] Z. Wei, Z.G. Wang, Macromolecules 28 (1995) 7215.
[56] C.B. Tang, E.M. Lennon, G.H. Fredrickson, E.J. Kramer, C.J. Hawker, Science 322 (2008) 429.
[57] H. Nikos, P. Stergios, F. George, in: (Ed.)^(Eds.)Block Copolymers, 2003, p 383.
[58] J. O' Sullivan, G.C. Wood, Proceedings of the Royal Society of London Series a-Mathematical and Physical Sciences 317 (1970) 511.
[59] H. Masuda, K. Fukuda, Science 268 (1995) 1466.
[60] O. Jessensky, F. Muller, U. Gosele, J. Electrochem. Soc. 145 (1998) 3735.
[61] S.Z. Chu, K. Wada, S. Inoue, M. Isogai, A. Yasumori, Adv. Mater. 17 (2005) 2115.
[62] W. Lee, R. Ji, U. Gosele, K. Nielsch, Nat. Mater. 5 (2006) 741.
[63] K. Schwirn, W. Lee, R. Hillebrand, M. Steinhart, K. Nielsch, U. Gosele, ACS Nano 2 (2008) 302.
[64] K. Lee, Y. Tang, M. Ouyang, Nano Lett. 8 (2008) 4624.
[65] W. Lee, K. Schwirn, M. Steinhart, E. Pippel, R. Scholz, U. Gosele, Nat. Nanotechnol. 3 (2008) 234.
[66] M.L. Tian, S.Y. Xu, J.G. Wang, N. Kumar, E. Wertz, Q. Li, P.M. Campbell, M.H.W. Chan, T.E. Mallouk, Nano Lett. 5 (2005) 697.
[67] N. Petkov, N. Stock, T. Bein, J. Phys. Chem. B 109 (2005) 10737.
[68] R. Fan, S. Huh, R. Yan, J. Arnold, P.D. Yang, Nat. Mater. 7 (2008) 303.
[69] A. Yamaguchi, F. Uejo, T. Yoda, T. Uchida, Y. Tanamura, T. Yamashita, N. Teramae, Nat. Mater. 3 (2004) 337.
[70] J. Fan, S.W. Boettcher, C.K. Tsung, Q. Shi, M. Schierhorn, G.D. Stucky, Chem. Mat. 20 (2008) 909.
[71] A. Firouzi, D.J. Schaefer, S.H. Tolbert, G.D. Stucky, B.F. Chmelka, J. Am. Chem. Soc. 119 (1997) 9466.

ACCEPTED MANUSCRIPT

[72] S.H. Tolbert, A. Firouzi, G.D. Stucky, B.F. Chmelka, Science 278 (1997) 264.
[73] Y. Yamauchi, M. Sawada, T. Noma, H. Ito, S. Furumi, Y. Sakka, K. Kuroda, Journal of Materials Chemistry 15 (2005) 1137.
[74] Y. Yamauchi, M. Sawada, A. Sugiyama, T. Osaka, Y. Sakka, K. Kuroda, Journal of Materials Chemistry 16 (2006) 3693.
[75] H. Miyata, Y. Kawashima, M. Itoh, M. Watanabe, Chem. Mat. 17 (2005) 5323.
[76] H. Miyata, K. Kuroda, Adv. Mater. 11 (1999) 1448.
[77] H. Miyata, K. Kuroda, Chem. Mat. 11 (1999) 1609.
[78] H. Miyata, K. Kuroda, J. Am. Chem. Soc. 121 (1999) 7618.
[79] H. Miyata, K. Kuroda, Chem. Mat. 12 (2000) 49.
[80] H. Miyata, T. Noma, M. Watanabe, K. Kuroda, Chem. Mat. 14 (2002) 766.
[81] C.T. Black, Appl. Phys. Lett. 87 (2005).
[82] Y.S. Jung, W. Jung, C.A. Ross, Nano Lett. 8 (2008) 2975.
[83] R.L. Rice, D.C. Arnold, M.T. Shaw, D. Iacopina, A.J. Quinn, H. Amenitsch, J.D. Holmes, M.A. Morris, Adv. Funct. Mater. 17 (2007) 133.
[84] C.W. Wu, T. Ohsuna, T. Edura, K. Kuroda, Angew. Chem.-Int. Edit. 46 (2007) 5364.
[85] B. Su, X.M. Lu, Q.H. Lu, Langmuir 24 (2008) 9695.
[86] E.M. Freer, L.E. Krupp, W.D. Hinsberg, P.M. Rice, J.L. Hedrick, J.N. Cha, R.D. Miller, H.C. Kim, Nano Lett. 5 (2005) 2014.
[87] A. Walcarius, E. Sibottier, M. Etienne, J. Ghanbaja, Nat. Mater. 6 (2007) 602.
[88] E.K. Richman, T. Brezesinski, S.H. Tolbert, Nat. Mater. 7 (2008) 712.
[89] B. Platschek, N. Petkov, D. Himsl, S. Zimdars, Z. Li, R. Kohn, T. Bein, J. Am. Chem. Soc. 130 (2008) 17362.
[90] R.A. Segalman, H. Yokoyama, E.J. Kramer, Adv. Mater. 13 (2001) 1152.
[91] Y. Morikawa, S. Nagano, K. Watanabe, K. Kamata, T. Iyoda, T. Seki, Adv. Mater. 18 (2006) 883.
[92] M. Kimura, M.J. Misner, T. Xu, S.H. Kim, T.P. Russell, Langmuir 19 (2003) 9910.
[93] M.W. Wu, R.A. Register, P.M. Chaikin, Phys. Rev. E 74 (2006).
[94] H.W. Li, W.T.S. Huck, Nano Lett. 4 (2004) 1633.
[95] S. Park, O. Yavuzcetin, B. Kim, M.T. Tuominen, T.P. Russell, Small 5 (2009) 1064.
[96] B.C. Berry, A.W. Bosse, J.F. Douglas, R.L. Jones, A. Karim, Nano Lett. 7 (2007) 2789.
[97] C.B. Tang, A. Tracz, M. Kruk, R. Zhang, D.M. Smilgies, K. Matyjaszewski, T. Kowalewski, J. Am. Chem. Soc. 127 (2005) 6918.
[98] I. Bita, J.K.W. Yang, Y.S. Jung, C.A. Ross, E.L. Thomas, K.K. Berggren, Science 321 (2008) 939.
[99] S.M. Park, M.P. Stoykovich, R. Ruiz, Y. Zhang, C.T. Black, P.E. Nealey, Adv. Mater. 19 (2007) 607.
[100] S.G. Xiao, X.M. Yang, E.W. Edwards, Y.H. La, P.F. Nealey, Nanotechnology 16 (2005) S324.
[101] D. Sundrani, S.B. Darling, S.J. Sibener, Langmuir 20 (2004) 5091.
[102] D. Sundrani, S.B. Darling, S.J. Sibener, Nano Lett. 4 (2004) 273.
[103] J.Y. Cheng, A.M. Mayes, C.A. Ross, Nat. Mater. 3 (2004) 823.
[104] C.T. Black, O. Bezencenet, IEEE Trans. Nanotechnol. 3 (2004) 412.
[105] R.A. Segalman, A. Hexemer, E.J. Kramer, Macromolecules 36 (2003) 6831.
[106] R.A. Segalman, Mater. Sci. Eng. R-Rep. 48 (2005) 191.
[107] T.G. Fitzgerald, R.A. Farrell, N.P. Petkov, M.T. Shaw, J.P.F. Charpin, J.P. Gleeson, J.D. Holmes, M.A. Morris, Langmuir 25 (2009) 13551.
[108] J.Y. Cheng, C.A. Ross, E.L. Thomas, H.I. Smith, G.J. Vancso, Appl. Phys. Lett. 81 (2002) 3657.
[109] J.Y. Cheng, C.A. Ross, E.L. Thomas, H.I. Smith, G.J. Vancso, Adv. Mater. 15 (2003) 1599.
[110] T.G. Fitzgerald, F. Borsetto, J.M. O'Callaghan, B. Kosmala, J.D. Holmes, M.A. Morris, Soft Matter 3 (2007) 916.

ACCEPTED MANUSCRIPT

[111] C. Harrison, D.H. Adamson, Z.D. Cheng, J.M. Sebastian, S. Sethuraman, D.A. Huse, R.A. Register, P.M. Chaikin, Science 290 (2000) 1558.
[112] R. Ruiz, R.L. Sandstrom, C.T. Black, Adv. Mater. 19 (2007) 587.
[113] S.-J. Jeong, J.E. Kim, H.-S. Moon, B.H. Kim, S.M. Kim, J.B. Kim, S.O. Kim, Nano Lett. 9 (2009) 2300.
[114] R. Ruiz, N. Ruiz, Y. Zhang, R.L. Sandstrom, C.T. Black, Adv. Mater. 19 (2007) 2157.
[115] J. Chai, J.M. Buriak, ACS Nano 2 (2008) 489.
[116] J. Chai, D. Wang, X.N. Fan, J.M. Buriak, Nat. Nanotechnol. 2 (2007) 500.
[117] S. Park, B. Kim, O. Yavuzcetin, M.T. Tuominen, T.P. Russell, ACS Nano 2 (2008) 1363.
[118] Y.S. Jung, W. Jung, H.L. Tuller, C.A. Ross, Nano Lett. 8 (2008) 3776.
[119] L. Sundstrom, L. Krupp, E. Delenia, C. Rettner, M. Sanchez, M.W. Hart, H.C. Kim, Y. Zhang, Appl. Phys. Lett. 88 (2006).
[120] J.Y. Cheng, J. Pitera, O.H. Park, M. Flickner, R. Ruiz, C.T. Black, H.C. Kim, Appl. Phys. Lett. 91 (2007).
[121] S. Kim, J. Lee, S.M. Jeon, H.H. Lee, K. Char, B.H. Sohn, Macromolecules 41 (2008) 3401.
[122] A.M. Welander, P.F. Nealey, H. Cao, R. Bristol, J. Vac. Sci. Technol. B 26 (2008) 2484.
[123] C.T. Black, K.W. Guarini, Y. Zhang, H.J. Kim, J. Benedict, E. Sikorski, I.V. Babich, K.R. Milkove, IEEE Electron Device Lett. 25 (2004) 622.
[124] L. Rockford, S.G.J. Mochrie, T.P. Russell, Macromolecules 34 (2001) 1487.
[125] R. Ruiz, H.M. Kang, F.A. Detcheverry, E. Dobisz, D.S. Kercher, T.R. Albrecht, J.J. de Pablo, P.F. Nealey, Science 321 (2008) 936.
[126] M.P. Stoykovich, H. Kang, K.C. Daoulas, G. Liu, C.C. Liu, J.J. de Pablo, M. Mueller, P.F. Nealey, ACS Nano 1 (2007) 168.
[127] M.P. Stoykovich, M. Muller, S.O. Kim, H.H. Solak, E.W. Edwards, J.J. de Pablo, P.F. Nealey, Science 308 (2005) 1442.
[128] G.M. Wilmes, D.A. Durkee, N.P. Balsara, J.A. Liddle, Macromolecules 39 (2006) 2435.
[129] J.Y. Cheng, C.T. Rettner, D.P. Sanders, H.C. Kim, W.D. Hinsberg, Adv. Mater. 20 (2008) 3155.
[130] X.M. Yang, L. Wan, S.G. Xiao, Y.A. Xu, D.K. Weller, ACS Nano 3 (2009) 1844.
[131] H. Asoh, K. Nishio, M. Nakao, T. Tamamura, H. Masuda, J. Electrochem. Soc. 148 (2001) B152.
[132] H. Masuda, A. Abe, M. Nakao, A. Yokoo, T. Tamamura, K. Nishio, Adv. Mater. 15 (2003) 161.
[133] H. Masuda, H. Asoh, M. Watanabe, K. Nishio, M. Nakao, T. Tamamura, Adv. Mater. 13 (2001) 189.
[134] W. Lee, R. Ji, C.A. Ross, U. Gosele, K. Nielsch, Small 2 (2006) 978.
[135] A.P. Robinson, G. Burnell, M.Z. Hu, J.L. MacManus-Driscoll, Appl. Phys. Lett. 91 (2007).
[136] C.Y. Liu, A. Datta, Y.L. Wang, Appl. Phys. Lett. 78 (2001) 120.
[137] B.Y. Kim, S.J. Park, T.J. McCarthy, T.P. Russell, Small 3 (2007) 1869.
[138] H. Masuda, K. Nishio, N. Baba, Appl. Phys. Lett. 63 (1993) 3155.
[139] C.S. Cojocaru, J.M. Padovani, T. Wade, C. Mandoli, G. Jaskierowicz, J.E. Wegrowe, A.F.I. Morral, D. Pribat, Nano Lett. 5 (2005) 675.
[140] J. Luo, J. Zhu, Nanotechnology 17 (2006) S262.
[141] T.E. Mallouk, Science 291 (2001) 443.
[142] C.R. Martin, Science 266 (1994) 1961.
[143] M. Steinhart, R.B. Wehrspohn, U. Gosele, J.H. Wendorff, Angew. Chem.-Int. Edit. 43 (2004) 1334.
[144] K. Nielsch, F. Muller, A.P. Li, U. Gosele, Adv. Mater. 12 (2000) 582.
[145] M. Lahav, T. Sehayek, A. Vaskevich, I. Rubinstein, Angew. Chem.-Int. Edit. 42 (2003) 5575.
[146] B.B. Lakshmi, P.K. Dorhout, C.R. Martin, Chem. Mat. 9 (1997) 857.
[147] N. Petkov, P. Birjukovs, R. Phelan, M.A. Morris, D. Erts, J.D. Holmes, Chem. Mat. 20 (2008) 1902.
[148] Y.Q. Liang, C.G. Zhen, D.C. Zou, D.S. Xu, J. Am. Chem. Soc. 126 (2004) 16338.

ACCEPTED MANUSCRIPT

[149] J.G. Wang, M.L. Tian, T.E. Mallouk, M.H.W. Chan, J. Phys. Chem. B 108 (2004) 841.
[150] (2005).
[151] J. Mallet, M. Molinari, F. Martineau, F. Delavoie, P. Fricoteaux, M. Troyon, Nano Lett. 8 (2008) 3468.
[152] T.E. Bogart, S. Dey, K.K. Lew, S.E. Mohney, J.M. Redwing, Adv. Mater. 17 (2005) 114.
[153] J. Hangfeng, M. Kuball, R.A. Burke, J.M. Redwing, Nanotechnology 18 (2007) 445704.
[154] T. Shimizu, T. Xie, J. Nishikawa, S. Shingubara, S. Senz, U. Gosele, Adv. Mater. 19 (2007) 917.
[155] T. Shimizu, Z. Zhang, S. Shingubara, S. Senz, U. Gosele, Nano Lett. 9 (2009) 1523.
[156] H. Jagannathan, M. Deal, Y. Nishi, H.C. Kim, E.M. Freer, L. Sundstrom, T. Topuria, P.M. Rice, J. Vac. Sci. Technol. B 24 (2006) 2220.
[157] F.M. Davidson, A.D. Schricker, R.J. Wiacek, B.A. Korgel, Adv. Mater. 16 (2004) 646.
[158] F.M. Davidson, R. Wiacek, B.A. Korgel, Chem. Mat. 17 (2005) 230.
[159] Z.L. Li, J. Andzane, D. Erts, J.M. Tobin, K.X. Wang, M.A. Morris, G. Attard, J.D. Holmes, Adv. Mater. 19 (2007) 3043.
[160] D.C. Lee, T. Hanrath, B.A. Korgel, Angew. Chem.-Int. Edit. 44 (2005) 3573.
[161] H.Y. Tuan, D.C. Lee, B.A. Korgel, Angew. Chem.-Int. Edit. 45 (2006) 5184.
[162] P.S. Shah, T. Hanrath, K.P. Johnston, B.A. Korgel, J. Phys. Chem. B 108 (2004) 9574.
[163] H.C. Luan, D.R. Lim, K.K. Lee, K.M. Chen, J.G. Sandland, K. Wada, L.C. Kimerling, Appl. Phys. Lett. 75 (1999) 2909.
[164] N. Petkov, T. Bein, in: F. Laeri, F. Schüth, U. Simon, M. Wark, (Ed.)^(Eds.)Host-Guest-Systems Based on Nanoporous Crystals, 2005, p 393.
[165] X. Ju, N. Petkov, W. Xueyan, D. Lacopino, A.J. Quinn, G. Redmond, T. Bein, M.A. Morris, J.D. Holmes, ChemPhysChem 8 (2007) 235.
[166] T. Jiang, G.A. Ozin, Journal of Materials Chemistry 8 (1998) 1099.
[167] M.B. Sigman, B.A. Korgel, Chem. Mat. 17 (2005) 1655.
[168] Y. Yu, C.H. Jin, R.H. Wang, Q. Chen, L.M. Peng, J. Phys. Chem. B 109 (2005) 18772.
[169] N. Petkov, J. Xu, M.A. Morris, J.A. Holmes, J. Phys. Chem. C 112 (2008) 7345.
[170] N.I. Kovtyukhova, B.K. Kelley, T.E. Mallouk, J. Am. Chem. Soc. 126 (2004) 12738.
[171] L.F. Liu, H.F. Tian, S.S. Xie, W.Y. Zhou, S.C. Mu, L. Song, D.F. Liu, S.D. Luo, Z.X. Zhang, Y.J. Xiang, X.W. Zhao, W.J. Ma, J. Shen, J.Q. Li, C.Y. Wang, G. Wang, J. Phys. Chem. B 110 (2006) 20158.
[172] X.T. Tang, G.C. Wang, M. Shima, J. Appl. Phys. 99 (2006).
[173] X.H. Huang, I.H. El-Sayed, W. Qian, M.A. El-Sayed, Nano Lett. 7 (2007) 1591.
[174] A. Manjavacas, F.J.G. de Abajo, Nano Lett. 9 (2009) 1285.
[175] M.S. Sander, R. Gronsky, T. Sands, A.M. Stacy, Chem. Mat. 15 (2003) 335.
[176] R.M. Penner, C.R. Martin, Anal. Chem. 59 (1987) 2625.
[177] J. Choi, G. Sauer, K. Nielsch, R.B. Wehrspohn, U. Gosele, Chem. Mat. 15 (2003) 776.
[178] P. Evans, W.R. Hendren, R. Atkinson, G.A. Wurtz, W. Dickson, A.V. Zayats, R.J. Pollard, Nanotechnology 17 (2006) 5746.
[179] K. Yasui, T. Morikawa, K. Nishio, H. Masuda, Jpn. J. Appl. Phys. Part 2 - Lett. Express Lett. 44 (2005) L469.
[180] Y.T. Pang, G.W. Meng, Y. Zhang, Q. Fang, L.D. Zhang, Appl. Phys. A-Mater. Sci. Process. 76 (2003) 533.
[181] K. Nielsch, R.B. Wehrspohn, J. Barthel, J. Kirschner, U. Gosele, S.F. Fischer, H. Kronmuller, Appl. Phys. Lett. 79 (2001) 1360.
[182] Y.T. Pang, G.W. Meng, L.D. Zhang, Y. Qin, X.Y. Gao, A.W. Zhao, Q. Fang, Adv. Funct. Mater. 12 (2002) 719.
[183] G. Kartopu, S. Habouti, M. Es-Souni, Mater. Chem. Phys. 107 (2008) 226.
[184] B. Wildt, P. Mali, P.C. Searson, Langmuir 22 (2006) 10528.
[185] N.B. Chaure, J.M.D. Coey, J. Magn. Magn. Mater. 303 (2006) 232.
ACCEPTED MANUSCRIPT

ACCEPTED MANUSCRIPT
[186] Y. Dahmane, L. Cagnon, J. Voiron, S. Pairis, M. Bacia, L. Ortega, N. Benbrahim, A. Kadri, J. Phys. D-Appl. Phys. 39 (2006) 4523.
[187] X.L. Fei, S.L. Tang, R.L. Wang, H.L. Su, Y. Du, Solid State Commun. 141 (2007) 25.
[188] S. Thongmee, H.L. Pang, J.B. Yi, J. Ding, J.Y. Lin, L.H. Van, Acta Mater. 57 (2009) 2482.
[189] G. Sharma, M.V. Pishko, C.A. Grimes, J. Mater. Sci. 42 (2007) 4738.
[190] Y.N. Xia, P.D. Yang, Y.G. Sun, Y.Y. Wu, B. Mayers, B. Gates, Y.D. Yin, F. Kim, Y.Q. Yan, Adv. Mater. 15 (2003) 353.
[191] D.M. Davis, M. Moldovan, D.P. Young, M. Henk, X.G. Xie, E.J. Podlaha, Electrochem. Solid State Lett. 9 (2006) C153.
[192] G. Tourillon, L. Pontonnier, J.P. Levy, V. Langlais, Electrochem. Solid State Lett. 3 (2000) 20.
[193] J.C. Bao, C.Y. Tie, Z. Xu, Q.F. Zhou, D. Shen, Q. Ma, Adv. Mater. 13 (2001) 1631.
[194] X. Shouhong, C. Chuanbao, Z. Hesun, J. Mater. Sci. 41 (2006) 5598.
[195] W. Lee, R. Scholz, K. Niesch, U. Gosele, Angew. Chem.-Int. Edit. 44 (2005) 6050.
[196] M. Daub, M. Knez, U. Goesele, K. Nielsch, J. Appl. Phys. 101 (2007).
[197] M.D. Dickey, E.A. Weiss, E.J. Smythe, R.C. Chiechi, F. Capasso, G.M. Whitesides, ACS Nano 2 (2008) 800.
[198] Y.Y. Wu, G.S. Cheng, K. Katsov, S.W. Sides, J.F. Wang, J. Tang, G.H. Fredrickson, M. Moskovits, G.D. Stucky, Nat. Mater. 3 (2004) 816.
[199] N. Petkov, B. Platschek, M.A. Morris, J.D. Holmes, T. Bein, Chem. Mat. 19 (2007) 1376.
[200] J.Y. Cheng, C.A. Ross, V.Z.H. Chan, E.L. Thomas, R.G.H. Lammertink, G.J. Vancso, Adv. Mater. 13 (2001) 1174.
[201] T. Thurn-Albrecht, J. Schotter, C.A. Kastle, N. Emley, T. Shibauchi, L. Krusin-Elbaum, K. Guarini, C.T. Black, M.T. Tuominen, T.P. Russell, Science 290 (2000) 2126.
[202] M. Bal, A. Ursache, M.T. Tuominen, J.T. Goldbach, T.P. Russell, Appl. Phys. Lett. 81 (2002) 3479.
[203] K. Xu, L. Qin, J.R. Heath, Nat. Nanotechnol. 4 (2009) 368.
[204] A. Subramani, D. Geerpuram, A. Domanowski, V. Baskaran, V. Medushko, Physica C 404 (2004) 241.
[205] D. Whang, S. Jin, C.M. Lieber, Nano Lett. 3 (2003) 951.
[206] A.D. Wissner-Gross, Nanotechnology 17 (2006) 4986.
[207] Y. Huang, X.F. Duan, Q.Q. Wei, C.M. Lieber, Science 291 (2001) 630.
[208] G.Y. Jung, E. Johnston-Halperin, W. Wu, Z.N. Yu, S.Y. Wang, W.M. Tong, Z.Y. Li, J.E. Green, B.A. Sheriff, A. Boukai, Y. Bunimovich, J.R. Heath, R.S. Williams, Nano Lett. 6 (2006) 351.
[209] B.S. Doyle, S. Datta, M. Doczy, S. Hareland, B. Jin, J. Kavalieros, T. Linton, A. Murthy, R. Rios, R. Chau, IEEE Electron Device Lett. 24 (2003) 263.
[210] Y. Kamata, A. Kikitsu, H. Hieda, M. Sakurai, K. Naito, J. Appl. Phys. 95 (2004) 6705.
[211] H. Hieda, Y. Yanagita, A. Kikitsu, T. Maeda, K. Naito, J. Photopolym Sci. Technol. 19 (2006) 425.
[212] C.T. Black, K.W. Guarini, K.R. Milkove, S.M. Baker, T.P. Russell, M.T. Tuominen, Appl. Phys. Lett. 79 (2001) 409.
[213] Y. Lei, W.P. Cai, G. Wilde, Prog. Mater. Sci. 52 (2007) 465.
[214] S.G. Cloutier, R.S. Guico, J.M. Xu, Appl. Phys. Lett. 87 (2005).
[215] Z.P. Huang, X.X. Zhang, M. Reiche, L.F. Liu, W. Lee, T. Shimizu, S. Senz, U. Gosele, Nano Lett. 8 (2008) 3046.
[216] G. Moore, Electronics magazine (1965).
[217] S.E. Thompson, M. Armstrong, C. Auth, S. Cea, R. Chau, G. Glass, T. Hoffman, J. Klaus, Z.Y. Ma, B. McIntyre, A. Murthy, B. Obradovic, L. Shifren, S. Sivakumar, S. Tyagi, T. Ghani, K. Mistry, M. Bohr, Y. El-Mansy, IEEE Electron Device Lett. 25 (2004) 191.
[218] R. Chau, B. Doyle, S. Datta, J. Kavalieros, K. Zhang, Nat. Mater. 6 (2007) 810.
[219] D.C. Edelstein, Proceedings of the 12th International IEEE VLSI Multilevel Interconnection Conference (1995) 301.
ACCEPTED MANUSCRIPT

ACCEPTED MANUSCRIPT
[220] K. Maex, M.R. Baklanov, D. Shamiryan, F. Iacopi, S.H. Brongersma, Z.S. Yanovitskaya, J. Appl. Phys. 93 (2003) 8793.
[221] K. Mosig, T. Jacobs, K. Brennan, M. Rasco, J. Wolf, R. Augur, Microelectron. Eng. 64 (2002) 11.
[222] R.A. Farrell, N. Petkov, K. Cherkaoui, H. Amenitsch, J.D. Holmes, P.K. Hurley, M.A. Morris, ChemPhysChem 9 (2008) 1524.
[223] A.P. Singh, P. Victor, P.G. Ganesan, O. Nalamasu, G. Ramanath, Appl. Phys. Lett. 87 (2005).
ACCEPTED MANUSCRIPT

ACCEPTED MANUSCRIPT

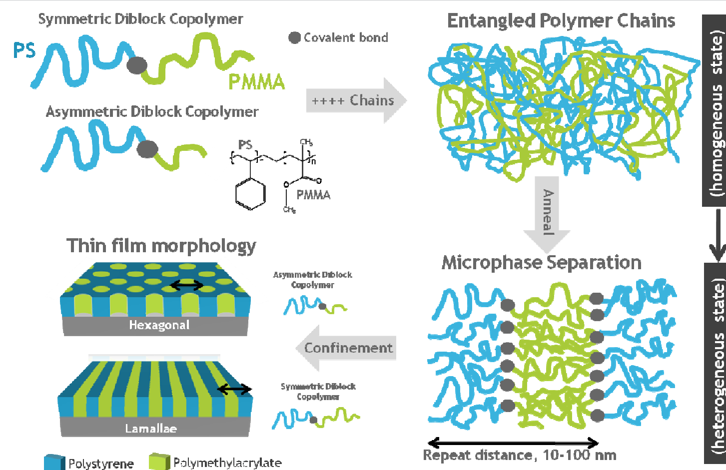

The review article describes the use of self-assembled nanoscale porous architectures as hosts for templating one dimension (1D) nano-entities for a wide range of electronic, photonic, magnetic and environmental applications. Special attention is given to the different ways of directing self-assembly with a focus on properties such as uni-directional alignment, precision placement and registry of the self-assembled structures to hierarchal or top down architectures.

ACCEPTED MANUSCRIPT